THE ROLE OF MYELOID STAT3 IN EXPERIMENTAL AUTOIMMUNE ENCEPHALOMYELITIS AND POSTNATAL BRAIN DEVELOPMENT

A Dissertation

by

HSUEH-CHUNG LU

Submitted to the Office of Graduate and Professional Studies of
Texas A&M University
in partial fulfillment of the requirements for the degree of

DOCTOR OF PHILOSOPHY

Chair of Committee,	Jianrong Li
Committee Members,	Beiyan Zhou
	C. Jane R. Welsh
	Gregg B. Wells
Head of Department,	C. Jane R. Welsh

August 2017

Major Subject: Neuroscience

ABSTRACT

Multiple sclerosis (MS) is a debilitating disease characterized by demyelination and neurodegeneration in the CNS. Both activated microglia and infiltrating myeloid cells are thought to contribute to disease progression of experimental autoimmune encephalomyelitis (EAE), a widely used animal model of MS. Signal transducer and activator of transcription 3 (STAT3) regulates multiple cellular functions including cell differentiation, survival, and inflammation, and is a critical signaling molecule for the interleukin-6 family of cytokines. Additionally, not only *Stat3* is a risk factor for MS, but its increased phosphorylation has been detected in the MS patient myeloid cells.

To investigate the role of STAT3 in myeloid cells and neuroinflammation, we generated myeloid STAT3-deficient mice (*LysMcre/Stat3*$^{fl/fl}$) and investigated their susceptibility to MOG_{35-55}-induced EAE. Whereas *Stat3*$^{fl/fl}$ control mice developed typical symptoms of EAE, *LysMcre/Stat3*$^{fl/fl}$ mice rather resistant to EAE and exhibited diminished antigen-specific helper T-cell responses in the periphery. Splenic myeloid cells isolated from immunized *LysMcre/Stat3*$^{fl/fl}$ mice exhibited impaired antigen-presenting and co-stimulatory functions. In contrast to active EAE, *LysMcre/Stat3*$^{fl/fl}$ mice were partially susceptible to EAE induced by adoptive transfer of encephalitogenic T-cells, suggesting the importance of myeloid STAT3 in differentiation of helper T-cells during the initiation phase of EAE. Consistent with these findings, mice with STAT3 inactivated in microglial cells were indistinguishable from control mice in MOG_{35-55}-

induced EAE, suggesting that microglial STAT3 signaling does not play a critical role in EAE.

We also investigated the role of microglial STAT3 on brain development and behaviors. Our preliminary investigation indicated that neonatal inactivation of microglial STAT3 signaling resulted in a transient reduction of microglial number at the second postnatal week, although the microglial population was largely recovered by P30. In addition, the *Cx3cr1creER/Stat3*$^{fl/fl}$ mice exhibited altered marble burying behaviors. These results suggest that microglial STAT3 signaling plays important roles in normal postnatal brain development and that transient perturbation of microglial functions may have long-term functional consequences.

In summary, this study highlights the importance of STAT3-dependent pathways in myeloid cells in the development of autoimmunity during EAE, as well as STAT3 in microglia in postnatal brain development and behaviors.

DEDICATION

This study is dedicated to many people afflicted with multiple sclerosis and other autoimmune diseases, as well as my family and SO for their love and support.

ACKNOWLEDGEMENTS

I would like to thank my committee chair, Dr. Jianrong Li, for her guidance, patience, and funding for my research. If not for her patience and enthusiasm, my research would not have come to fruition. I also thank my committee members, Dr. Beiyan Zhou, Dr. Jane Welsh, and Dr. Gregg Wells, for their advice during my research. The diverse backgrounds from my committee members have greatly broadened my knowledge pertaining to my research.

I would like to thank the former and present lab members for their guidance and help in the experiments. Particularly, I would like to thank Dr. Andrew Steelman, for sparking my interest in neuroimmunology, forming my research philosophy, and teaching me all the important research techniques from the ground up; Dr. Sunja Kim for collaboration on numerous experiments, such as EAE analysis and co-cultures, and her advice and troubleshooting tips when techniques do not work as intended; Danielle Michaud for arranging the cell sorting and RNA sequencing for the co-culture experiments; Bianca Barth for caring the mice and conducting the behavioral tests; Adam Bowling and Guillermo Obregon for the quantitation of microglial cell numbers; as well as Chris Gillis, Yu Kong, and Jeffery Thompson, for their general support and friendship.

Additionally, I would like to thank my colleagues for their help. Particularly, I would like to thank Dr. Beiyan Zhou again for demonstrating the bone marrow isolation and retro-orbital injection techniques and allowing access to the qRT-PCR thermocycler

and flow cytometer; Wei Ying for collaboration of the bone marrow transplantation experiments; Dr. Roger Smith and Dr. Gus Wright for flow cytometry and cell sorting; Dr. Andrew Hillhouse for multiplex and RNA sequencing; Dr. David Threadgill for allowing access to the behavioral test devices; staff in the CMP for animal care; as well as the staff in the TAMIN and VIBS for the registration and paperwork.

I would also like to thank my community college biology teachers, Mr. Ken Marr and Mr. Steven Brumbaugh, for training me to be open-minded and think critically and giving me the chance to practice English speaking. I also thank Dr. Jaime Olavarria and Robyn Laing at the University of Washington for my first experience in a laboratory and my interest in behavioral neuroscience.

Finally, I would like to thank my parents, Wen Yu Lu and Sharon Ou, for their everlasting love and support, my brother Vincent for his help accommodating to live in the United States, my SO Alex for the encouragement when needed the most, and my former and present small furry friends, Gray, Poring, Duo, and Allo, for their company.

CONTRIBUTORS AND FUNDING SOURCES

Contributors

This work was supervised by a dissertation committee consisting of Professor Jianrong Li and Dr. Jane Welsh of the Department of Veterinary Integrative Biosciences, Dr. Gregg Wells of the Texas A&M University Health Science Center, and Dr. Beiyan Zhou now at the University of Connecticut Health Center.

The bone marrow derived macrophages and bone marrow transplantation in section 2 was completed by the student, in collaboration with Dr. Beiyan Zhou of the Department of Veterinary Pathobiology at the time of the experiments. The multiplex in section 2 was completed with the assistance of Dr. Andrew Hillhouse of the Department of Veterinary Pathobiology. All other work conducted for the dissertation was completed by the student independently.

Funding Sources

My graduate study was supported by Dr. Jianrong Li and a fellowship from Texas A&M University Institute for Neuroscience.

This work was made possible in part by NIH under Grant Number R01NS060017 and by National Multiple Sclerosis Society under Grant Number RG1507-05632.

NOMENCLATURE

ADEM	Acute Disseminated Encephalomyelitis
AIR	Anti-inflammatory Response
APC	Antigen Presenting Cell
BBB	Blood Brain Barrier
BMDM	Bone Marrow Derived Macrophage
CCL	C-C Motif Chemokine Ligand
CD	Cluster of Differentiation
CFA	Complete Freund's Adjuvant
CNS	Central Nervous System
CSF	Cerebrospinal Fluid
CVEC	Cerebrovascular Endothelial Cell
DC	Dendritic Cell
DIV	Day *in vitro*
DPI	Day post Immunization
E	Embryonic Day
EAE	Experimental Autoimmune Encephalomyelitis
ECM	Extracellular Matrix
GA	Glatiramer Acetate
G-CSF	Granulocyte-Colony Stimulating Factor
GM-CSF	Granulocyte Monocyte-Colony Stimulating Factor

HLA	Human Leukocyte Antigen
ICAM-1	Intracellular Adhesion Molecule-1
IFN	Interferon
iNOS	Inducible Nitric Oxide Synthase
IL	Interleukin
JAK	Janus Kinase
LFA-1	Lymphocyte Function-Associated Antigen
MBP	Myelin Basic Protein
M-CSF	Monocyte-Colony Stimulating Factor
MHC	Major Histocompatibility Complex
MMP	Matrix Metalloproteinase
MOG	Myelin Oligodendrocyte Glycoprotein
MS	Multiple Sclerosis
MWM	Morris' Water Maze
NO	Nitric Oxide
P	Postnatal Day
PBMC	Peripheral Blood Mononuclear Cell
PML	Progressive Multifocal Leukoencephalopathy
PLP	Proteolipid Protein
PT	Pertussis Toxin
ROS	Reactive Oxygen Species
SC	Spinal Cord

SOCS	Suppressor of Cytokine Signaling
STAT	Signal Transducer and Activator of Transcription
TGFβ	Transforming Growth Factor beta
T_H	T-Helper
TMEV	Theiler's Murine Encephalomyelitis Virus
TNF	Tumor Necrosis Factor
VCAM-1	Vascular Cell Adhesion Molecule-1
VLA-4	Very Late Antigen-4

TABLE OF CONTENTS

Page

LIST OF FIGURES

Page

LIST OF TABLES

Page

1. INTRODUCTION

1.1 Multiple Sclerosis

1.1.1 Overview of Multiple Sclerosis

Multiple sclerosis (MS) is a debilitating disease characterized by demyelination and neurodegeneration in the CNS, and was first described in detail by Charcot in 1868 [1]. Its prevalence is 0.09% of human population worldwide [2], has unknown etiology and likely involves with genetics and environmental factors. Its occurrence is higher in the further away from the equator, and as determined by migration studies, is not accounted for solely by population genetics [3]. Its prevalence is also correlated with the socioeconomic level of the country, and is hypothesized to relate to the delayed exposure of infections during childhood, known as the hygiene hypothesis [4]. It occurs in more females than males with the ratio being roughly 2:1, suggesting hormones as one of the risk factors [2]. The first onset of MS is usually between age 20-40 [5]. Patients experience a wide array of symptoms including vision problems, numbness, vertigo, ataxia, and more. Most patients initially undergo a relapse-remitting stage (RRMS), in which neurological symptoms occur and last a few days before remission. Later in life, most patients undergo a secondary progressive stage (SPMS), in which the symptoms and lesions grow progressively worse and become irresponsive to treatments [4, 6]. There is also a primary progressive form of MS (PPMS) that occurs in roughly 10% - 15% of the patients [7], in which the patients do not undergo the relapse-remitting stage, but instead directly enter the progressive stage and exhibit continuously worsening

symptoms. During RRMS, T2-hyperintense lesions commonly occur in the periventricular white matter regions, indicating a wide variety of pathologies such as inflammation, demyelination, and axonal loss, whereas T1-hypointense lesions are common in the supratentorial brain regions and indicate brain atrophy [8]. MS lesions in the CNS are multifocal and heterogeneous in nature and can be characterized into several groups based on distribution of immune cells and other criteria [9]. Specifically, the lesions are characterized into groups that feature autoimmune encephalomyelitis and groups that feature oligodendrocyte dystrophy [9], suggesting the possible involvement of multiple different mechanisms.

1.1.2 Genetic Risks of MS

The cause of MS is not completely clear. The fact that MS is heterogeneous in both its symptoms and pathologies suggest it may involve multiple different mechanisms. MS is widely known to have a genetic component, as it has a modest familial risk [10]. The concordance rate of MS in female homozygotic twins has been determined to be around 25% [11], strongly suggesting that MS has genetic association to some degree but non-genetic factors are also involved. Genome-wide association studies have shown that MS susceptibility is linked to many different genes on multiple different chromosomes, and many are related to immune functions, such as TNFα, IFNγ, IL-2R, IL-7R, IL-10, CCR2, CCR5, ICAM-1, CTLA-4, and STAT3 [4, 12]. Alleles in the HLA complex confers the biggest genetic risk factor [13]. HLA alleles associated with MS susceptibility may have binding properties with better affinity to self-myelin antigen. When transgenic mice co-express certain HLA alleles associated with MS and

myelin basic protein (MBP)-specific T-cell receptor (TCR) derived from MS patients, the mice develop spontaneous experimental autoimmune encephalomyelitis (EAE) [14, 15]. These studies provide strong evidence that MS is related to genetics that influence the immune functions.

1.1.3 MS and Autoimmunity

According to Witebsky's postulate and Rose and Bona's revision of the criteria for autoimmune-mediated diseases, the transfer of autoantibodies or autoimmune T-cells to another healthy host must be sufficient to reproduce the disease [16, 17]. However, due to ethical concerns, it would be difficult to provide direct proof that MS is an autoimmune-mediated disease. While this is the case, many studies provide indirect evidence that MS has an autoimmune component. For example, autoimmune T-cells can be found in the cerebrospinal fluid (CSF) of the MS patients [18]. Infiltrating myeloid cells and lymphocytes were found to be associated with lesion areas [19]. HLA alleles, responsible for interaction with the antigens and lymphocytes, represent the strongest genetic risk [13]. Immunosuppressive therapies such as glatiramer acetate and mitoxantrone help relieving the symptoms during relapse [20] [21]. In addition, natalizumab, which blocks α4β1 integrin and T-cell infiltration, as well as fingolimod, which prevents lymphocytes from leaving the secondary lymphoid organs, are both effective treatments [22, 23]. Given the number of studies and the common use of immunosuppressive therapies, today MS is widely acknowledged to be an autoimmune disease.

1.1.4 Environmental Factors of MS

Although many genes have been identified to be related to MS susceptibility, the concordance rate in homozygotic twins is only 25%, meaning that the onset of MS cannot be explained solely by genetics. Moreover, the latitude difference in MS prevalence cannot be explained by population genetics, as migration to a region of higher or lower prevalence before the age of 15-16 years old grants the associated higher or lower risk in that region [24]. These studies suggest that there are likely environmental triggers associated with MS onset. As reviewed by Sospedra and Martin [4], a number of viruses exists that cause demyelinating diseases in human as well as other animals. It is possible that through the mechanisms of molecular mimicry and bystander activation, viral infection could lead to breakage of immune tolerance and cause autoimmunity. While the theory seems plausible and several viral candidates exist, thus far no single virus has been identified to cause MS.

1.1.5 Animal Models of MS

Due to the complex nature of MS, different animal models are used to help understand different aspects of MS. For example, toxin-induced models such as cuprizone and lysolecithin help to understand the process of demyelination, injury responses, and remyelination [25, 26]; Virus-based models such as Theiler's murine encephalomyelitis virus (TMEV) aim to understand possible environmental cause by viral infection and is clinically relevant to primary progressive MS [27]; Autoimmune-driven models such as EAE excels at studying the autoimmune aspect of the disease. EAE was originally developed to study acute disseminated encephalomyelitis (ADEM)

[28]. Since then, EAE has gradually become the most widely used model for MS and has led to successful immunosuppressive/immunomodulatory therapies such as glatiramer acetate, natalizumab, and fingolimod. Although MS likely has a different etiology than EAE, EAE is still a very valuable tool in terms of studying the process of $CD4^+$ T-cell mediated autoimmunity and cell trafficking, which are the major aims of this study.

1.2 Experimental Autoimmune Encephalomyelitis

1.2.1 The Origin of Experimental Autoimmune Encephalomyelitis

Experimental autoimmune encephalomyelitis (EAE), the most widely used and accepted animal model of MS, was first described by Rivers and others [28, 29] in attempt to experimentally produce acute disseminated encephalomyelitis (ADEM). ADEM occurs in the recovery stage after certain viral diseases, e.g., smallpox and measles, as well as after rabies vaccination [30]. Patients typically exhibit limb paresis and fast recovery, but more severe cases can cause mortality [30]. Its pathology is characterized by demyelination and perivascular infiltration [30]. Because ADEM only occurs in rare cases, Rivers and others attempted repeated injections of rabies vaccine component in monkeys. Surprisingly, in monkeys receiving uninfected rabbit brain as a control, ADEM-like symptoms occurred with perivascular infiltration and demyelination. Although the authors did not know whether the experimental disease they created was really ADEM itself (as would occurred after rabies vaccination), their studies indicate that a specific immune response in the CNS, autoimmune or allergic, may be elicited using exogenous CNS tissue.

Because Rivers and others' work required many injections to achieve a decent disease onset rate, other studies started using the complete Freund's adjuvant (CFA), which contains killed *Mycobacterium tuberculosis* in an oil-based emulsion, along with the brain emulsions [31, 32]. The use of CFA made the induction much more reliable. The monkeys developed relapsing-remitting symptoms with leukocyte infiltration into the perivascular space. Soon after, EAE with brain homogenates were produced in other animals including mice, which was first described by Olitsky and Yager [33] and used homologous brain tissue and CFA.

Because demyelination is a common feature in EAE, hypotheses arose that autoimmunity to the myelin component is what causes the disease. Laatsch, Kies [34] isolated myelin and found that it possesses greater disease-causing capability than whole brain homogenate. Since then, myelin basic protein (MBP) and subsequently other myelin proteins such as proteolipid protein (PLP) and myelin oligodendrocyte glycoprotein (MOG) and their derived epitopes were discovered and used to generate EAE in different mouse strains. For example, whole MBP, whole PLP, and several of their peptides containing encephalitogenic epitopes can be used in SJL mice to cause relapsing-remitting EAE, whereas MOG_{35-55} can be used in C57BL/6 mice to cause monophasic chronic EAE [35].

1.2.2 Disease Mechanisms of EAE

Since CFA contains ligands for Toll-like receptors and elicit a strong immune response [36], myelin antigen emulsified in CFA become phagocytosed by the activated professional antigen presenting cells (APCs), processed and presented on MHC Class II

molecules in the draining lymph nodes [37]. Through the interaction of antigen presentation, co-stimulation, and cytokine crosstalk, naïve helper T-cells proliferate and differentiate into effector T-cells (Figure 1). Co-stimulation involves recognition of CD80/CD86 on APCs to CD28 on T cells as well as CD40 to CD154 [38]. The cytokine interleukin (IL)-12 from APCs drives T cells towards T_H1 subset, whereas a combination of IL-6 and transforming growth factor β (TGFβ) drives towards T_H17 subset [39]. In other words, an adaptive immune response is induced artificially, much like the process of vaccination.

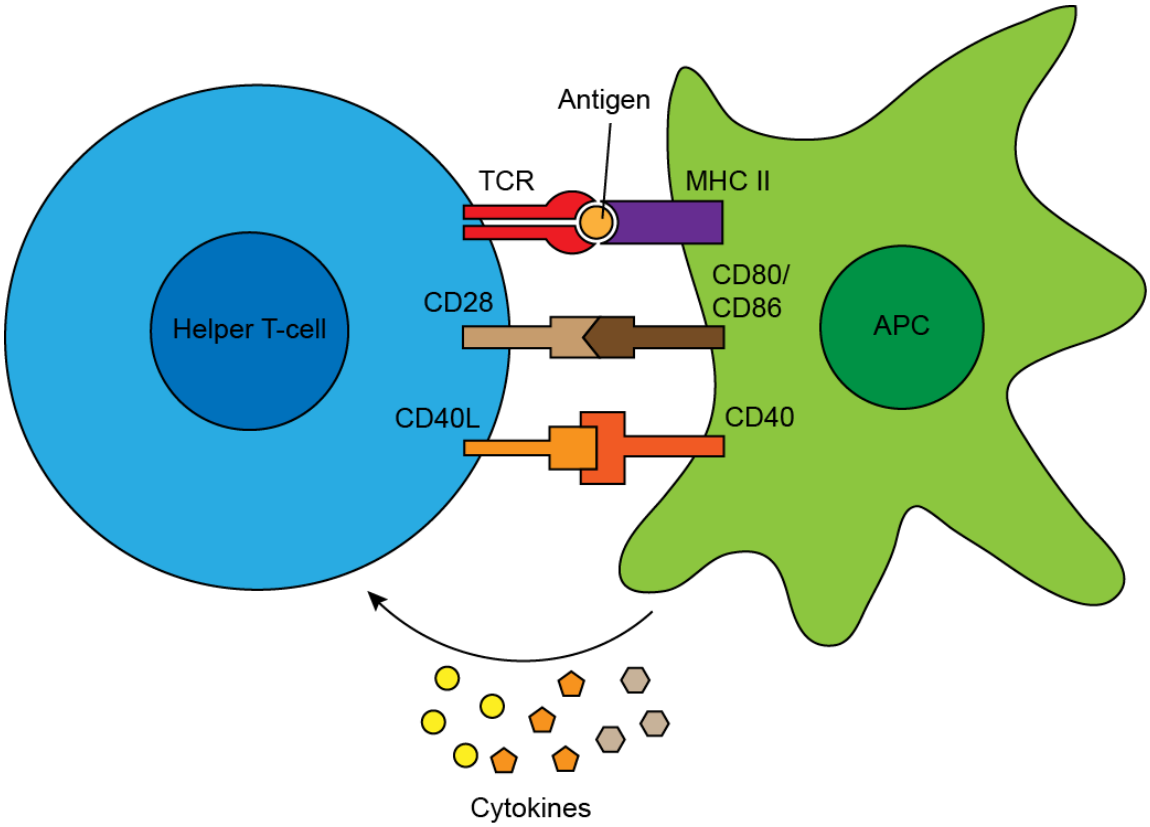

Figure 1. Antigen-specific interaction between APCs and helper T-cells.

Activated T cells travel to the CNS, where they meet their target antigen. In regards to the access of T cells to the CNS, it is generally believed that the pertussis toxin (PT) used in MOG-induced EAE in C57BL/6 mice as well as MBP-induced EAE in SJL mice is required at the time of induction because it opens the blood brain barrier (BBB) to allow leukocytes to pass through and cause damage [40]. However, this does not explain why PLP-induced EAE in SJL mice does not require PT, despite that these EAE models essentially work in the same principles. Moreover, since PT is administered at the time of induction and 48 hours later, by the time the effector T cells are in the circulation, which takes roughly a week, the transient effect of PT on BBB should have diminished already [40]. Thus, it is conceivable that the role of PT in EAE induction may not be about BBB permeability. PT is an exotoxin derived from the bacterium *Bordetella pertussis*, and is involved in inhibiting macrophage and neutrophil recruitment by altering chemokine secretion during whooping cough [41]. It is also a G protein couple receptor antagonist and has other different actions [42]. Furthermore, it was reported that PT-induced production of IL-1β is required for the clonal expansion of helper T-cells [43]. Therefore, PT is likely to exert its effect on cytokine signaling during EAE induction.

Although the exact mechanism about how the autoreactive T cells gain entry to the healthy CNS (as the case in EAE) is not completely understood, evidence points towards APC and T-cell interaction in the leptomeninges. Kivisakk, Mahad [44] found that memory T-cells regularly enter the cerebrospinal fluid (CSF) in the subarachnoid space through choroid plexus via P-selectin/ligand and ICAM-1/LFA-1 interaction for

purpose of immune surveillance. Later the same group [45] isolated macrophages and dendritic cells from meninges in animals before EAE onset, co-cultured with naïve 2D2 T cells in the presence of MOG, and found that the T cells did proliferate. With BrdU injected prior to disease onset, they found T cells were proliferating in the meninges in pre-clinical animals. Using time-lapsed microscopy on isolated meninges stained with cell markers, the authors found close interactions between APCs and T cells. Their findings suggest a possible mechanism by which EAE develops: Autoimmune T cells polarized in the peripheral immune organs move to the CSF for daily surveillance, where they meet local macrophages and dendritic cells which are presenting antigens drained and collected from the interstitial fluid in the CNS. The interaction of MOG presented on MHC II and MOG-specific T-cells triggers T-cell reactivation and thereby causing meningitis. The local inflammation caused tissue damage and activated adjacent macrophages and microglia, which then secreted proinflammatory cytokines and chemokines and MMPs, causing disruption of BBB and infiltration of leukocytes into the CNS parenchyma. Consistent with this hypothesis, it was demonstrated in a rat EAE model that effector T-cells can move along the CSF, encounter the interaction with APCs in the leptomeninges, and gain access to the parenchyma [46]. In addition, lymphatic vessels that run along the dural sinuses in the CNS has been recently discovered [47]. These lymphatic vessels are connected to the cervical lymph nodes and can carry immune cells to the CSF, where the cells conduct immune surveillance.

EAE is mediated by $CD4^+$ T-cells, as evidenced not only by the fact that T_H1 and T_H17 subsets are necessary for the disease's development [48, 49], but also that adoptive

transfer of differentiated MOG-specific T cells is sufficient to trigger EAE [50]. Both T_H1 [49] and T_H17 subsets [48] were shown to be important in the pathogenesis. Through proinflammatory cytokine crosstalk with microglia and recruited macrophages/monocytes, the immune response causes damage to the myelin and other structures in the CNS.

1.2.3 Strengths and Pitfalls of EAE

Studies in EAE have proven to have tremendous benefits in our understanding of demyelination. EAE is not only a good model for ADEM, but also a good model for studying autoimmunity. It has led to the discovery of T_H17 subset of helper T-cells [48]. It has enabled studies in the contribution of various immune cell types, numerous cytokines, and other molecules in autoimmunity. It has helped the understanding of genetic susceptibility in autoimmunity. It has led to many studies on cell trafficking into the CNS, from the role of matrix metalloproteinases [51, 52] to T-cell immune surveillance in the CSF [44, 45], and has advanced our understanding of the BBB and the so-called CNS immune privilege. On the practical side, EAE has allowed the development of several successful immunosuppressive/immunomodulatory therapies, *e.g.*, glatiramer acetate (GA), natalizumab, and fingolimod. GA was originally developed as a random copolymer of 4 amino acids to mimic MBP [20]. It was shown to suppress EAE, has immunomodulatory properties such as inducing M2 and T_H2 phenotypes, and was proven useful in reducing relapses in MS [20]. Natalizumab, the VLA-4 antibody, was developed utilizing the knowledge of molecular signatures that T-cells use to adhere to endothelial cells and transmigrate into target tissue. It was tested

and shown effective in suppressing EAE, and later on proven useful in treating MS [53]. Although the unfortunate side effect of developing progressive multifocal leukoencephalopathy (PML) in some patients, a fatal disease caused by JC virus, led to its temporary withdrawal [53], the benefits it provided eventually lead to its return to the market. From this lesson, we also learned about the potential consequences of attempting to shut down the immune system. Fingolimod, a first-in-class oral drug that utilizes the inhibition of T-cell trafficking, downregulates sphingosine-1-phosphate receptor 1 (S1PR1) and prevented T-cells from exiting the secondary lymphoid organs, was shown to suppress EAE and proven to help in RRMS [54].

Although studies using EAE have greatly advanced our knowledge in autoimmunity, the main criticism about EAE as an MS model is its limited value in understanding MS etiology. EAE pathogenesis shares similarities with MS, namely the perivascular cell infiltration, autoimmune inflammation, demyelination, gliosis, and the sparing of neuronal cell bodies [55]. The knowledge of pathogenesis has led to successful treatments. However, the knowledge of causation is required for an effective cure. While EAE is purely autoimmune-mediated and can be abolished by blocking essential immune pathways [48, 49], it remains to be proven that MS is also purely autoimmune-mediated for reasons aforementioned. MS is partially genetic and likely occurs in predisposed individuals under certain environmental conditions. Several viruses, *e.g.,* human herpesvirus 6 and Epstein-Barr virus, were shown to be potential candidates as infectious agents [4]. If MS is indeed caused by infectious agents that lead to autoimmunity via molecular mimicry and/or bystander activation, then therapies

developed from EAE will not be helpful to prevent MS progression in the long term. Although EAE shares features with MS, they also have clear differences. For example, inflammation in EAE is primarily driven by $CD4^+$ T-cells, whereas $CD8^+$ T-cells are found in greater numbers is MS lesions [56]. Focusing on EAE can thus lead to negligence in the contribution of certain cell types that are important in MS. Due to the fundamental differences between EAE and MS, it is not surprising that most promising treatments tested in EAE fail in treating MS [57]. Because of these shortcomings, researchers should bear in mind the applicability when conducting research in EAE. EAE is still a useful model for understanding mechanisms of autoimmunity and cell trafficking, which are the main focuses of this study. In relating EAE studies to MS, one should always evaluate the relevance of the molecule or gene of interest to MS, and consider also using other models, such as TMEV, that can recapitulate different aspects of MS.

1.3 Myeloid Cells

1.3.1 Myeloid Lineage Cells of the Immune System

Hematopoiesis occurs at different sites during different developmental states, starting from the yolk sac as early as E7.5 in mice, to the aorta-gonad mesonephros region, fetal liver, and eventually the bone marrow after birth [58]. Hematopoiesis at different stages features production of different cell lineages. For example, during primitive hematopoiesis, which occurs from E7.5 in mice, the erythro-myeloid progenitors (EMPs) in the yolk sac give rise to tissue-resident macrophages including

the Kupffer cells in the liver [59], Langerhans cells in the epidermis [59, 60], alveolar macrophages in the lung [61, 62], intestinal macrophages [63], and microglia in the CNS [64-67]. In addition, the EMPs from the yolk sac also contributes to development of fetal red blood cells, monocytes, and granulocytes [59]. During definitive hematopoiesis, hematopoietic stem cells (HSCs) in the bone marrow first differentiate into more committed progenitors for the myeloid lineage and the lymphoid lineage according to the classical model [68]. The lymphoid lineage gives rise to B-cells, T-cells, and natural killer cells. The myeloid lineage gives rise to erythrocytes, megakaryocytes, granulocytes, monocytes, and dendritic cells. Interestingly, the HSC-derived cells replace the fetal erythrocytes, granulocytes, monocytes, and intestinal macrophages [63], but not certain populations such as the Kupffer cells, Langerhans cells, and microglia [59]. These populations primarily maintain their yolk sac origin. The granulocytes, monocytes, macrophages, and dendritic cells are often grouped together and collectively referred to as the myeloid cells.

As reviewed by Kawamoto and Minato [69] and Zhu, Yamane [39], myeloid cells in the immune system are essential for the host's innate immune functions. Myeloid cells respond to chemoattractants and can gather at the injury or infection sites. Myeloid cells express an array of pathogen recognition receptors (PRRs) such as Toll-like receptors that recognize pathogen associated molecular patterns (PAMPs) and initiate innate immune responses. For example, Toll-like receptor 4 recognizes lipopolysaccharide (LPS), a component in the cell wall of gram-negative bacteria, and triggers the macrophages to develop a proinflammatory phenotype, called the M1

phenotype. M1 macrophages secrete molecules such as tumor necrosis factor α (TNFα) and nitric oxide (NO) to combat the pathogens. Professional phagocytes such as macrophages and neutrophils also destroy the pathogens by phagocytosing them and fusing the phagosomes with lysosomes, thereby breaking them down. While myeloid cells have various receptors for phagocytosis, their phagocytic activity can be enhanced by the complement system and immunoglobulin receptors. Macrophages and dendritic cells then process the broken-down pathogens and present their antigens on the MHC Class II molecules on the cell surface that can be recognized by the helper T-cells. Myeloid cells also produce various cytokines to instruct the type of T-cell differentiation. The interaction between the antigens presented on MHC Class II by the dendritic cells and the T-cell receptor on T-cells, along with two other signals known as co-stimulation and cytokine expression, induce activation and differentiation of T-cells and development of adaptive immune response, which then in turn enhance the functions of the innate immune system.

1.3.2 Roles of Myeloid Cells in MS and EAE

Accumulation of dendritic cells and macrophages as well as microglial activation have been observed in MS lesions [70-72], suggesting the involvement of myeloid cells in MS pathology. Although the specific role of myeloid cells in MS is still unclear, HLA Class II molecules are not only the strongest genetic factor [4], analysis in MS patient peripheral blood mononuclear cells (PBMCs) also showed increased HLA Class II expression [73]. Therefore, myeloid cells may be involved in MS through their role in antigen presentation, presumably causing autoimmunity. Consistent with these findings,

APCs from cervical lymph nodes of MS patients have been found presenting brain derived antigens [74]. In addition to antigen presentation, proinflammatory cytokines such as TNFα were found to be up-regulated in MS patient PBMCs [73], and nitric oxide synthase (NOS) was found in MS lesion areas [75]. Therefore, myeloid cells likely cause damage in MS through their innate immune functions.

While the importance of myeloid cells in MS is difficult to prove, they have been shown to be essential in development of EAE. Indeed, depleting macrophages with either HSV-TK or clodronate liposome abolishes EAE [76, 77]. Since EAE is mediated by $CD4^+$ helper T-cells, myeloid cells are necessary for EAE due to their role to differentiate $CD4^+$ T-cells into T_H1 and T_H17 subsets and subsequently re-activate them. Consistent with this, dendritic cells were shown to require the expression of MHC Class II molecules for developing adoptive transfer EAE in mice [78]. Furthermore, two-photon microscopy revealed direct interactions between T-cells and antigen presenting cells at leptomeninges during EAE [79]. Similar observations have been made using time-lapsed microscopy on isolated meninges from EAE mice [45]. Macrophages are also important in their function to break down the extracellular matrix in order to gain entry to the CNS, as double knockout of matrix metalloproteinase (MMP)-2 and MMP-9 suppresses EAE symptoms [52]. These studies indicate that myeloid cells play an indispensable role in EAE.

1.3.3 Myeloid Cells and Leukocyte Trafficking into the CNS

During an inflammation, myeloid cells in the immune system secrete chemokines such as CCL2, CCL3, and CCL5 to attract leukocytes by chemical gradient. Myeloid

cells also stimulate the endothelial cells of the blood vessel to express ICAM-1 and VCAM-1, which are recognized by their respective ligands, LFA-1 and VLA-4, expressed by T-cells, and cause the T-cells in the bloodstream to halt and pass through the endothelial cell layer into the inflammatory site [80].

The transmigration of immune cells into the CNS parenchyma during a CNS injury or infection is complicated by the fact that access to CNS involves passing the blood-brain barrier (BBB) [52]. Across the cerebrovascular endothelial cell (CVEC) layer, there is a basal membrane and associated with it is the glial limitan. This basal membrane contains various extracellular matrix (ECM) proteins such as laminin and fibronectin. The glial limitan consists of astrocyte end feet anchored to the basal membrane, as well as pericytes. The space between the CVEC layer and the glial limitan is called perivascular space. Depleting monocytes/macrophages with clodronate liposome causes T cells to accumulate in the perivascular space, but not into the CNS parenchyma during EAE, thus preventing disease progression [76]. This suggests that myeloid cells have a role in assisting T cells to transmigrate through the parenchymal basal membrane.

Toft-Hansen *et al.* [81] found that leukocytes spontaneously accumulate in the perivascular space of CCL2 overexpressing mice, and treatment with pertussis toxin (PT) causes the cells to infiltrate into the parenchyma. The authors also found that using a broad-spectrum matrix metalloproteinase (MMP) inhibitor prevents this infiltration. Using an *in vitro* model, Abraham *et al.* [82] showed that T cell migration through Matrigel-coated transwell inserts induced by chemokines CCL5 and CXCL10 was

inhibited by MMP inhibitors. These results suggest a dependence of MMPs to break down the ECM to allow efficient leukocyte infiltration.

As reviewed in Yong *et al.* [83], MMP-2, 7, 9, and 12 are elevated in MS and are correlated with increased gadolinium enhancement in MRI scans, which is an indication of disruption in BBB integrity. Toft-Hansen *et al.* [51] examined all members of the metalloproteinase family and found an increase of MMP-2, 8, 9, 10, 12, as well as TIMP-1 during EAE, with macrophages being the major source and only a few exceptions, making the study of MMPs in EAE highly relevant to MS. Agrawal *et al.* [52] found that MMP-2 and MMP-9 targets β-dystroglycan, which anchors astrocyte endfeet to the parenchymal basal membrane through high affinity binding to laminin. These authors also found that double knockout of MMP-2 and MMP-9 inhibits EAE. As the major cellular source of MMP-2 and MMP-9, macrophages thus contribute to the breakdown of glial limitan during EAE, allowing leukocytes to infiltrate into the CNS parenchyma. While these findings indicate the importance of myeloid MMPs in EAE, it is to be noted that as Yong, Zabad [83] pointed out, single MMP deficiency does not necessarily confer resistance to EAE. MMP-9 KO mice are less susceptible to EAE only in younger age (3-4w). MMP-2 KO and MMP-12 KO in fact caused more severe EAE due to compensatory increases in other MMPs. Therefore, studying and interpretation of MMPs' role in EAE have to proceed with caution.

While some studies suggest that leukocytes can accumulate in the perivascular cuff but myeloid cells are required to break through the blood brain barrier basal membrane, Agrawal *et al.* [52] reported that they did not observe accumulation of

leukocytes in the perivascular cuff in their MMP-2 and MMP-9 double knockout mice. Thus, it is possible that myeloid cells are not only needed for breaking through the parenchymal basal membrane, but also for transmigrating across the cerebrovascular endothelial layer as well. In support of this, Kivisakk and others [44] discovered that memory T-cells carry out immune surveillance at the subarachnoid space. The interaction between antigen presenting cells and T-cells at the leptomeninges has been observed [45, 79]. Moreover, the CNS lymphatic system has recently been discovered [47]. Together with the common observation that EAE pathology begins at the meninges, these suggest a possible mechanism by which EAE develops: Autoimmune T-cells polarized in the peripheral immune organs move to the CSF for daily surveillance, where they meet local macrophages and dendritic cells that are presenting antigens drained and collected from the interstitial fluid in CNS. The interaction of MOG presented on MHC II and MOG specific T-cells triggers T-cell reactivation and thus causing meningitis. The local inflammation caused tissue damage and activated adjacent macrophages and microglia, which then secreted proinflammatory cytokines and chemokines and MMPs, causing disruption of BBB and infiltration of leukocytes into the CNS parenchyma. Therefore, myeloid cells are important in assisting leukocyte transmigration due to their role in presenting antigens at the leptomeninges for immune surveillance as well as the secretion of proteases such as MMPs to break down the blood brain barrier.

1.4 Signal Transducer and Activator of Transcription (STAT)-3

1.4.1 Overview of STAT3

STAT3 is a 89 kDa protein of the STATs family, which contains 7 proteins, STAT1, STAT2, STAT3, STAT4, STAT5A, STAT5B, and STAT6, and are involved in transducing cytokines and growth factors and control of gene expression. STAT3 exists in two forms: full-length and abundantly expressed STAT3α, and a truncated STAT3β formed by alternative splicing. STAT3α contains an N-terminal domain, a coiled coil domain, a DNA binding domain, a linker domain, an SH2 domain, and a transactivation domain. STAT3β lacks the transactivation domain and can competitively inhibit the transcriptional factor functions of STAT3α [84], but has also been shown to have its own functions [85].

As illustrated in Figure 2, Certain receptors of cytokines or growth factors, e.g., the IL-6 receptor family, form dimer or oligomer complex upon ligand binding, and recruit and phosphorylate Janus kinases (JAKs). The resulted complex provides docking site for the SH2 domain on STAT3 and can phosphorylate STAT3 at its tyrosine 705 residue near the C-terminus [86]. STAT3 phosphorylated at tyrosine 705 (pSTAT3-Y705) forms homodimers via the SH2 domains, and are translocated into the nucleus with the help of members of the importin protein family [87]. STAT3 then forms complex with other transcriptional factors and coactivators or repressors to regulate gene expression. While tyrosine phosphorylation enables the transcriptional functions of STAT3, STAT3 is also phosphorylated at serine 727 by JNK and p38 MAPK, resulting in enhanced and sustained transcriptional functions [88]. In addition, serine

phosphorylation in STAT3 can aid in respiratory functions in mitochondria, as STAT3 deficiency reduces the activities in the electron transport chain [89]. Other than the tyrosine and serine phosphorylation, unphosphorylated STAT3 has also been shown to function independently of the phosphorylated dimers. For example, unphosphorylated STAT3 interacts with NF-κB and drives transcription of genes such as CCL5 [90]. STAT3 signaling is negatively regulated by suppressor of cytokine signaling (SOCS)-3, which can be induced by IL-6 signaling as a negative feedback. SOCS3 acts by ubiquitination of phospho-JAKs and phospho-STATs or by binding to specific cytokine receptor and JAK complexes [91]. Although SOCS3 can inhibit multiple JAKs, *e.g.*, JAK1, JAK2, and TYK2, and multiple STATs, *e.g.*, STAT1, STAT3, and STAT4 [91], its inhibiting activity is limited to specific receptor and JAK complexes rather than individual molecules. For example, SOCS3 can inhibit IL-6 induced STAT3 signaling by binding to gp130 and JAK2 [91], but not IL-10 induced STAT3 signaling, which is via IL-10 receptor complex and JAK1 [92].

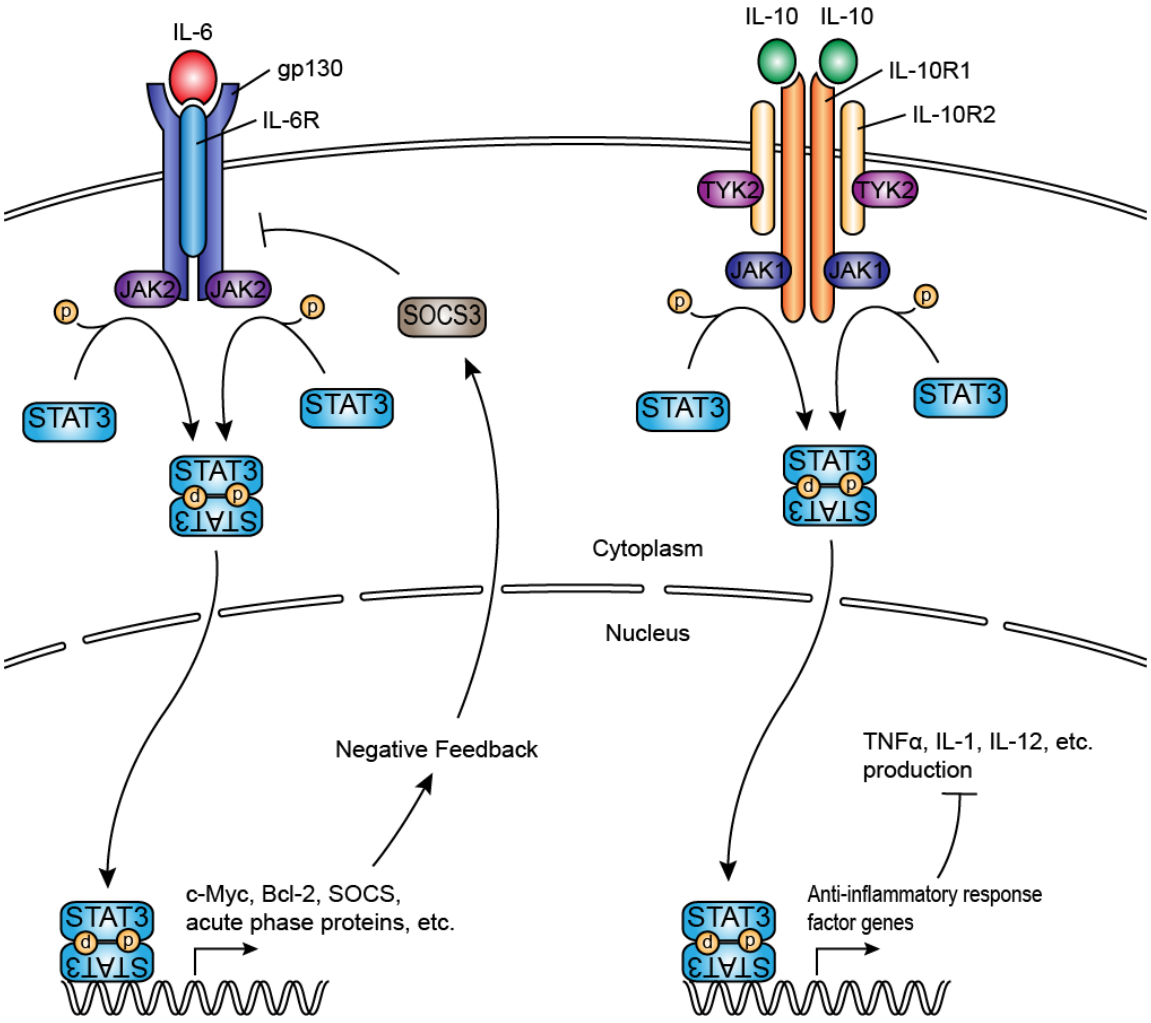

Figure 2. STAT3 signaling.

Generally, STAT3 functions in regulating genes that are involved in cell cycle and cell survival. STAT3 is essential for transducing leukemia inhibitory factor (LIF)-induced embryonic stem cell self-renewal, as it targets transcription factors such as Klf4 and Klf5 and many others that, knockdown of which leads to reduced self-renewal [93]. Using a fusion protein consisting of STAT3 and the estrogen receptor that can be activated by 4-hydroxytamoxifen, it was shown that STAT3 signal can maintain

embryonic stem cell self-renewal in the absence of LIF [94]. Because STAT3 is important in the maintenance of embryonic stem cells, its universal knockout leads to embryonic death in mice at E6.5 – 7.5 [95]. STAT3 transduces the signal from IL-6 and gp130 receptor and activates the transcription of c-Myc gene, a gene that promotes cell cycle [96]. In the CNS, STAT3 has been shown to be activated during IL-15-induced proliferation of neural stem cells in the subventricular zone [97]. STAT3 has also been shown to be involved in ciliary neurotrophic factor (CNTF)-induced as well as IL-6- and LIF-induced astrogliogenesis [98, 99]. STAT3 inhibits apoptosis by activating Bcl-2 transcription, thereby mediating IL-6-induced maintenance of human HSC self-renewal [100]. Blocking of STAT3 reduced expression of Bcl-xL, another anti-apoptotic gene, in a human cancer cell line and induced apoptosis, suggesting the importance of STAT3 in inhibition of apoptosis [101]. In addition, IL-6 induces miR-21 expression and contributes to anti-apoptotic functions in myeloma cells, and this pathway is STAT3-dependent [102]. In the CNS, STAT3 has been shown to signal anti-apoptotic functions of IL-9 in neonatal cortical neurons by down regulation of Bax [103]. Because STAT3 is involved in cell survival and is constitutively activated in cancer cells, many cancer studies have focused on STAT3 as a therapeutic target. This also includes glioma, in which STAT3 is aberrantly activated [104].

In addition to regulation of gene expression involved in cell cycle, studies have found that STAT3 also has many other functions particularly in the CNS. For example, leptin regulates energy balance and is mediated through STAT3 signaling in the hypothalamus [105]. Disrupting STAT3 in neurons thus causes obesity and diabetes

[106]. In the oligodendrocytes, STAT3 has been shown to promote oligodendrocyte survival and differentiation and is required for efficient remyelination after lysolecithin injection [107]. STAT3 is also shown to be involved in synaptic plasticity. Inhibiting STAT3 with AG490 impairs spatial memory, suggesting its role in synaptic plasticity and implications in pathogenesis of Alzheimer's disease [108]. NMDA receptor-dependent long term depression was shown to be blocked by AG490 [109].

1.4.2 STAT3 and Neutrophils

Neutrophils are the first responders during an infection or inflammation. Neutrophil infiltration has been observed during the onset phase of EAE, correlating to demyelination at the lesion sites [110]. Granulocyte-colony stimulating factor (G-CSF) signals through STAT3 and is a key cytokine in neutrophil maturation and migration. G-CSFR mutation causes severe neutropenia and accumulation of immature myeloid progenitors, but expression of a constitutively active STAT3 rescues the phenotype [111], suggesting an important role of STAT3 in neutrophil functions. However, conditional deletion of STAT3 in hematopoietic progenitors using *Mx-Cre/Stat3*$^{fl/fl}$ resulted in higher number of neutrophils, which exhibited normal respiratory burst, phagocytosis, and bacteria killing capabilities [112], similar to the neutrophilia observed in hematopoietic lineage specific SOCS3 deficient mice [113]. Interestingly, mice deficient of SOCS3 in myeloid cells develop an atypical and non-resolving form of EAE characterized by enhanced recruitment of neutrophils into the cerebellum [114]. It is possible that the conditional deletion of STAT3, causing a prolonged and enhanced proinflammatory response in the absence of IL-10 signaling, compensates for the

impaired G-CSF signaling in neutrophil functions. The role of STAT3 in neutrophil functions thus requires further investigation.

1.4.3 STAT3 and CD4$^+$ T-Cells

CD4$^+$ T-cells are part of the adaptive immune system and can secrete various cytokines to help other cells' functions. Naïve CD4$^+$ T-cells can be differentiated into different effector subsets depending on immune context and cytokine crosstalk. For example, IL-12 signals through STAT4 and drives the production of IFNγ, which acts in an autocrine fashion and signals through STAT1, driving the expression of T-bet and T_H1 differentiation [115]. In the case of T_H17, TGFβ signaling first induces the production of RORγt. IL-6 signals through STAT3 to produce IL-21. IL-21 acts in an autocrine fashion and drives IL-23 receptor expression through a STAT3- and RORγt-dependent pathway. The autocrine loop of IL-21 ensures sustained activation of STAT3, and IL-23 is important in the maintenance of T_H17 phenotype. These signals together lead to fully committed IL-17 producing T_H17 cells [116, 117]. Without the signal starting from IL-6, TGFβ-driven transcriptional factor Foxp3 suppresses the activity of RORγt and shifts the differentiation towards regulatory T-cells (Tregs). Since both T_H1 and T_H17 cells are essential in the induction of EAE [48, 49], and STAT3 mediates T_H17 differentiation [116, 117], selective deletion of STAT3 in CD4$^+$ T-cells completely prevents the development of EAE [118], suggesting the pathogenic function of STAT3 in CD4$^+$ T-cells in autoimmune demyelination diseases. However, the importance of STAT in innate immune cells such as myeloid cells in the context of MS and EAE have not been directly investigated and was investigated in this study.

1.4.4 STAT3 in Myeloid Cells and MS

Genome-wide association studies identified *Stat3* as a risk factor in MS [12, 119], suggesting its role in MS disease pathology. Elevated pSTAT3 has been detected in $CD4^+$ T-cells, $CD8^+$ T-cells, and $CD14^+$ monocytes in peripheral blood mononuclear cells (PBMCs) from relapsing MS patients [120]. While the functions of STAT3 in $CD4^+$ T-cells and its importance in EAE have been well documented, its functions in myeloid cells in the context of MS and EAE pathologies are not as clearly understood. $CD14^+$ monocytes in PBMCs from relapsing MS patients showed elevated pSTAT3 compared to remitting patients and healthy individuals [120]. pSTAT3 was found in macrophages and microglia in post-mortem CNS tissue from MS patients [121]. Collectively, these suggest that myeloid STAT3 may also be involved in MS.

STAT3 has a nonredundant role in signaling IL-10 anti-inflammatory response (AIR) in myeloid cells [122]. IL-10 signals through the IL-10 receptor complex, which contains two IL-10R1 and two IL-10R2 chains and are expressed by most leukocytes. The receptor complex signals through JAK1 and STAT3, which participates in AIR by turning on "AIR factor" genes that inhibit the production of proinflammatory mediators. These include but are not exclusive to Bcl3 and Etv3, both of which inhibit NF-κB, Nfil3 to inhibit IL-12 production, and Zfp36 that degrades TNFα mRNA [122]. IL-10 deficiency in mice results in exacerbated EAE [123]. Loss of STAT3 in myeloid cells over time induces chronic enterocolitis [124] due to enhanced proinflammatory responses in the absence of AIR. Therefore, loss of STAT3, causing an enhanced and prolonged immune response, perceivably could be detrimental to autoimmune diseases

such as EAE. On the other hand, STAT3 mediates IL-6 signaling, which is involved in inflammatory events such as acute phase responses [125]. IL-6/STAT3 signaling in dendritic cells also causes proinflammatory responses and drives production of TNFα and several chemokines [126]. The authors also found that whether STAT3 participates in proinflammation or anti-inflammation depends on the length of activation. Because SOCS3 targets the IL-6R complex but not IL-10R complex, IL-6 signaling results in transient activation of STAT3 and proinflammatory responses, and IL-10 signaling results in prolonged activation of STAT3 and AIR. However, it is still unclear which pathway will dominate in the case of conditional deletion or pharmaceutical inhibition. As aforementioned, conditional deletion of SOCS3 in myeloid cells causes exacerbated EAE [127], supporting a hypothesis that inhibiting STAT3 may be beneficial. Interestingly, double knockout of MMP-2 and MMP-9 confers resistance to EAE [52], and both MMP-2 and MMP-9 were shown to be at least in part regulated by STAT3 [128, 129], indicating that myeloid STAT3 may have a role in transmigration and its inhibition may be beneficial in treating autoimmune diseases. In this study, we investigated the role of STAT3 in autoimmunity during EAE by generating mice with targeted ablation of STAT3 in the myeloid cells.

2. DELETION OF STAT3 IN PERIPHERAL MYELOID CELLS RENDERS C57BL/6 MICE LESS SUSCEPTIBLE TO MOG_{35-55}-INDUCED EAE

2.1 Introduction

Multiple sclerosis (MS) is a debilitating disease characterized by demyelination and neurodegeneration in the central nervous system (CNS) [130]. MS lesions in the CNS are multifocal and heterogeneous in nature and can be characterized into several groups based on the distribution of immune cells and other criteria [9]. Specifically, the lesions are characterized into groups that feature autoimmune encephalomyelitis and groups that feature oligodendrocyte dystrophy[9]. The heterogeneity in both its symptoms and pathologies suggest it may involve multiple different mechanisms. Currently, MS is believed to occur in genetically predisposed individuals under specific environmental cues and involves autoimmune mechanisms [4, 131, 132].

Myeloid cells are an indispensable part of the innate immune system. Accumulating dendritic cells and macrophage/microglial activation have been observed in MS lesions [70-72]. The number of infiltrating monocytes/macrophages usually outnumbers T-cells, suggesting the importance of myeloid cells in MS pathology. Moreover, not only certain HLA Class II molecules are the strongest genetic factor in MS [4], analysis in MS PBMCs also showed increased HLA Class II expression during acute relapse [73]. Therefore, myeloid cells are likely involved in MS pathogenesis through their role in antigen presentation. Consistent with these findings, APCs from cervical lymph nodes (LNs) of MS patients have been found to be presenting brain

derived antigens [74]. In addition, pro-inflammatory cytokines such as TNFα was found to be up-regulated in MS patient PBMCs [73], and NOS was found in MS lesion areas [75]. Therefore, myeloid cells may cause damage in MS through their innate immune functions.

Experimental autoimmune encephalomyelitis (EAE) is an autoimmune-driven animal model of MS. Macrophages have been shown to be critical in the development and progression of EAE, as depleting monocytes/macrophages abolishes EAE [76, 77]. Since EAE is mediated by $CD4^+$ helper T-cells [49, 50, 133], myeloid cells are necessary for EAE due to their role in differentiating $CD4^+$ T-cells into T_H1 and T_H17 subsets and subsequently re-activating them. Consistent with this, the expression of MHC Class II molecules on DCs has been shown to be necessary for the development of adoptive transfer EAE in mice [78]. Furthermore, antigen-presenting cells (APCs) were found to directly interact with and activate T-cells during EAE in the leptomeninges and in newly developing CNS lesions [45, 79]. Myeloid cells are also important in their function to break down the extracellular matrix and increase BBB permeability, as double ablation of MMP-2 and MMP-9 suppressed EAE [52].

STAT3 is an 89 kDa protein of the STATs family and transduces signals of many cytokines including LIF, IL-6, G-CSF, IL-2, IL-7, IL-21, IL-10, and more [117]. Genome-wide association studies identified *Stat3* as a risk factor in MS [12, 119], suggesting its role in MS disease pathology. Elevated pSTAT3 has been detected in $CD4^+$ T-cells, $CD8^+$ T-cells, and $CD14^+$ monocytes in PBMCs from relapsing MS patients compared to remitting patients and healthy subjects [120]. pSTAT3 was found

in macrophages and microglia in post-mortem CNS tissue from MS patients [121]. These studies suggest that STAT3 signaling in myeloid cells may be involved in the pathogenesis of MS.

STAT3 has a nonredundant role in signaling IL-10 anti-inflammatory responses (AIR) in monocytes/macrophages [122]. *Il10* deficiency causes exacerbated EAE [123]. Loss of *Stat3* in myeloid cells over time induces chronic enterocolitis [124] due to enhanced proinflammatory responses in the absence of AIR. Therefore, loss of STAT3 could aggravate autoimmune diseases such as EAE. On the other hand, STAT3 mediates IL-6 signaling, which involves inflammatory events such as acute phase responses [125]. Furthermore, conditional deletion of SOCS3 in myeloid cells, an inhibitor of STAT3, causes exacerbated EAE [127], suggesting that inhibiting STAT3 may suppress EAE.

To study the role of myeloid STAT3 signaling in EAE, we generated conditional STAT3 mutant mice by crossbreeding *LysMcre* and $Stat3^{fl/fl}$ mice and subjected them to MOG_{35-55}-induced active EAE. We found that $LysMcre/Stat3^{fl/fl}$ mice are significantly more resistant to actively induced EAE but are susceptible to passive EAE induced by transfer of encephalitogenic T-cells. We also found that loss of STAT3 in myeloid cells decreased the surface expression of antigen presenting and co-stimulatory molecules and impaired antigen-specific activation of $CD4^+$ helper T-cells in *ex vivo* co-cultures. Our study highlights the importance of myeloid STAT3 in autoimmune T-cell generation, and our data suggest that STAT3 may be a potential therapeutic target for autoimmune diseases.

2.2 Materials and Methods

2.2.1 Human Tissue and Sample Preparation

Preparation of CNS tissue from human MS and control subjects was described previously [134]. Briefly, frozen brain tissues from MS patients with clinical diagnosis and confirmed pathologies and from control subjects were obtained from the Rocky Mountain MS Center (Englewood, CO) and the Human Brain and Spinal Fluid Resource Center (Los Angeles, CA). The tissues were divided with one half for homogenization and the other half for immunohistochemistry.

2.2.2 Animals

Stat3$^{fl/fl}$ mice contain two loxP sites that flank exon 22 of Stat3 gene [135] and were a generous gift from Dr. Shizuo Akira (Hyogo College of Medicine, Nishinomiya, Japan). Upon arrival, the *STAT3*$^{fl/fl}$ mice were backcrossed to C57BL/6 mice for 8 generations. *LysMcre* mice express Cre recombinase driven by the Lyz2 promoter and were described previously [136]. *Cx3cr1creER* mice express an enhanced yellow fluorescent protein (EYFP) and a Cre recombinase linked to a mutated estrogen receptor under the control of endogenous *Cx3cr1* promoter [137]. Conditional knockout mice were generated by crossbreeding *Stat3*$^{fl/fl}$ mice to either *LysMcre* or *Cx3cr1creER* mice. B6.129P2-Lyz2$^{tm1(cre)Ifo}$/J mice (*LysMcre*), B6.129P2(Cg)-Cx3cr1$^{tm2.1(cre/ERT2)Litt}$/WganJ mice (*Cx3cr1creER*), B6.SJL-Ptprc^{a} Pepc^{b}/BoyJ mice (C57BL/6 CD45.1), C57BL/6-Tg(Tcra2D2,Tcrb2D2)1Kuch/J mice (2D2), B6;129S6-Gt(ROSA)26Sor$^{tm14(CAG-tdTomato)Hze}$/J mice (*rosa26-Ai14*) were obtained from Jackson Laboratory (Bar Harbor, ME). Mice were under husbandry and bred in the animal facility in Texas A&M

University Comparative Medicine Program. All animal studies were approved by the Institutional Animal Care and Use Committee at Texas A&M University.

2.2.3 Administration of Tamoxifen

Tamoxifen (T5648, Sigma-Aldrich) was administered in either 5-week old *Cx3cr1-creER/Stat3*$^{fl/fl}$ mice. Tamoxifen was first dissolved in corn oil (C8267, Sigma-Aldrich) at 40 mg/ml by incubating while shaking at 37°C for 30 min followed by pulse sonication. Each mouse at age of 5 weeks received 2 doses of 8 mg tamoxifen (in 200 µl corn oil) by oral gavage, 48 hr apart.

2.2.4 Induction of MOG$_{35-55}$-induced Active EAE

MOG-induced EAE was carried out as previously described [138] with modifications. Briefly, 20 ml of Incomplete Freund's adjuvant (263910, Difco, Detroit, MI) was mixed with 100 mg heat killed *Mycobacterium tuberculosis* H37 RA (231141, Difco) and vortexed for 5 min to make complete Freund's adjuvant (CFA). MOG_{35-55} peptide (AS-60130-10, Anaspec Inc., Fremont, CA) was reconstituted in sterile PBS at 2 mg/ml. CFA was emulsified with MOG_{35-55} at a 1:1 volume ratio by short bursts of sonication using Microson Ultrasonic Cell Disrupter XL2000 (Misonix, Farmingdale, NY) and concurrent addition of MOG_{35-55} drop-wise for 20 min, followed by vigorous vortexing for 45 min. Mice were anesthetized with *i.p.* injection of 100 mg/kg body weight ketamine and 10 mg/kg body weight xylazine, and followed by *s.c.* injection of 200 µl MOG_{35-55}-containing CFA, containing 200 µg MOG_{35-55} peptide and 500 µg *M. tuberculosis*) and *i.p.* injection of 400 ng pertussis toxin (#180, List Biological Laboratories, Inc., Campbell, CA) in 100 µl PBS. The second dose of 500 ng pertussis

toxin was administered 48 hrs later. Mice were weighted and clinical symptoms were assessed on a daily basis. Clinical symptoms were scored according to the following criteria: 1, tail paralysis; 2, hind limb paresis; 3, unilateral hind limb paralysis; 4, bilateral hind limb paralysis; 5, moribund or death.

2.2.5 Passive EAE Induction by Adoptive Transfer

Passive induction of EAE was previously described [50] with modifications. Briefly, donor C57BL/6 mice were immunized for MOG_{35-55} using the same procedure as in active EAE induction. Pertussis toxin was not administered. Ten days after immunization, draining LNs were isolated from donor mice and single cell suspension was prepared from draining LNs and cultured at 5.0×10^7 cells in 10 ml complete RPMI 1640 medium (11875-085; Life Technologies), containing 10% FBS, 4 mM L-glutamine, 1 mM sodium pyruvate (P2256; Sigma-Aldrich), 50 μM β-mercaptoethanol (M7154; Sigma-Aldrich), and 100 IU/ml Penicillin and 100 μg/ml Streptomycin (15140; Life Technologies), in 100 mm petri dishes in the presence of 20 μg/ml MOG_{35-55} for 4 days. After 4 days of culture, cells were rinsed off and washed with original RPMI 1640 medium, and resuspended in original RPMI 1640 medium at RT at the density of 1.0 - 2.0×10^7 cells/ml. Cells were aliquoted 5 ml into several 15 ml conical tubes. One volume of Lympholyte M (CL5031; Cedarlane, Burlington, NC) was layered using a Pasteur pipette to the bottom of tubes. The tubes were then centrifuged at 1,000 × *g* at RT for 20 min with the brake set to 0. Cells at the interphase were collected using a Pasteur pipette, washed twice with sterile PBS, centrifuged at 600 × *g* at 4°C for 10 min, and resuspended at the density of 1.5×10^7 cells in 200 μl sterile PBS. Cells ($1.5 – 2.0 \times$

10^7) were injected *r.o.* into recipient mice that were sublethally irradiated by 400 rad a day before cell transfer. 400 ng pertussis toxin was injected *i.p.* on the same day of cell injection and then 48 hrs after. Clinical symptoms were assessed on a daily basis following the same criteria as for active EAE.

2.2.6 Bone Marrow Chimera

Mouse bone marrow was isolated as previously described [139]. Briefly, donor mice (5-8 weeks) were euthanized with isoflurane (5260-04-05, Abbott Laboratories, North Chicago, IL) followed by cervical dislocation. Skin around the hind limbs was removed, and the hind limbs were isolated with scissors without the femur bones damaged. Muscle tissue around the femur and tibia bones was removed. The bone heads were trimmed with scissors to have bone marrow slightly exposed. The bone marrow was ejected from the bone using a 23G needle and a 3 ml syringe loaded with PBS containing 2% FBS and was made into single cell suspension by passing through the needle twice and filtering through a 70 um cell strainer. The red blood cells were lysed with red blood cell lysing buffer (R7757, Sigma-Aldrich, St. Louis, MO) for 5min on ice, and then washed and reconstituted in sterile PBS at the density of 3.33×10^7 cells/ml.

Recipient mice of age 5-6 weeks were constrained in perforated 50 ml conical tubes and subject to 10-Gray X-ray irradiation. Within the same day, the mice were anesthetized with isoflurane and injected 5.0×10^6 bone marrow cells *r.o.* in 150 µl PBS. Animals were housed in autoclaved cages and supplied with irradiated food and drinking water with 1.25% antibiotics (sulfamethoxazole and trimethoprim; 50383, Hi-Tech

Pharmacal Co. Inc., Amityville, NY) for 2 weeks before being switched back to regular housing. At 6 weeks post transplantation, active EAE was induced as described above.

2.2.7 Tissue Collection

The mice at desired age or EAE stage were deeply anesthetized with ketamine and xylazine. Blood was collected by cardiac puncture and mixed 2:1 with 10 usp/ml heparin solution (H3393, Sigma-Aldrich) for preparation of single cell suspension or placed in empty Eppendorf tubes for preparation of serum. The mice were then perfused through the left ventricle with 20 ml of PBS. The spleen and draining lymph nodes (inguinal, axillary, and cervical) were removed and placed in Eppendorf tubes with PBS containing 2% FBS on ice. For histological analysis of the CNS, the brain and spine were removed and fixed in 4% paraformaldehyde (PFA; P6148, Sigma-Aldrich) in PBS overnight at 4°C. For analysis of CNS infiltrating leukocytes, the spinal cord was ejected from the spine with a 10 ml syringe attached to a 20G cannula and filled with ice-cold PBS. For analysis of cytokine mRNA expression in the CNS, the brain and ejected spinal cord were flash frozen with liquid nitrogen and stored at -80°C until use.

2.2.8 Isolation of CNS Infiltrating Leukocytes

Brain and spinal cord from EAE mice were disrupted with scissors and digested in 5 ml of Stempro Accutase (A11105-01; Life Technologies, Carlsbad, CA) for 30 min at 37°C. The enzyme activity of Accutase was then blocked by addition of 2 ml 100% FBS. Tissues were then filtered through a 70 μm cell strainer with the help of a 3 ml syringe plunger to make single cell suspension. Cells were centrifuged and resuspended in 35% Percoll (P4937; Sigma-Aldrich) in PBS. 70% Percoll was slowly added to the

bottom with a Pasteur pipette attached to a rubber bulb. The tubes were then centrifuged at 2,000 × *g* for 20 min at 18°C with the brake set to 0. Cells in the interphase between 35% and 70% Percoll were harvested with a Pasteur pipette, washed and resuspended in complete RPMI 1640 medium (11875-085; Life Technologies), containing 10% FBS, 4 mM L-glutamine, 1 mM sodium pyruvate (P2256; Sigma-Aldrich), 50 μM β-mercaptoethanol (M7154; Sigma-Aldrich), and 100 IU/ml penicillin and 100 μg/ml streptomycin (15140; Life Technologies).

2.2.9 Preparation of Single Cell Suspensions from Spleen, Lymph Nodes, and Blood

Spleen and draining lymph nodes from EAE mice were disrupted with a 3 ml syringe plunger and passed through a 70 μm cell strainer. Splenocytes were centrifuged and resuspended in 3 ml of RBC lysis buffer (R7757, Sigma-Aldrich) and incubated at room temperature for 2 min, then washed in complete RPMI 1640 medium.

200 μl of blood collected from the mice were mixed with 100 μl heparin (10 usp/ml; H3393; Sigma-Aldrich). 1 ml of RBC lysis buffer was added, and the samples were incubated at room temperature for 15 min. Cells were then centrifuged and resuspended in PBS containing 2% FBS. If no clear white pellet was observed after centrifugation, the lysis procedure was repeated once.

2.2.10 Magnetic selection of $CD11b^+$ and $CD4^+$ cells

Single cell suspension of splenocytes prepared from mice was resuspended in BD iMAG buffer (552362, BD Biosciences, San Jose, CA) at the density of 2.0×10^7 cells/ml in a 15 ml conical tube and incubated with 20 μg/ml α-CD11b-biotin (40 μl per ml; 13-0112, eBioscience, San Diego, CA) or 10 μg/ml α-CD4-biotin (20 μl per ml; 13-

0042, eBioscience) for 15 min on ice. The cells were then washed twice and resuspended in iMAG buffer at the density of 4.0×10^7 cells/ml. Streptavidin (557812, BD Biosciences) was added (10 µl per 1.0×10^7 cells) and incubated at 8°C for 30 min. The volume was then brought to 2.0×10^7 cells/ml and the tube was placed onto a cell separation magnet (#552311; BD Biosciences) and incubated at room temperature for 8 min. The negative portion was removed while the tube was still on the magnet, and the positive portion was resuspended in iMAG buffer at 2.0×10^7 cells/ml. The separation was repeated two more times with 4 min incubation at room temperature each time. After the last separation, the positive portion was resuspended in complete RPMI 1640 medium.

2.2.11 Preparation of Cell Cultures

Primary Mixed Glia and Microglia. Neonatal mouse pups of age postnatal day 0-3 (P0-3) were ice anesthetized and then decapitated. Under a dissecting microscope, the brains were isolated, and the meninges were carefully peeled off using two pairs of tweezers. Tissue was disrupted with a razor blade and digested in HBSS containing 0.01% trypsin (T8253, Sigma-Aldrich) and 10 µg/ml DNase (D5025, Sigma-Aldrich) at 37°C for 10 min, and passed through a 70-µm cell strainer to make single cell suspension. Cells were washed, resuspended and cultured in poly-D-lysine (P0899, Sigma-Aldrich) coated plates or flasks with complete DMEM medium containing 10% FBS, 4mM L-glutamine (G8540, Sigma-Aldrich), 1mM sodium pyruvate (P2256, Sigma-Aldrich), 100 IU/ml penicillin and 100 µg/ml streptomycin (15140, Life Technologies), for 10-14 days before experiments were conducted. Media was

replenished every other day. Microglia mono-culture was obtained by shaking the mixed glia flasks (25-cm^2 or 75-cm^2) at 200 rpm for 1 hr and collecting the supernatant as previously described [140].

BMDM. The preparation of BMDMs was previously described [139]. Briefly, L929 cells (ATCC#CCL-1; a generous gift from Dr. Beiyan Zhou) were cultured at the density of 5.0 x 10^5 cells in 15 ml complete DMEM medium per 75-cm^2 culture flask. At div 5, the culture was centrifuged at 400 × *g*, and the conditioned medium were collected and stored in -20°C until use. Bone marrow cells isolated as described above were resuspended in IMDM medium (Hyclone, #SH30228.01) containing 15% L929-conditioned medium and 10% FBS at the density of 1.0 x 10^6 cells/ml. 1.0 x 10^7 cells per 100-mm petri dish were cultured for 7 days. The medium was replenished at div 3. At div 7, the cells were incubated in HBSS containing 5 mM EDTA at 4°C for 40 min, then harvested by flushing with a P1000 Eppendorf pipette. Mature BMDMs were washed and resuspended in IMDM medium containing 10% FBS for experiments. BMDM maturity was analyze with CD11b and F4/80 staining and flow cytometry.

2.2.12 Western Blotting

To determine the functional effect of STAT3 deletion, BMDMs from *Stat3$^{fl/fl}$* and *LysMcre/Stat3$^{fl/fl}$* mice were stimulated with 10 ng/ml rmIL-6 (1830-SR, R&D Systems, Minneapolis, MN) in IMDM medium containing 10% FBS for 30 min at 37°C. Cells were then lysed with ice-cold lysing buffer, which contains 20 mM Tris-HCl, 150 mM NaCl, 1 mM Na_2EDTA, 1 mM EGTA, 1% triton-X100, 10 mM $Na_4P_2O_7$, 10 mM NaF, 1.0% PIC (P8340, Sigma-Aldrich), 100 mM Na_3VO_4, and 100 mM PMSF, and was

sonicated in short bursts for several seconds using a Microson ultrasonic cell disrupter at level 2. Protein in the supernatant was collected after centrifugation at 16,000 × *g* for 15 min at 4°C. Protein level was quantitated using a DC Protein Assay kit (5000116, Bio-Rad, Hercules, CA), and the concentration was equalized by adding ddH_2O. After denaturing and linearizing by boiling and adding 2% SDS and 1% β-mercaptoethanol, proteins were separated in an 8% polyacrylamide gel by SDS-PAGE, and transferred to a PVDF membrane. The membrane was blocked with 5% BSA for 1 hr at room temperature, and probed with α-STAT3 (9132, Cell Signaling Technology Inc., Danvers, MA) and α-pSTAT3(Y705) (9145, Cell Signaling Technology Inc.) antibodies at 4°C for overnight. The membrane was then washed with TBS with 0.1% Tween (P7949, Sigma Aldrich) three times for 5 min each, and incubated with α-rabbit IgG-HRP antibody (115-035-062, Jackson ImmunoResearch, West Grove, PA) for 1 hr at room temperature and was developed with SuperSignal West Pico substrate (34080, Thermo Scientific, Rockford, IL). Images were acquired on a Bio-Rad Chemidoc XRS System (Bio-Rad, Hercules, CA). Densitometric data were obtained using Quantity One software (Bio-Rad, Hercules, CA).

2.2.13 RNA Isolation and Quantitative RT-PCR

For tissue, flash frozen spinal cord from EAE mice were thawed, incubated in 1 ml Tri Reagent (T9424, Sigma Aldrich), homogenized in a tissue homogenizer, and transferred to a 1.5-ml Eppendorf tube. For cell culture, the supernatant was first collected at the end of stimulation. Next, 1 ml Tri Reagent was added into the well, pipette-flushed several times and transferred to a 1.5-ml Eppendorf tube. The sample

tubes were incubated for 5 min at room temperature. 200 µl of chloroform (#4440, Macron Fine Chemicals) was added, and the tubes were vigorously hand-shaken for 15 sec and vortexed for another 15 sec. The tubes were centrifuged at 12,000 × *g* for 15 min at 4°C. 500 µl of liquid in the clear upper phase was collected and added with 500 µl isopropanol. After sitting for 10 min at room temperature, the tubes were centrifuged at 12,000 × *g* for 30 min in 4°C. The supernatant was removed and the pellets were resuspended in 1 ml 75% ethanol, and centrifuged at 7,500 × *g* for 5 min at 4°C. The supernatant was then removed again, and the pellets were dissolved by adding 100 µl nuclease free H_2O (#10336503, Fisher Scientific, Fair Lawn, NJ) and incubating at 56°C for 10 min. The isolated RNA was quantitated using a NanoDrop 1000 Spectrophotometer (Thermo Scientific) and stored at -80°C until use.

500 ng RNA samples were treated with 0.1 UI/µl DNase I (#18068, Invitrogen, Carlsbad, CA) for 15 min at room temperature to remove DNA contamination. 2.5 mM EDTA was added and samples were incubated for 10 min at 56°C to inactivate DNase activity. Samples were then reverse transcribed to cDNA in a reaction mixture of 5 mM magnesium chloride, 0.25 mM dATP, 0.25 mM dTTP, 0.25 mM dCTP, 0.25 mM dGTP, 0.75 U/ml reverse transcriptase (M510F, Promega, Madison, WI), 25 µg/ml random primers (C118A, Promega), and 1 U/ml RNase inhibitor (N251B, Promega), and incubated in the following thermal cycling parameters: 25°C 10 min, 42°C 15 min, 95°C 5 min. DNA contamination was checked by reverse transcribing samples without reverse transcriptase and amplifying β-actin with PCR. 10 ng cDNA was amplified with quantitative PCR in a reaction mixture of 1x SYBR Green PCR Master Mix (#4309155,

applied biosystems, UK) and 1 μM forward and reverse primers in the following thermal cycling parameters: 95°C 10 min, [95°C 15 sec, 60°C 1 min] × 40 cycles. Changes of the expression levels relative to β-actin were calculated using the formula: $2^{(-\Delta\Delta CT)}$. The primer pairs used were listed in Table 1.

Table 1. Primer sets for PCR.

Gene	Forward Primer	Reverse Primer
β-actin	AGACTTCGAGCAGGAGATGG	CAACGTCACACTTCATGATGG
Tnfα	TGTCCCTTTCACTCACTGGC	CATCTTTTGGGGGAGTGCCT
Il1β	CGACAAAATACCTGTGGCCT	CGACAAAATACCTGTGGCCT
Ifnγ	AAGACTGTGATTGCGGGGTT	GCACCAGGTGTCAAGTCTCT
Trem	GGCTGAGGTCCTGCAGAAAG	GCACCCTCGAAACTCGATGA
Cd206	AAGGCATGCGTTGCACATAC	ATTCTGCTCGATGTTGCCCA
Ccl2	GGCTCAGCCAGATGCAGTTA	GCTGCTGGTGATCCTCTTGT
Ccl3	CCGGAAGATTCCACGCCAAT	GTCTCTTTGGAGTCAGCGCA
Ccl5	GCCAGCTTGGGGATGCCACTC	CAGAGCCTCGGAGCAGCTGAG
Il6	TGGTGACAACCACGGCCTTCC	AGCCTCCGACTTGTGAAGTGGT
Il12p40	CGCAGCAAAGCAAGATGTGT	CGTGTCACAGGTGAGGTTCA

2.2.14 Enzyme Linked Immunosorbant Assay (ELISA)

Levels of secreted cytokines in cell culture supernatants were analyzed with Ready-SET-Go!® ELISA kits (mouse IFNγ, #88-7314; mouse IL-17A, #88-7371; mouse TNFα, #88-7324; mouse IL-1β, #88-7013; mouse CCL2, #88-7391; mouse IL-6, #88-7064; mouse IL-12p70, #88-7121; eBioscience, San Diego, CA) following the manufacturer's instructions.

2.2.15 Flow Cytometry

1.0-5.0 × 10^5 cells were resuspended in 50 μl PBS containing 2% FBS. Nonspecific binding of Fc receptors was blocked by incubating with 5 μg/ml α-ms

CD16/32 antibody (#14-0161, eBioscience) for 10 min on ice. Cells were then stained with fluorochrome-conjugated antibodies (α-ms CD11b FITC, #11-0112; α-ms Ly-6G PE, #61-9668; α-ms F4/80 APC, #17-4801; α-ms CD8 FITC, #11-0081; α-ms CD19 PE, #12-0193; α-ms CD4 APC, #17-0041; α-ms CD11c PE, #12-0114; α-ms Ly-6C APC, #17-5932; α-ms/rt CD40 FITC, #11-0402; α-ms CD80 PE, #12-0801; α-ms CD86 APC, #17-0862; α-ms MHC II APC, #17-5321; α-ms CD45 PE-Cy5.5, #35-0451; α-ms CD45.1 FITC, #11-0453; α-ms CD45.2 APC, #17-0454; eBioscience) at 1/200 dilution in a total volume of 100 µl for 20 min on ice in dark, and subsequently washed and resuspended in PBS with 2% FBS. Flow cytometric data were acquired on a BD Accuri C6 flow cytometer (BD Biosciences, San Jose, CA). Color compensation, gating, and data analysis were performed on the proprietary software from the manufacturer.

2.2.16 Multiplex Immunoassay

Levels of multiple cytokines in the myeloid and T-cell co-culture experiment were analyzed with ProcartaPlex Mix&Match Mouse 15-plex kit (eBioscience, EPX150-25074-801) following the manufacturer's instructions.

2.2.17 Immunohistochemistry/Immunocytochemistry

Brain and vertebral column were isolated from normal and EAE mice and fixed in 4% PFA in PBS at 4°C overnight. The next day, the spinal cord was carefully isolated from the spine using scissors and forceps, and fixed in 4% PFA again for an additional 4 hr. The tissues were then cryoprotected with 30% sucrose in PBS for roughly two days until sunk. Tissues were embedded in Tissue-Tek O.C.T. Compound (#4583, Sakura Finetek USA, Inc., Torrance, CA) and frozen sectioned into 10 µm sections on Leica

CM1950 cryostat (Leica, Nusslock, Germany). Sections were adhered onto Superfrost Plus Microscope Slides (Fisher Scientific, Waltham, MA) and stored at -20°C until use. Slides were thawed and dried for 30 min to 1 hr at 37°C prior to staining. For visualization of myelin structure and integrity, the sections were stained with Oil-Red-O solution by overnight incubation in 0.5% (w/v) Oil-Red-O (00625, Sigma-Aldrich) dissolved in propylene glycol (S264, Poly Scientific R&D Corp, Bay Shore, NY) at room temperature. For immunofluorescence, appropriate regions of the slides were marked with an ImmEdge hydrophobic barrier pen (Vector Lab, Inc. Burlingame, CA) to separate different sections. The sections were rinsed in PBS for 5 min to remove O.C.T. Compound. Sections were blocked for unspecific binding and permeabilized with PBS containing 5% goat serum and 0.3% Triton X-100 (T9284, Sigma Aldrich) for 1 hr at room temperature, and incubated with rabbit α-Iba-1 (1:400; #019-19741, Wako, Richmond, VA), rat α-CD68 (1:400; MCA1957, BioRAD, Hercules, CA), rabbit α-GFAP (1:100; 18-0063, Invitrogen), tomatolectin (B-1175, Vector Labs), rat α-ms ICAM-1 (1:100; 14-0542-81, eBioscience), rat α-ms PECAM-1 (1:50; 553370, BD Biosciences), rat α-ms CD3 (1:100, 14-0032, eBioscience), rat α-ms CD4 (1:100, 14-0042, eBioscience), rabbit α-pSTAT3(Y705) (1:100; #9145, Cell Signaling), ms α-human CD11b (ab63317, AbCam) diluted in PBS containing 5% goat serum and 0.1% Triton X-100 at 4°C overnight. The next day, tissue sections were washed in PBS three times for 5 min each, and incubated with goat α-rb IgG conjugated to Alexa Fluor 488 (A11034, Invitrogen, Eugene, OR) or goat α-ms IgG conjugated to Alexa Fluor 488 (A11029, Invitrogen, Eugene, OR) diluted 1:1000 in PBS containing 5% goat serum and

0.1% Triton X-100 for 1 hr at room temperature in dark. Cell nuclei were stained with Hoechst 33342 (Invitrogen) at 1:1000 dilution in PBS for 1 min. Human MS CNS tissue was also stained with Sudan black by incubation in 0.3% (w/v) Sudan black (Sigma-Aldrich) dissolved in 70% (v/v) ethanol at room temperature for 2 min to decrease autofluorescence in the lipid. Images were acquired with an Olympus IX71 microscope (Olympus, Tokyo, Japan) with constant settings across different sections/samples. Post-processing (image merging and background removal) was performed in a uniform fashion in Adobe Photoshop software.

2.2.18 Data Analysis

When appropriate, differences between two groups were analyzed with two-tailed Student's *t* test. Differences between more than two groups were analyzed with multivariate analysis of variance followed by Bonferroni's post hoc test. The cumulative EAE scores of *Stat3*$^{fl/fl}$ and *LysMcre/Stat3*$^{fl/fl}$ mice were analyzed with Wilcoxon rank-sum test. The rate of EAE onset of *Stat3*$^{fl/fl}$ and *LysMcre/Stat3*$^{fl/fl}$ mice was analyzed with Pearson chi-square test and Fisher's exact test. Differences were considered statistically significant if $p < 0.05$.

2.3 Results

2.3.1 STAT3 Is Activated in Myeloid Cells in Human MS CNS

We first investigated whether STAT3 is activated in myeloid cells in MS lesions. As shown in Figure 3A, the level of pSTAT3 (Y705) and total STAT3 were evaluated by Western blotting analysis of postmortem brain tissue from MS patients and control

subjects (Table 2). pSTAT3 (Y705) was increased by ~4.9 fold, and total STAT3 was increased by ~2.3 fold in MS patients compared to control individuals (Figure 3B). Next, we examined whether STAT3 is activated in specifically infiltrating myeloid cells in MS lesions with immunofluorescence. As shown in Figure 3C, in actively demyelinating lesions, we found multiple $pSTAT3^{+}$ cells, some of which co-localized with $CD11b^{+}$ cells. In contrast, we did not find any pSTAT3 (Y705) signal in control patients. These data indicate that STAT3 is activated in subsets of myeloid cells in active MS lesion and suggest that STAT3 may be involved in the pathogenesis of MS.

Table 2. Summary of pathological information on MS patients and control subjects.

Diagnosis	ID	Age/Sex	Clinical Diagnosis/Cause of Death
Control	#C-1	86/F	Clinical diagnosis of MS
	#C-2	74/M	Progressive Supranuclear Palsy
	#C-3	19/M	Gun shot (abdomen)
	#C-4	15/M	Accidental hanging
	#C-5	31/M	Anemia, pencytopenia
	#C-6	29/M	Motor cycle accident
MS	#MS-1	69/M	MS
	#MS-2	44/M	MS (chronic progressive), aspiration pneumonia, grand mal seizure with status epilepticus
	#MS-3	40/F	MS (progressive, severe, unrelenting for 10 yrs)
	#MS-4	63/F	MS, Sleep Apnea, Chronic urinary tract infection, respiratory failure, Hypertension
	#MS-5	52/F	MS (secondary progressive)
	#MS-6	51/F	MS (secondary progressive)
	#MS-7	75/F	MS, hypertension, kidney stone surgery, Goiter surgery, Hypothyroidism, Migraine,Chronic uninary tract infection
	#MS-8	54/F	MS (relapse-remitting)

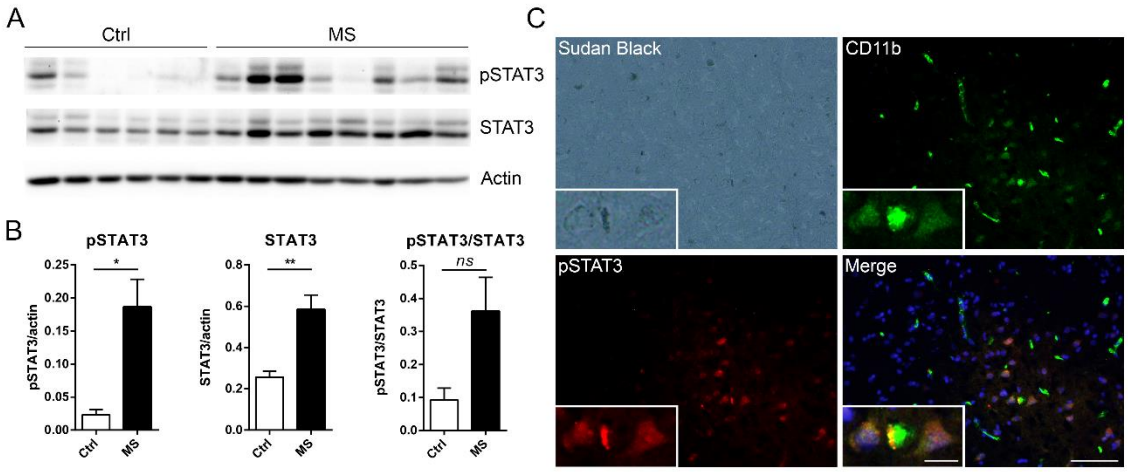

Figure 3. Increased STAT3 phosphorylation in active MS lesions. A, Protein lysates from non-neurological controls (n = 6) and MS patients (n = 8) were immunoblotted with antibodies against pSTAT3 (Y705) and total STAT3. Each lane represents one individual. **B**, Level of pSTAT3 and total STAT3 was quantitated with densitometry. Data represent mean ± SEM. *$p < 0.05$, **$p < 0.01$. **C**, Representative pictures of MS patient CNS tissue. Tissue was stained with α-CD11b (green), α-pSTAT3 (Y705) (red), Hoechst (blue), and Sudan black. Scale bar, 50 µm. Scale bar, 10 µm (insert).

2.3.2 STAT3 Is Activated in MOG_{35-55}-induced EAE in C57BL/6 Mice

Next, we investigated whether STAT3 is activated during MOG_{35-55}-induced EAE in C57BL/6 mice. Using markers for myeloid cells, astrocytes, and T-cells, we examined the activation of STAT3 in SC lumbar cord sections from EAE mice 14 dpi (Figure 4). We found that pSTAT3 was colocalized to $CD68^+$ (Figure 4A), $tomatolectin^+$ (Figure 4D), and $CD11b^+$ (Figure 4E) myeloid cells at or near inflammatory locations in the parenchyma during active EAE (indicated by white arrows), whereas only a few $pSTAT3^+$ cells colocalized to $GFAP^+$ astrocytes (Figure 4B) or $CD4^+$ T-cells (Figure 4F). In contrast to EAE, pSTAT3 signal was absent in normal naïve spinal cord (Figure 4C). Together, these data suggest that activation of STAT3 in myeloid cells may contribute to the pathogenesis of EAE.

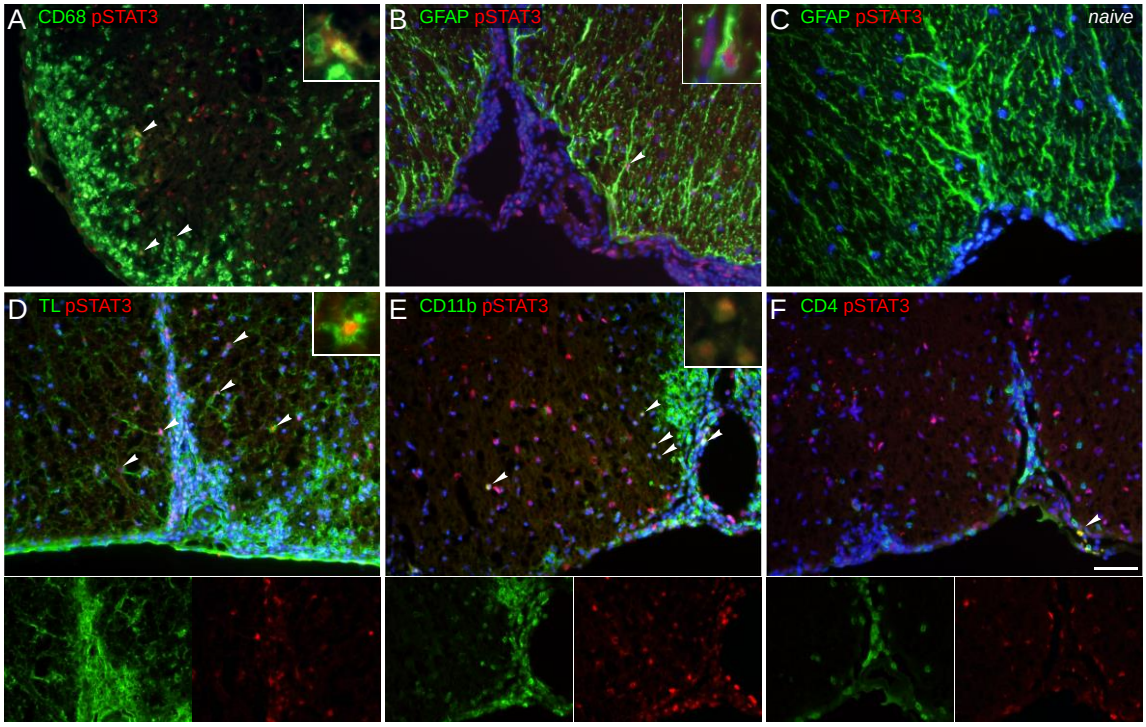

Figure 4. STAT3 is activated in the myeloid cells during EAE. Spinal cord sections from EAE C57BL/6 mice at 14 dpi (**A, B, D-F**) or naïve C57BL/6 mice (**C**) were analyzed with immunofluorescence. Shown are representative pictures of the mid ventral region. Arrows indicate double labeled cells. Inserts show higher magnification of double labeled cells. **A, B**, pSTAT3 was colocalized to $CD68^+$ activated microglia/macrophages but only to a few $GFAP^+$ astrocytes. **C**, pSTAT3 signal was absent in naïve spinal cord. **D**, Some $pSTAT3^+$ cells were also tomatolectin positive, which labels blood vessels and microglia/macrophages. **E**, Some $pSTAT3^+$ cells were also colocalized to $CD11b^+$ myeloid cells. **F**, pSTAT3 had only a few colocalizations with CD4 in the parenchyma. Some double labeled cells were found in the leptomeninges. Scale bar, 50 µm.

2.3.3 STAT3 Is Selectively Inactivated in Myeloid Cells in LysMcre/Stat3$^{fl/fl}$ Mice

To study the function of STAT3 in myeloid cells, we utilized the *loxP*/Cre system and crossed *LysMcre* line with *Stat3$^{fl/fl}$* line to obtain the conditional knockout. As shown in Figure 5A, Cre recombinase expressed under the control of the lysozyme M promoter causes recombination at the two loxP sites, resulting in the deletion of exon 22 in *Stat3* gene, which contains the Tyrosine 705 residue of which phosphorylation is critical for STAT3 activation and transcription activity. To confirm that the targeted

sequence is indeed deleted in myeloid cells upon Cre recombination, we designed primers to flank the entire deleted sequence. The deleted band (*Δdel*) of ~550 bp was amplified using the DNA from FACS-sorted $CD11b^+$ splenocytes from *LysMcre/Stat3*$^{fl/fl}$ mice, whereas the *flox* band of ~3500 bp was amplified from *Stat3*$^{fl/fl}$ mice (Figure 5B). These results demonstrated that *Stat3* exon 22 was indeed excised in the myeloid cells of *LysMcre/Stat3*$^{fl/fl}$ mice.

We next compared the extent of Tyrosine 705 phosphorylation upon brief IL-6 stimulation in cultured BMDMs prepared from *LysMcre/Stat3*$^{fl/fl}$ and littermate *Stat3*$^{fl/fl}$ control mice. Although the total protein level of STAT3 was not significantly decreased in the *LysMcre/Stat3*$^{fl/fl}$ BMDMs since only exon 22 was deleted, STAT3 phosphorylation was significantly impaired in the *LysMcre/Stat3*$^{fl/fl}$ BMDMs after 30 min stimulation of IL-6 (Figure 5C, D). These data demonstrated that STAT3 activation is functionally impaired in the *LysMcre/Stat3*$^{fl/fl}$ cells.

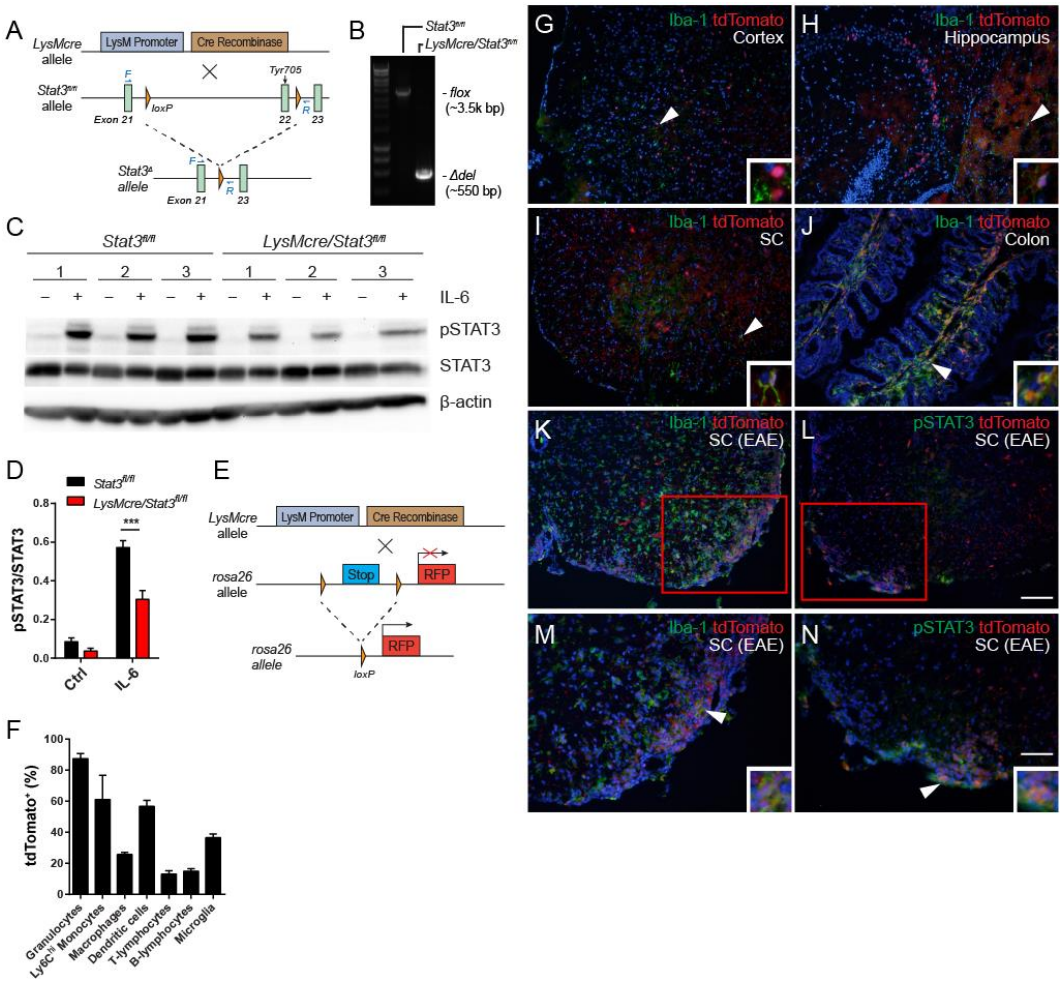

Figure 5. STAT3 was selectively inactivated in myeloid cells in *LysMcre/Stat3$^{fl/fl}$* mice. **A**, Exon 22 was flanked by two loxP sites and excised by Cre recombination. *F* and *R*, primers designed to flank the entire deleted sequence. Forward-CCTCTACCCCGACATTCCCAAGG, reverse-CACACAAGCCATCAAACTCTGGTCTC. **B**, DNA was purified from FACS-sorted CD11b^{+} cells from the spleen from *LysMcre/Stat3$^{fl/fl}$* mice. The *flox* band (~3500 bp) and the deleted band (*Δdel*; ~550 bp) was amplified with PCR using the primer in **A**. **C, D**, BMDMs from adult *LysMcre/Stat3$^{fl/fl}$* (n = 3) and *Stat3$^{fl/fl}$* (n = 3) mice were stimulated with 10 ng/ml rmIL-6 for 30 min. Cell lysates were immunoblotted with antibodies against pSTAT3 (Y705) and total STAT3 and quantitated with densitometry in **D**. Data represent mean ± SEM. ***$p < 0.005$. **E**, The reporter line *rosa26-Ai14* expresses RFP upon Cre recombination. **F**, Expression of reporter activity in the spleen and CNS in 9-month old *LysMcre/rosa26-Ai14* mice (n = 3) was analyzed with flow cytometry. Granulocytes, CD11b^{+}Gr-1^{+}; Ly6C^{hi} monocytes, CD11b^{+}Ly6C^{hi}; Macrophages, CD11b^{+}Ly6C^{lo}; Dendritic cells, CD11b^{+}CD11c^{+}; T-cells, CD3^{+}; B-cells, CD19^{+}; Microglia, CD11b^{+}CD45^{int}. Data represent Mean ± SEM. **G-J**, Expression of reporter activity in the cerebral cortex (**G**), hippocampus (**H**), spinal cord (**I**), and colon (**J**) from naïve adult *LysMcre/rosa26-Ai14* mice of ~2 months of age were analyzed with immunostaining of Iba-1. Representative pictures were shown. Arrows indicate the location of inserts. **K-N**, Spinal cord sections from *LysMcre/rosa26-Ai14* EAE mice were stained with α-Iba-1 (**K, M**) and α-pSTAT3 (**L, N**). Representative pictures were shown. **M**, Higher magnification of the boxed region in **K**. **N**, Higher magnification of the boxed region in **L**. Arrows indicate the location of inserts. Scale bar (**G-L**), 50 μm. Scale bar (**M, N**), 25 μm.

After establishing the efficacy of *Stat3* targeting and functional inactivation, we then asked where LysM-driven Cre recombination occurs *in vivo*, and more importantly what cell types undergo LysM-driven *Stat3* inactivation during EAE. We thus crossed *LysMcre* mice with the reporter line *rosa26-Ai14* to determine the efficiency of Cre recombinase activity in various cell types in the splenocytes and CNS mononuclear cells with flow cytometry. Granulocytes showed the highest tdTomato expression and are at 87.5% (Figure 5E). Monocytes and dendritic cells also showed abundant expression at 61.1% and 56.7%, respectively, whereas only 36.5% microglia expressed tdTomato (Figure 5E). Consistent with the flow cytometric data, there were sparing Iba-1^{+}tdTomato^{+} cells in the cerebral cortex (Figure 5H), hippocampus (Figure 5H), and spinal cord (Figure 5I), whereas relatively more abundant colocalizations could be found in the colon (Figure 5J). We also noticed distinct Iba-1^{-}tdTomato^{+} cells in the CA3 region of the hippocampus (Figure 5H) as well as in the gray matter of the spinal cord (Figure 5I), which suggests that LysM-driven Cre recombination may also occur in specific subsets of neurons. In contrast to naïve SC, Iba-1^{+}tdTomato^{+} cells were much more abundant in the inflamed region in EAE spinal cord (Figure 5K, M). STAT3 was activated in tdTomato^{+} cells during EAE (Figure 5L, N), but not in the naïve. Together, these data indicate that the animal model is sufficient in reducing activation of STAT3.

2.3.4 LysMcre/Stat3$^{fl/fl}$ Mice Are Significantly Less Susceptible to MOG$_{35-55}$-induced EAE

GWAS studies identified that *Stat3* is one of the MS susceptibility genes [12, 119]. Together with our finding that STAT3 is activated in myeloid cells in MS lesions

(Figure 3), this suggests that myeloid STAT3 activation may be involved in generation or regulation of autoimmune processes. To investigate this, we subjected *Stat3*$^{fl/fl}$ and *LysMcre/Stat3*$^{fl/fl}$ mice to MOG_{35-55}-induced EAE. While most *Stat3*$^{fl/fl}$ mice (81.8%) developed EAE two weeks after immunization, only 5.56% of *LysMcre/Stat3*$^{fl/fl}$ mice showed EAE clinical symptoms (Figure 6A, C). The onset of EAE symptoms often accompanies weight loss, and consistent with their decreased susceptibility, *LysMcre/Stat3*$^{fl/fl}$ mice did not exhibit as much weight loss as *Stat3*$^{fl/fl}$ mice (Figure 6B). In addition to the absence of classic EAE symptoms, there was no sign of demyelination in the lumbar cord of *LysMcre/Stat3*$^{fl/fl}$ mice (Figure 6D). When analyzed 2 weeks after immunization, *LysMcre/Stat3*$^{fl/fl}$ mice contained significantly less CNS infiltrating leukocytes including macrophages/monocytes and lymphocytes compared to *Stat3*$^{fl/fl}$ mice (Figure 6E, F). At 21 dpi, the spinal cord from *LysMcre/Stat3*$^{fl/fl}$ mice contained few activated macrophages (Figure 6G), and microglia mostly remained in a ramified resting state (Figure 6H). In agreement with this observation, *LysMcre/Stat3*$^{fl/fl}$ mice also expressed significantly less proinflammatory mediators in the spinal cord than *Stat3*$^{fl/fl}$ mice (Figure 6I). Together, these data demonstrated that loss of STAT3 signaling in myeloid cells suppressed leukocyte infiltration and neuroinflammation in MOG-immunized mice.

To investigate whether myeloid STAT3 deletion affects the transmigrating capability of the cells, we next investigated whether the suppressed leukocyte CNS infiltration in the *LysMcre/Stat3*$^{fl/fl}$ mice is associated with decreased expression of adhesion molecules and/or better structural integrity of the BBB (Figure 7). ICAM-1

mRNA was significantly increased in the immunized *Stat3*$^{fl/fl}$ mouse spinal cord, but *LysMcre/Stat3*$^{fl/fl}$ was not significantly different from those of naïve mice (Figure 7A). VCAM-1 showed a trend of increase only in the *Stat3*$^{fl/fl}$ (Figure 7A). Consistent with the mRNA data, immunostaining revealed that ICAM-1 was drastically increased in the vasculature of immunized *Stat3*$^{fl/fl}$ particularly in regions with infiltration of Iba-1+ macrophages/microglia during the peak stage of EAE (Figure 7B). In contrast, we only observed ICAM-1 staining in the leptomeninges but not within the spinal cord of the *LysMcre/Stat3*$^{fl/fl}$ mice (Figure 7B). We visualized the BBB area with PECAM and GFAP immunostaining and found many cells at the paravascular cuff in the *Stat3*$^{fl/fl}$ at peak stage of EAE, but not in the *LysMcre/Stat3*$^{fl/fl}$ (Figure 7C). Together, these data provide strong evidence that myeloid STAT3 signaling is essential in the development of MOG_{35-55}-induced EAE.

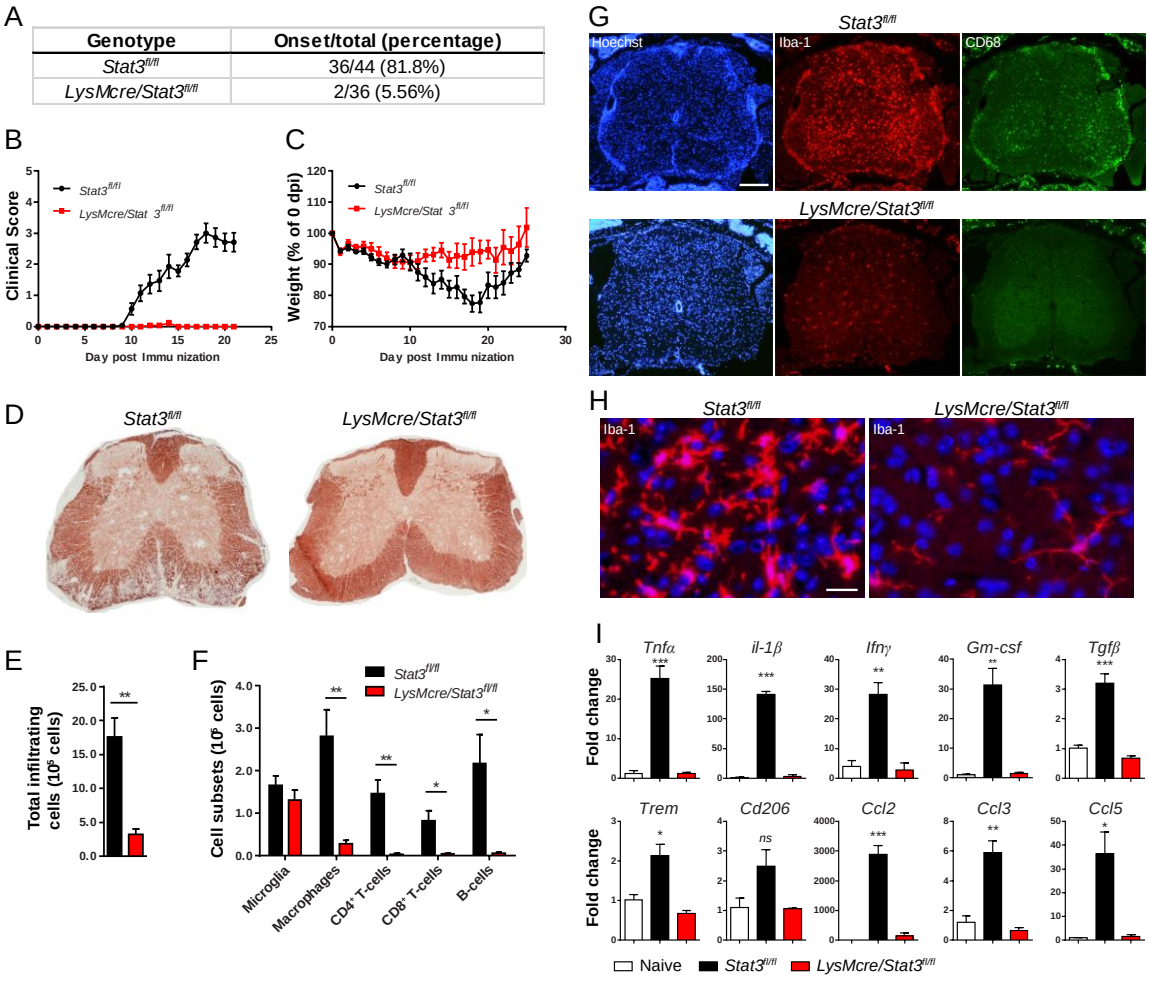

Figure 6. *LysMcre/Stat3$^{fl/fl}$* mice are resistant to actively induced EAE. A-C, *Stat3$^{fl/fl}$* (n = 44) and *LysMcre/Stat3$^{fl/fl}$* mice (n = 36) were immunized for MOG_{35-55}-induced EAE and evaluated on daily basis using the scoring criteria described in the methods section. **A**, Table of onset rate. **B**, Clinical scores up to 21 dpi. **C**, Percentage weight change. **D**, Myelin structure in the spinal cord sections from 21 dpi mice was analyzed with Oil-Red-O staining. Representative pictures were shown. **E, F**, CNS infiltrating leukocytes were isolated from *Stat3$^{fl/fl}$* (n = 4) and *LysMcre/Stat3$^{fl/fl}$* EAE mice (n = 4) at 14 dpi and analyzed with flow cytometry. Microglia, $CD11b^{+}CD45^{int}$; Macrophages, $CD11b^{+}CD45^{hi}$. **G, H**, Spinal cord sections from mice at 21 dpi were cryosectioned and stained with Hoechst (blue) and antibodies for Iba-1 (red) and CD68 (green). Representative pictures were shown. Scale bar (**G**), 200 μm. Scale bar (**H**), 50 μm. **I**, RNA was isolated from spinal cord of *Stat3$^{fl/fl}$* (n = 5) and *LysMcre/Stat3$^{fl/fl}$* mice (n = 5) at 14 dpi and analyzed with quantitative RT-PCR. Data represent fold expression compared to naïve group. Data represent mean ± SEM. $*p < 0.05$, $**p < 0.01$, $***p < 0.005$.

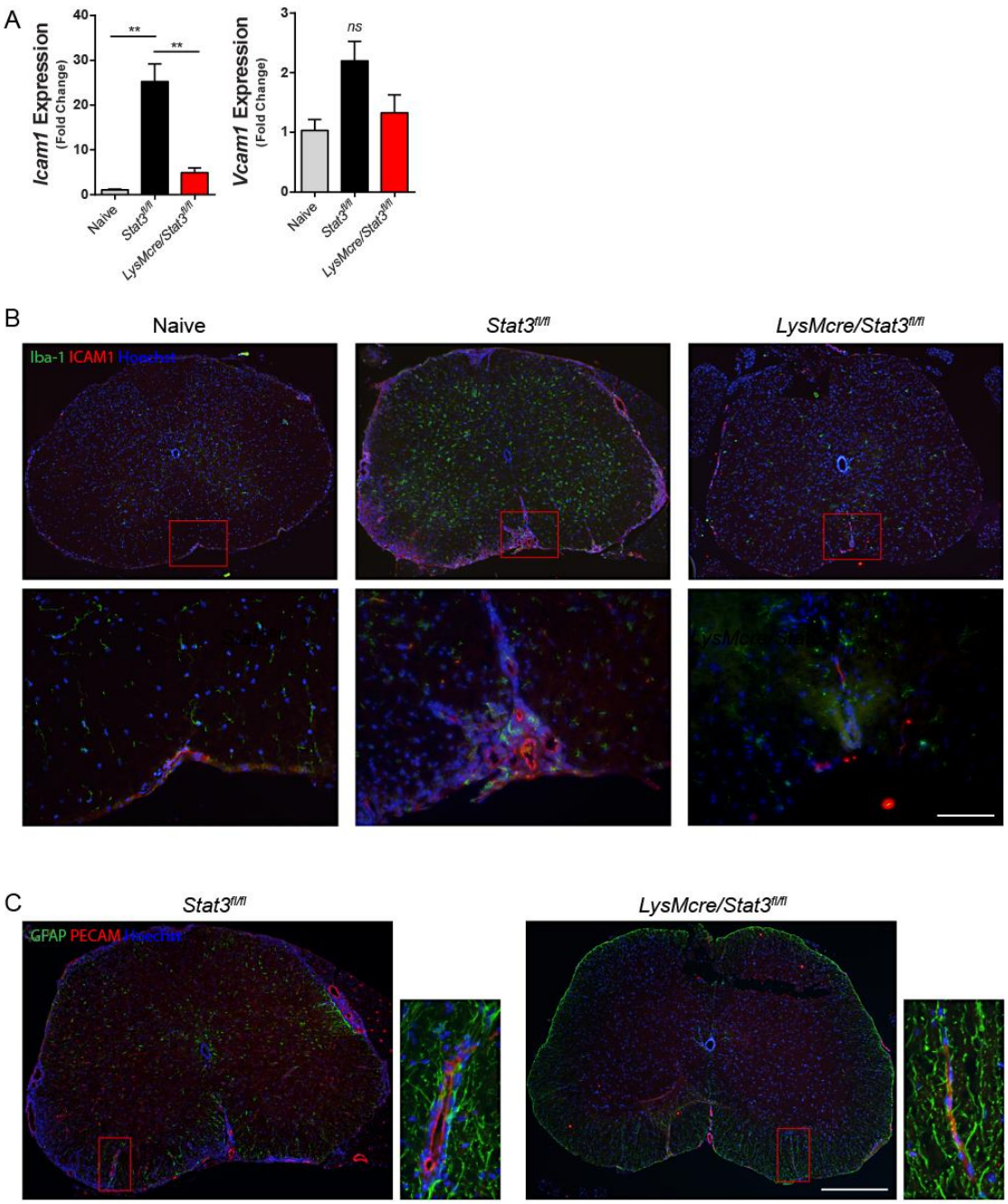

Figure 7. Expression of cell adhesion molecules during EAE. Active EAE was induced in the *Stat3*$^{fl/fl}$ and *LysMcre/Stat3*$^{fl/fl}$ mice. **A**, RNA was isolated form spinal cord from immunized mice at 14 dpi (*Stat3*$^{fl/fl}$, $n = 4$; *LysMcre/Stat3*$^{fl/fl}$, $n = 3$) and from naïve C57BL/6 mice ($n = 3$). Expression level of *Icam1* and *Vcam1* mRNA was analyzed by quantitative RT-PCR. Data represent mean ± SEM. $^{**}p < 0.01$. **B, C**, Spinal cord from mice at 14 dpi were cryosectioned and stained with Hoechst (blue) and antibodies for Iba-1 (green) and ICAM-1 (red, **B**) or PECAM (red, **C**). Representative pictures were shown. Lower panels are the magnified view of the red boxes in the upper panels. Scale bar, 50 μm.

2.3.5 Peripheral T_H1 and T_H17 Responses Are Reduced in LysMcre/Stat3$^{fl/fl}$ Mice during Pre-clinical and Onset Stages of EAE

Since EAE is an autoimmune-driven disease, the resistance to EAE may be attributable to diminished adaptive immune response in the peripheral immune system. Therefore, we evaluated the kinetics of peripheral immune response by performing $CD4^+$ T-cell cytokine recall experiments at different stages of EAE. During the pre-clinical and onset stages of EAE, *LysMcre/Stat3$^{fl/fl}$* splenocytes secreted significantly less IFNγ compared to *Stat3$^{fl/fl}$* (Figure 8A). Although a significant difference in IL-17A was not found, there was a consistent trend of decreased IL-17A secretion in the *LysMcre/Stat3$^{fl/fl}$* up until the peak stage (Figure 8B). We also found a significant decrease in GM-CSF (Figure 8C) and many cytokines and chemokines, namely TNFα, IL-1β, IL-6, IL-12p70, IL-18, IL-23, IP-10 and CCL5 (Figure 9) during the disease onset. During the post peak stage of EAE, none of the three cytokines showed significant differences between *Stat3$^{fl/fl}$* and *LysMcre/Stat3$^{fl/fl}$* (Figure 8A-C), nor did most other cytokines we tested (Figure 9).

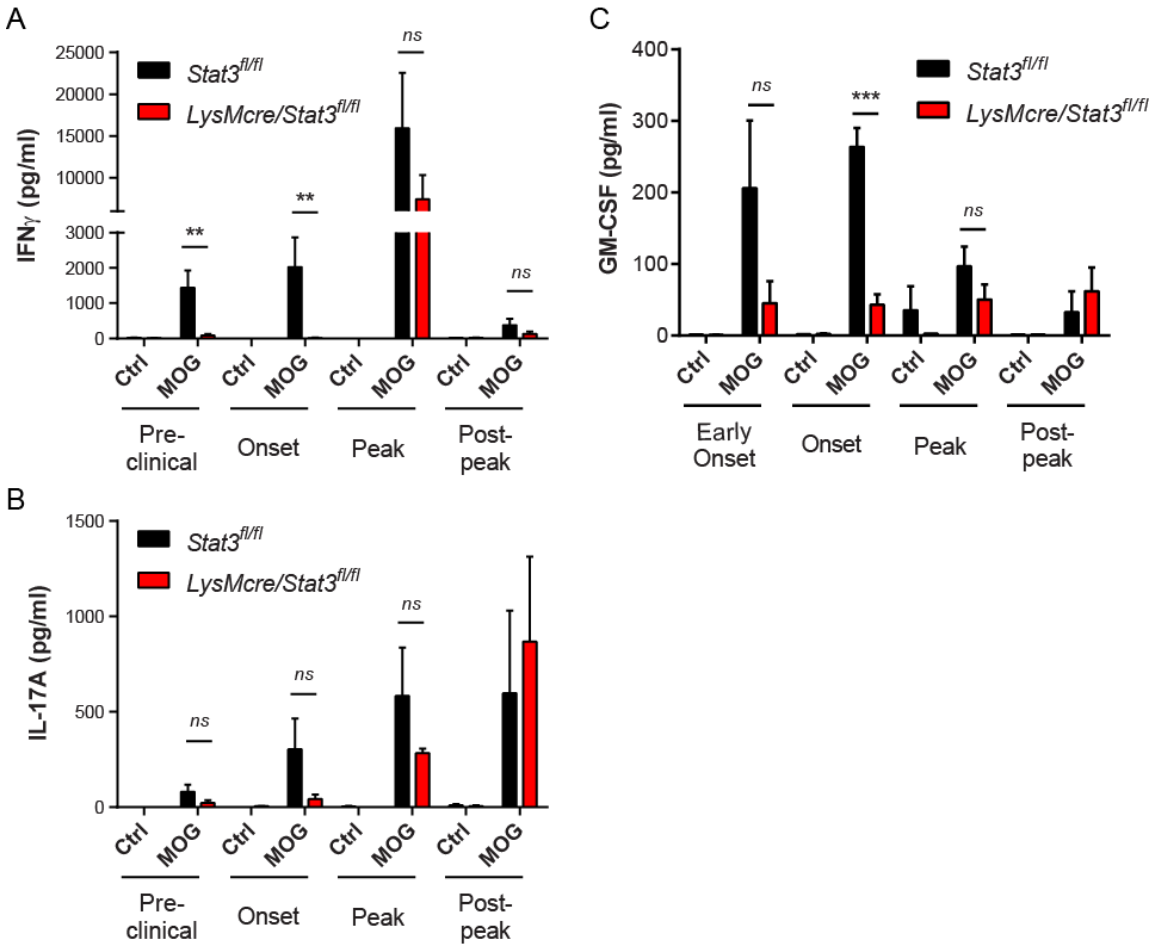

Figure 8. Peripheral MOG-specific T-cell responses were impaired during pre-clinical and onset of EAE. EAE was induced in *Stat3*$^{fl/fl}$ and *LysMcre/Stat3*$^{fl/fl}$ mice. Splenocytes were isolated at four different stages of disease and cultured at 5.0×10^5 cells per well in 96-well U-shaped plates in complete RPMI medium in the absence or presence of 30 µg/ml MOG_{35-55} for 3 d. Cytokine secretion into the supernatant was determined with ELISA. Pre-clinical, 12 dpi, *Stat3*$^{fl/fl}$, $n = 6$; *LysMcre/Stat3*$^{fl/fl}$, $n = 5$. Onset, 19 dpi, *Stat3*$^{fl/fl}$, $n = 6$; *LysMcre/Stat3*$^{fl/fl}$, $n = 4$. Peak, 28 dpi, *Stat3*$^{fl/fl}$, $n = 5$; *LysMcre/Stat3*$^{fl/fl}$, $n = 2$. Post-peak, 49 dpi, *Stat3*$^{fl/fl}$, $n = 3$; *LysMcre/Stat3*$^{fl/fl}$, $n = 2$. **A**, IFNγ. **B**, IL-17A. **C**, GM-CSF. Data represent mean ± SEM. $*p < 0.05$, $**p < 0.01$, $***p < 0.005$.

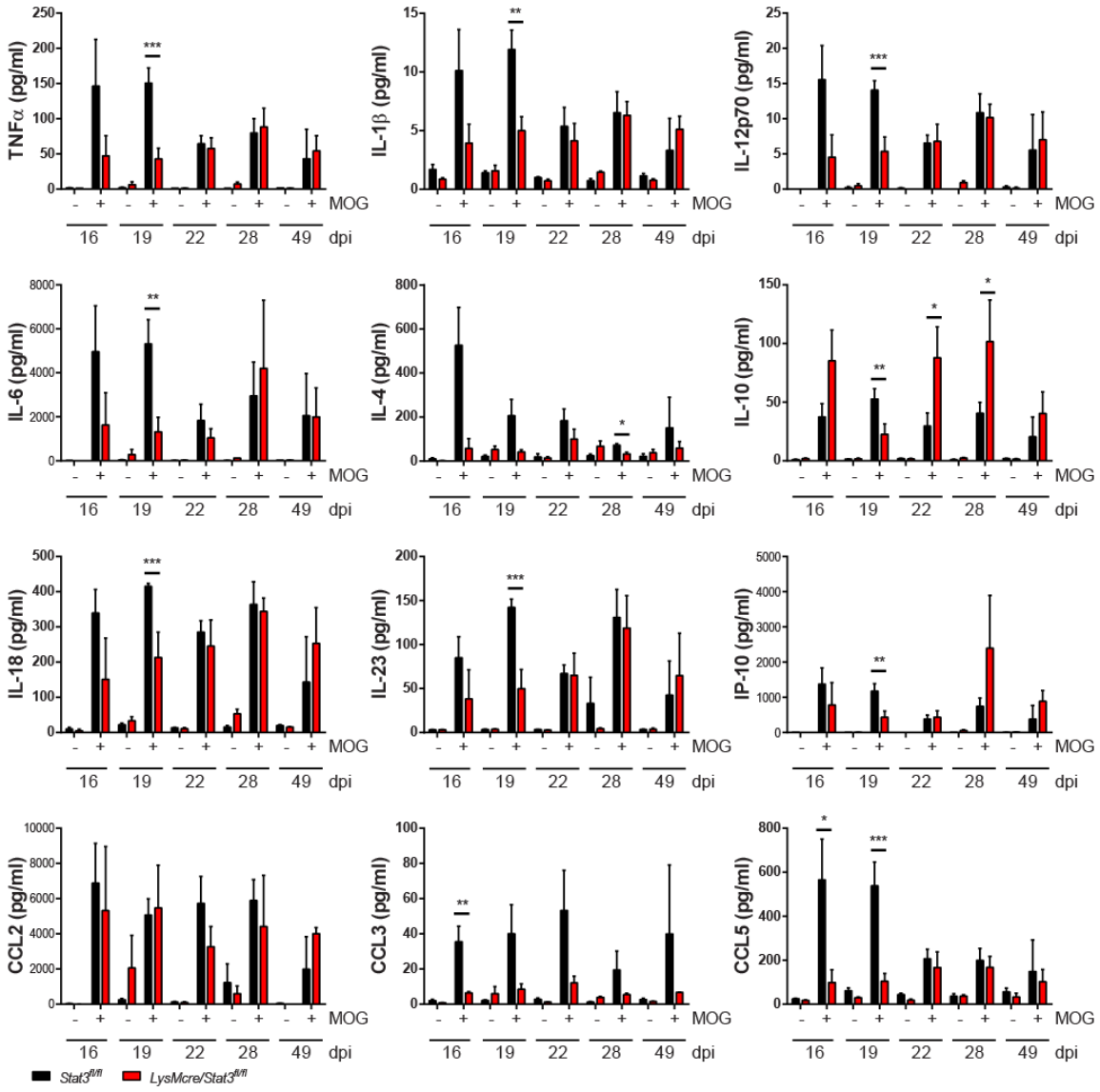

Figure 9. Cytokine responses during different stages of EAE development. EAE was induced in *Stat3*$^{fl/fl}$ and *LysMcre/Stat3*$^{fl/fl}$ mice. Splenocytes were isolated at different stages of disease and cultured at 5.0×10^5 cells per well in 96-well U-shaped plates in complete RPMI medium in the absence or presence of 30 µg/ml MOG_{35-55} for 3 d. Cytokine secretion into the supernatant was determined using multiplex immunoassay. 16 dpi, *Stat3*$^{fl/fl}$, $n = 4$; *LysMcre/Stat3*$^{fl/fl}$, $n = 3$. 19 dpi, *Stat3*$^{fl/fl}$, $n = 6$; *LysMcre/Stat3*$^{fl/fl}$, $n = 4$. 22 dpi, *Stat3*$^{fl/fl}$, $n = 4$; *LysMcre/Stat3*$^{fl/fl}$, $n = 4$. 28 dpi, *Stat3*$^{fl/fl}$, $n = 5$; *LysMcre/Stat3*$^{fl/fl}$, $n = 2$. 49 dpi, *Stat3*$^{fl/fl}$, $n = 3$; *LysMcre/Stat3*$^{fl/fl}$, $n = 2$. Data represent mean ± SEM. *$p < 0.05$, **$p < 0.01$, ***$p < 0.005$.

In addition to the levels of secreted cytokines, we also investigated the number of activated T_H1 and T_H17 cells in the spleen during EAE. The number of IFNγ-producing

T_H1 cells were significantly less in *LysMcre/Stat3*$^{fl/fl}$ at the onset stage of EAE as compared to *Stat3*$^{fl/fl}$ control mice (Figure 10A). Interestingly, this pattern was reversed during the peak and post peak stages of EAE (Figure 10A), although the differences were not statistically significant and the *LysMcre/Stat3*$^{fl/fl}$ mice did not exhibit any EAE clinical symptoms. In contrast to the differences in T_H1, there were no significant differences for IL-17A-secreting T_H17 cells between the genotypes at the onset or peak stages of EAE (Figure 10B). To rule out the possibility that the differences in cytokine recall may be due to a potential shift in immune cell population in the *LysMcre/Stat3*$^{fl/fl}$ mice, we analyzed cell profile of spleen and blood from mice at different EAE stages (Figure 11). During the pre-clinical stage of EAE, there was no differences in any of the myeloid cells or lymphocytes we tested between the genotypes (Figure 11A). During the onset stage of EAE, we observed a trend towards decreased percentage of myeloid populations in the blood as well as decreased percentage of lymphocyte populations in the spleen in the *LysMcre/Stat3*$^{fl/fl}$ mice (Figure 11B). This pattern is, however, not seen during the peak stage of EAE (Figure 11C). During the peak stage of EAE, we saw a trend towards increased neutrophil and monocyte population in the blood (Figure 11C). However, none of these differences were statistically significant. Last, we found no major differences in the cell profile at post-peak stage of EAE (Figure 11D). Therefore, the differences in cytokine responses between the genotypes are not likely to be due to a shift in major leukocyte populations. Taken together, these data indicate that loss of STAT3 signaling in myeloid cells results in decreased T_H1 responses primarily in pre-clinical and early peak stages of EAE as well as a trend in decreased T_H17 responses.

These data suggest that activation of STAT3 in myeloid lineage cells is required for generating antigen-specific T_H1 and T_H17 responses, and that the impaired T-cell responses in *LysMcre/Stat3*$^{fl/fl}$ mice render them less susceptible to EAE.

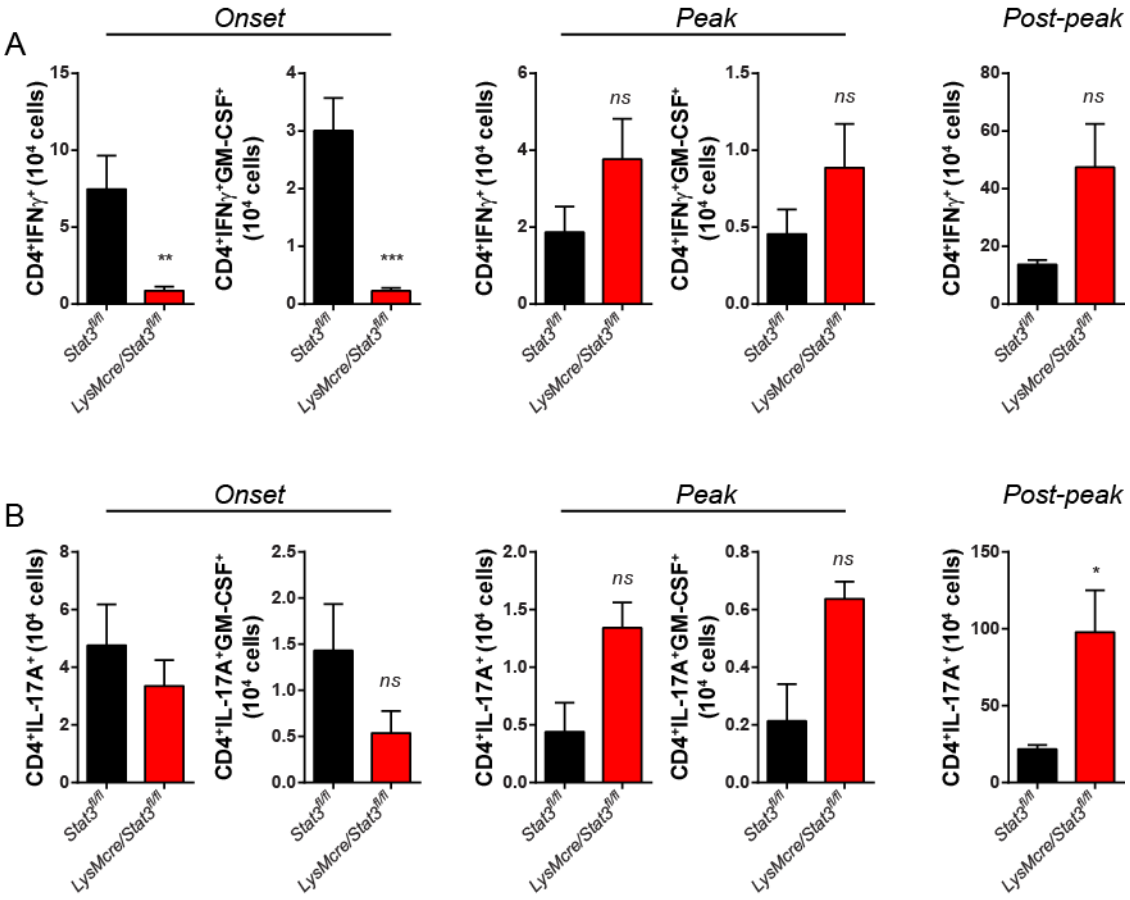

Figure 10. *LysMcre/Stat3*$^{fl/fl}$ mice' secondary lymphoid organs contained lower number of MOG-specific T_H1 cells at EAE onset. Active EAE was induced in *Stat3*$^{fl/fl}$ and *LysMcre/Stat3*$^{fl/fl}$ mice. Splenocytes were isolated at three different stages of disease and cultured in the presence of 100 µg/ml MOG_{35-55} in complete RPMI medium for 24 h. Cytokine secretion was blocked by Brefeldin A for the last 5 h. The cells were then fixed and stained with α-CD4, α-IFNγ, α-IL-17A, and α-GM-CSF, and analyzed with flow cytometry. **A**, T_H1 cells. **B**, T_H17 cells. Onset, 19 dpi, *Stat3*$^{fl/fl}$, $n = 6$; *LysMcre/Stat3*$^{fl/fl}$, $n = 4$. Peak, 22 dpi, *Stat3*$^{fl/fl}$, $n = 4$; *LysMcre/Stat3*$^{fl/fl}$, $n = 4$. Post-peak, 49 dpi, *Stat3*$^{fl/fl}$, $n = 3$; *LysMcre/Stat3*$^{fl/fl}$, $n = 2$. Data represent mean ± SEM. *$p < 0.05$, **$p < 0.01$, ***$p < 0.005$.

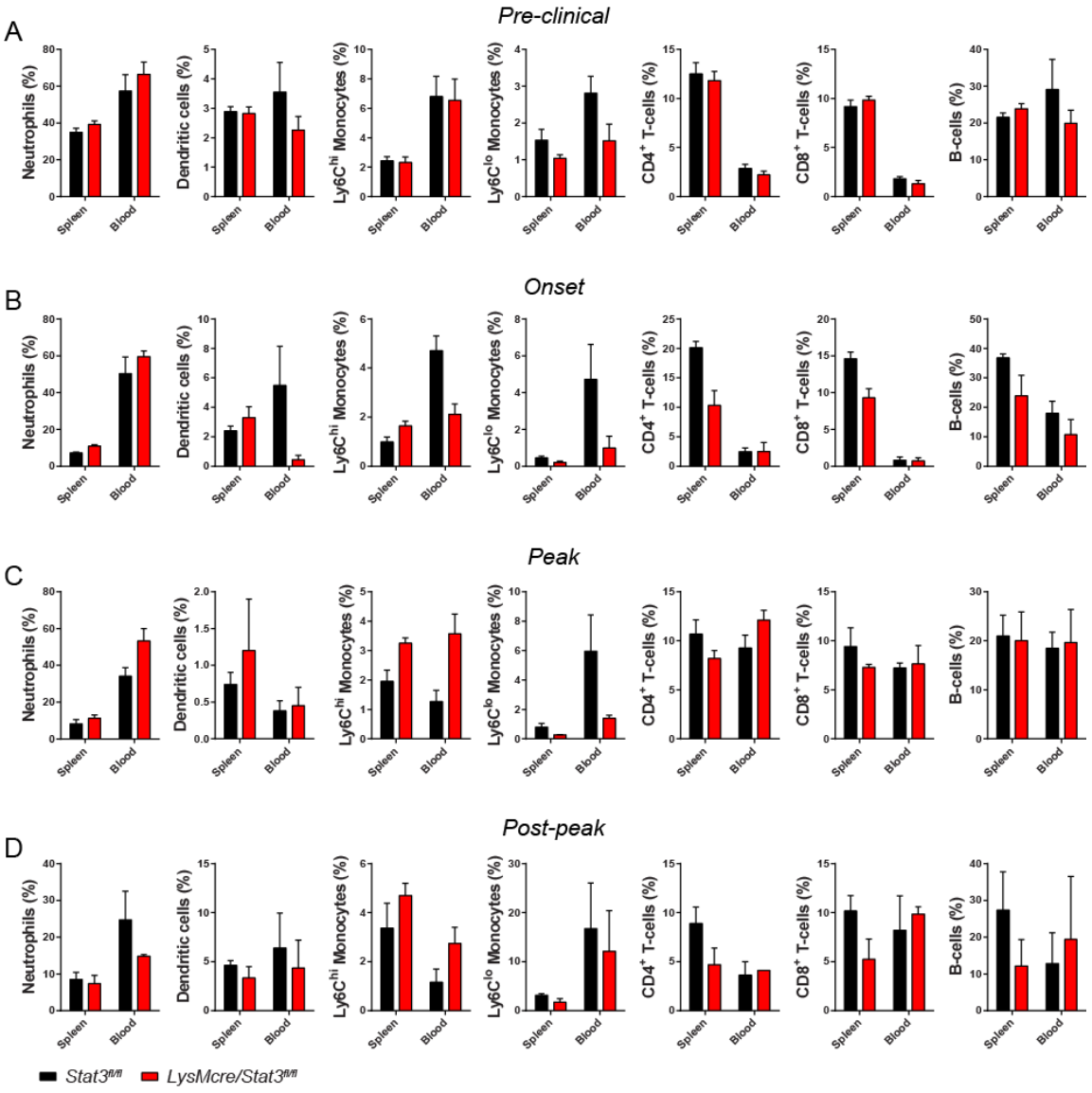

Figure 11. No major cell profile difference was found during EAE. Active EAE was induced in *Stat3$^{fl/fl}$* and *LysMcre/Stat3$^{fl/fl}$* mice. Splenocytes and blood were isolated at four different stages of disease and stained with antibodies for cell surface markers. Neutrophils, CD11b^{+}Ly6G^{+}; Dendritic cells, CD11b^{+}CD11c^{+}; Ly6C^{hi} monocytes, CD11b^{+}Ly6C^{hi}; Ly6C^{lo} monocytes, CD11b^{+}Ly6C^{lo}; CD4^{+} T-cells, CD4^{+}; CD8^{+} T-cells, CD8^{+}; B-cells, CD19^{+}. **A**, Pre-clinical, 12 dpi, *Stat3$^{fl/fl}$*, *n* = 6; *LysMcre/Stat3$^{fl/fl}$*, *n* = 5. **B**, Onset, 19 dpi, *Stat3$^{fl/fl}$*, *n* = 6; *LysMcre/Stat3$^{fl/fl}$*, *n* = 4. **C**, Peak, 28 dpi, *Stat3$^{fl/fl}$*, *n* = 5; *LysMcre/Stat3$^{fl/fl}$*, *n* = 2. **D**, Post-peak, 49 dpi, *Stat3$^{fl/fl}$*, *n* = 3; *LysMcre/Stat3$^{fl/fl}$*, *n* = 2. Data represent mean ± SEM.

2.3.6 Stat3 Deletion in Myeloid Cells Impairs Their Capability to Differentiate Naïve $CD4^+$ T-Cells ex vivo

Since certain myeloid cell types such as macrophages and dendritic cells are capable of differentiating naïve helper T-cells into effector T-cells, which are important in EAE, impairment in such capability may result in decreased T-cell response and resistance to EAE. To test this, we took an *ex vivo* co-culture approach and isolated $CD11b^+$ splenocytes from *LysMcre/Stat3*$^{fl/fl}$ mice 9-10 days after immunizing with MOG_{35-55} and co-cultured the $CD11b^+$ cells with naïve $CD4^+$ T-cells from 2D2 mice in the absence or presence of MOG_{35-55} peptide (Figure 12A). We first tested the purity of magnetic selection (Figure 13). Both CD11b and CD4 positive selection yielded highly enriched populations (84.3% and 89.9%, respectively; Figure 13A, B). There were no major differences in the cell populations in the isolated $CD11b^+$ cells between the genotypes (Figure 13C).

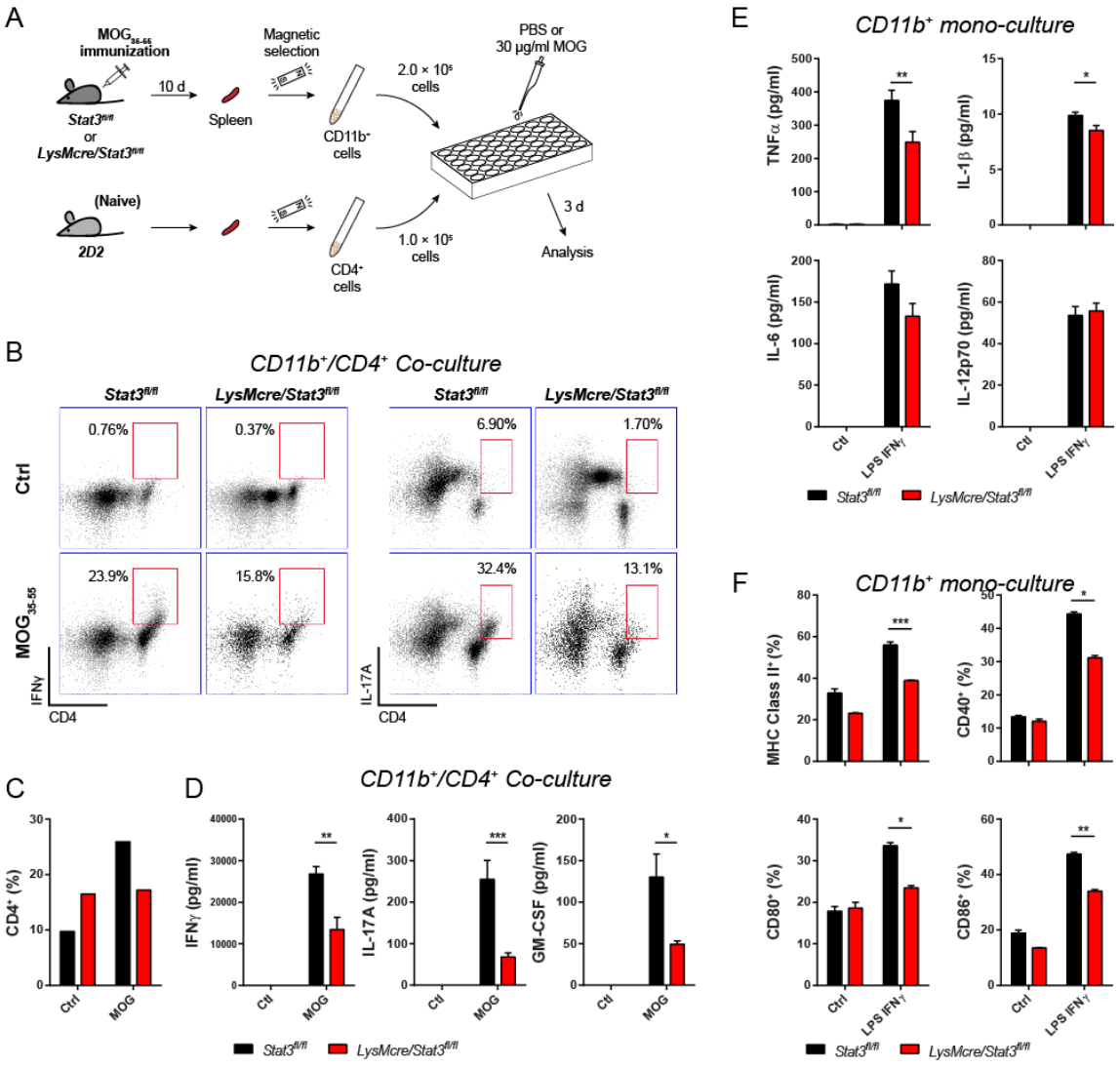

Figure 12. CD11b$^+$ myeloid cells from *LysMcre/Stat3$^{fl/fl}$* mice exhibit impaired capability to differentiate CD4$^+$ T-cells *ex vivo*. A-D, *Stat3$^{fl/fl}$* and *LysMcre/Stat3$^{fl/fl}$* mice were immunized with MOG_{35-55}, but PT was not administered. After 9-10 days, CD11b$^+$ cells from spleens of immunized *Stat3$^{fl/fl}$* and *LysMcre/Stat3$^{fl/fl}$* mice as well as CD4$^+$ cells from naïve 2D2 mice were isolated with magnetic selection. CD11b$^+$ and CD4$^+$ cells were co-cultured at a 2:1 ratio in the presence of 30 µg/ml MOG_{35-55} for 2-3 days before the supernatant and cells were harvested and analyzed. Cells from 3 *Stat3$^{fl/fl}$* and 3 *LysMcre/Stat3$^{fl/fl}$* mice were pooled and cultured in triplicates. **A**, The experimental design was depicted in a diagram. **B**, Number of IFNγ- and IL-17A-producing T-cells at div 2 were analyzed with intracellular staining and flow cytometry. Numbers next to red boxes indicate percentage of IFNγ$^+$ or IL-17A$^+$ of total CD4$^+$. **C**, Percentage of total CD4$^+$ cells at div 2 was analyzed with flow cytometry. **D**, Cytokine secretion from the co-culture at div 3 was analyzed with multiplex immunoassay. **E, F**, 2.0 × 10^5 CD11b$^+$ cells from the immunized mice were stimulated with 10 ng/ml LPS and 10 ng/ml IFNγ for 24 h. **E**, Expression of inflammatory cytokines was analyzed with multiplex immunoassay. **F**, Cells were stained with antibodies against MHC Class II, CD40, CD80, and CD86 and analyzed with flow cytometry. Data represent mean ± SEM. *$p < 0.05$, **$p < 0.01$, ***$p < 0.005$.

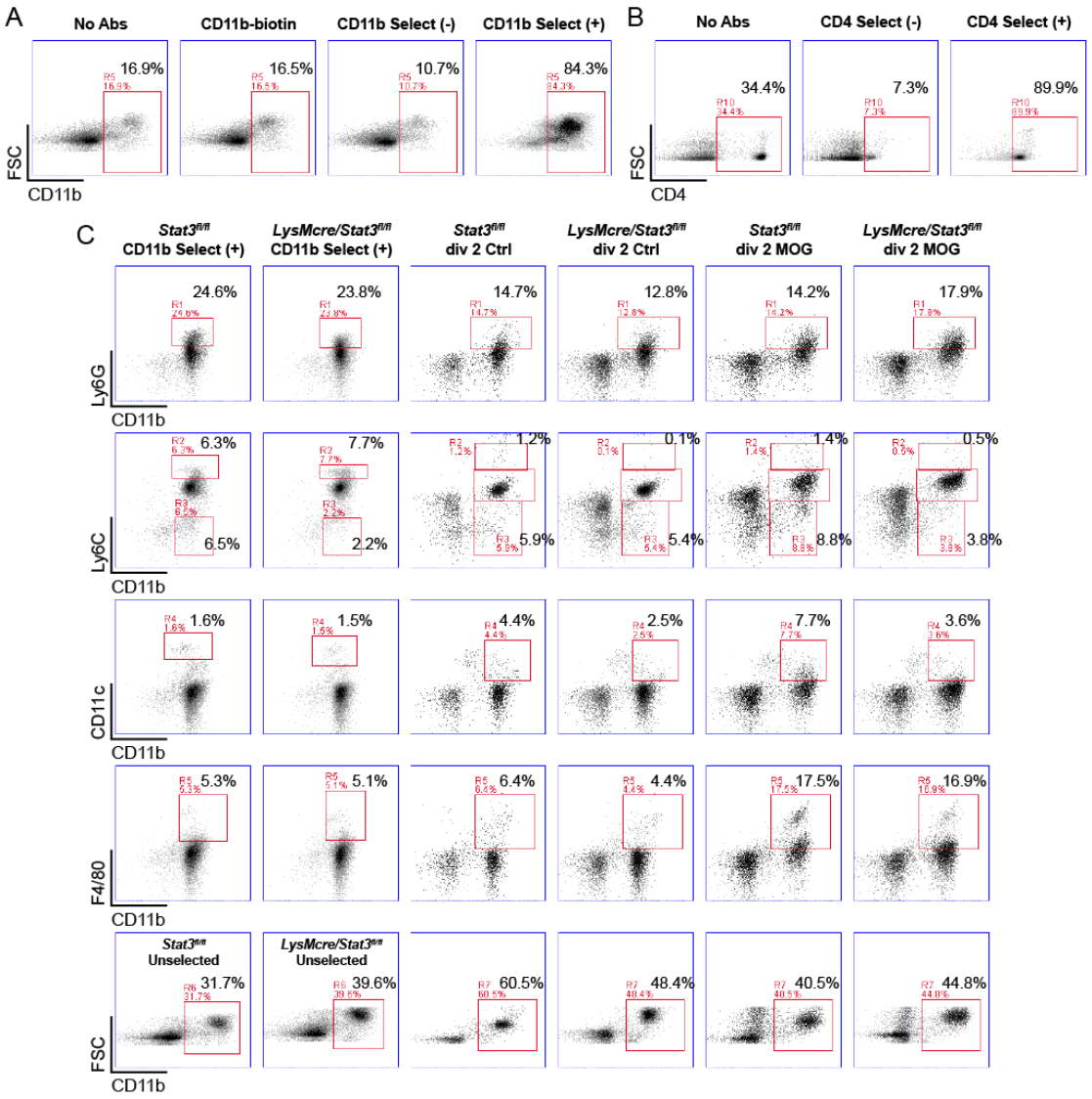

Figure 13. Efficiency and cell profile analysis of magnetic cell selection for the *ex vivo* co-culture experiment. $CD11b^+$ cells from splenocytes of immunized *Stat3*$^{fl/fl}$ and *LysMcre/Stat3*$^{fl/fl}$ mice as well as $CD4^+$ cells from naïve 2D2 mice were isolated with magnetic cell selection as described in the methods. **A, B**, Efficiency of selection was determined with staining of α-CD11b (**A**) or α-CD4 (**B**) and flow cytometry. **C**, Selected cells at div 0 as well as co-cultured cells at div 2 were stained with antibodies for various cells markers to investigate cell type differences.

To examine the capacity of $CD11b^+$ myeloid cells in activating and differentiating naïve 2D2 helper T-cells, we co-cultured them at ratio of 2:1 (myeloid:T-cells) for 2-3 days. After 2 days, the co- co-culture of mutant myeloid cells and 2D2 T-cells contained less total amount of $CD4^+$ T-cells as well as IFNγ-producing and IL-17A-producing T-cells compared to the co-culture of *Stat3*$^{fl/fl}$ myeloid cells and 2D2 T-cells (Figure 12B, C). At div 3, the co-culture of mutant myeloid cells and 2D2 T-cells secreted significantly less IFNγ, IL-17A, and GM-CSF than the co-culture of *Stat3*$^{fl/fl}$ myeloid cells and 2D2 T-cells (Figure 12D). We also saw decreased expression of many other inflammatory mediators including IL-4, TNFα, IL-1β, IL-6, IL-12, IL-18, IL-23, MIP-1a, and RANTES (Figure 14B). When *LysMcre/Stat3*$^{fl/fl}$ $CD11b^+$ splenocytes were cultured alone, we found a small decrease in the secretion of TNFα and IL-1β (Figure 12E). However, IL-6 and IL-12, the important cytokines for development of T_H17 and T_H1, respectively, were not significantly different (Figure 12E). We also saw decreased expression of IL-17A, MIP-1a, and RANTES, but not IL-4, IL-10, IL-18, IL-23, or IP-10 (Figure 14B). Interestingly, MCP-1 was increased in *LysMcre/Stat3*$^{fl/fl}$ $CD11b^+$ mono-culture (Figure 14C). These changes are unlikely to be due to differences in cell viability, as there was no significant difference in percentage of PI^+ cells (Figure 14A). While the change in cytokine expression in $CD11b^+$ mono-culture alone may not be sufficient to account for the impaired adaptive immune responses, we examined the antigen presenting and co-stimulatory molecules and found that *LysMcre/Stat3*$^{fl/fl}$ myeloid cells expressed significantly less MHC Class II, CD40, CD80, and CD86 upon LPS and IFNγ stimulation (Figure 12F). The decrease of expression in MHC Class II

and co-stimulatory molecules is likely responsible for the decreased T-cells responses in the co-culture, which in turn failed to provide enough positive feedback loop to the myeloid cells and resulted in decreased secretion of many other cytokines.

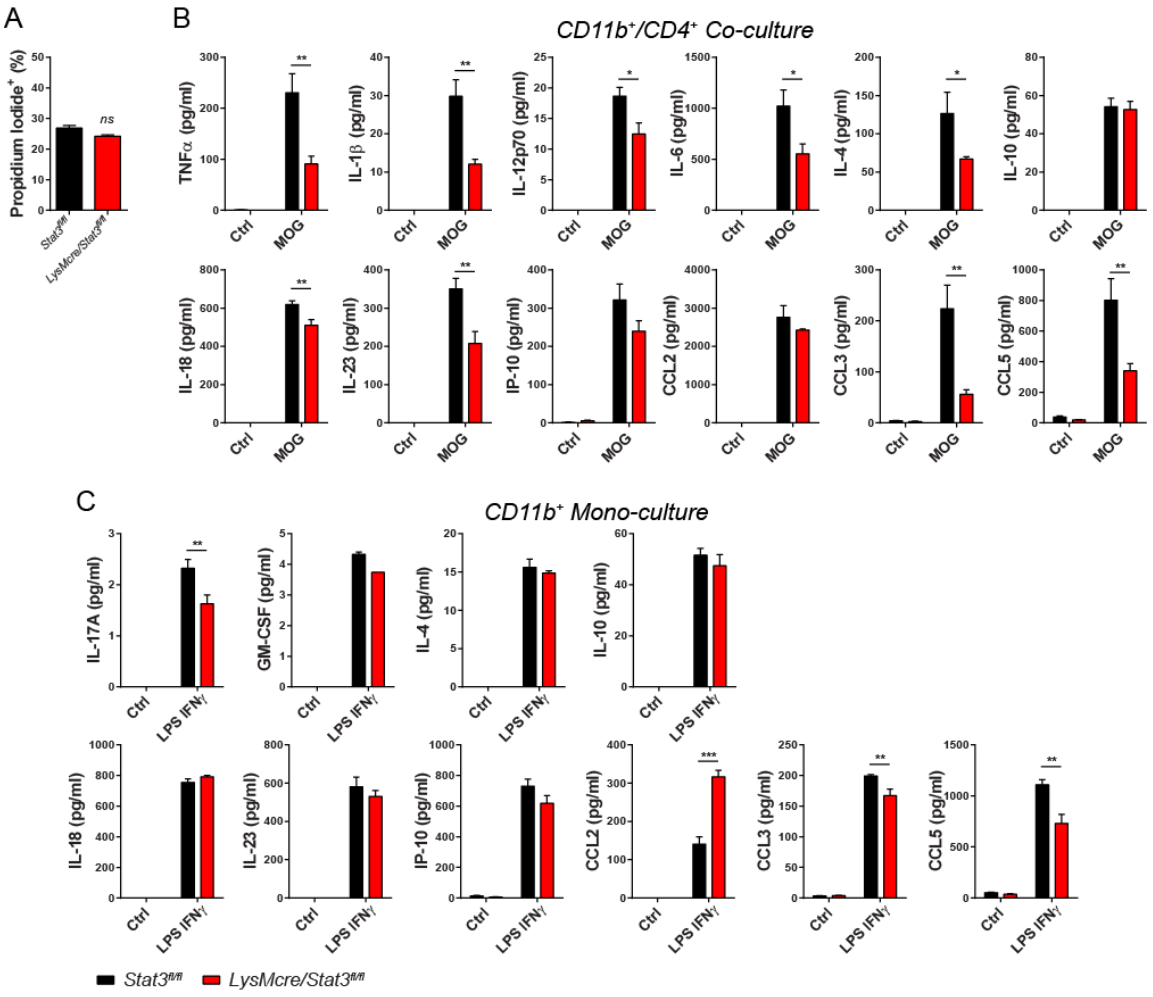

Figure 14. Cytokine analysis of the *ex vivo* CD11b$^+$/CD4$^+$ co-culture and CD11b$^+$ mono-culture. A, Cell viability of the CD11b$^+$ mono-culture stimulated with 10 ng/ml LPS and 10 ng/ml IFNγ for 24 h was evaluated with propidium iodide and flow cytometry. **B**, **C**, Cytokine expression of the CD11b$^+$/CD4$^+$ co-culture after MOG_{35-55} stimulation for 2 d (**B**) and the CD11b$^+$ mono-culture after LPS and IFNγ stimulation for 24 h (**C**) was measured by multiplex immunoassay. *Stat3$^{fl/fl}$*, $n = 3$. *LysMcre/Stat3$^{fl/fl}$*, $n = 3$ (technical replicates). Data represent mean ± SEM. *$p < 0.05$, **$p < 0.01$, ***$p < 0.005$.

Stat3 deletion in the peritoneal macrophages was previously reported to cause enhanced pro-inflammatory responses [124] due to its role in signaling IL-10 anti-inflammatory responses [122]. To further characterize STAT3-mediated immune responses of macrophages, we prepared BMDMs from bone marrow of *Stat3*$^{fl/fl}$ and *LysMcre/Stat3*$^{fl/fl}$ mice (Figure 15). The differentiation and maturity of BMDMs were first evaluated by flow cytometric analysis of cell surface expression of CD11b and F4/80 after 7 days of culture. Both *Stat3*$^{fl/fl}$ and *LysMcre/Stat3*$^{fl/fl}$ bone marrow cell cultures were mostly mature macrophages (92.8% and 95.7%, respectively; Figure 15A). When stimulated with IFNγ, *LysMcre/Stat3*$^{fl/fl}$ BMDMs expressed less CD40 and CD80, but more MHC Class II compared to *Stat3*$^{fl/fl}$ BMDMs (Figure 15B). *LysMcre/Stat3*$^{fl/fl}$ BMDMs also expressed more pro-inflammatory mediators, *e.g.*, TNFα, IL-1β, IL-6, IL-12, and MCP-1, at both mRNA (Figure 15C) and protein level (Figure 15D) upon stimulation with LPS. When co-cultured with pre-differentiated 2D2 T_H1 and T_H17 cells, the co-cultures secreted comparable amounts of IFNγ and IL-17A between the genotypes (Figure 15E). Our results confirmed the previous finding that *Stat3*-deficient macrophages exhibit enhanced innate immune responses [124]. However, our results also revealed that cultured BMDMs did not recapitulate the immune responses of myeloid cells that are acutely isolated from MOG-immunize mice (Figure 12 and Figure 14) and further underscore the importance of examining *Stat3*-dependent immune responses *in vivo*.

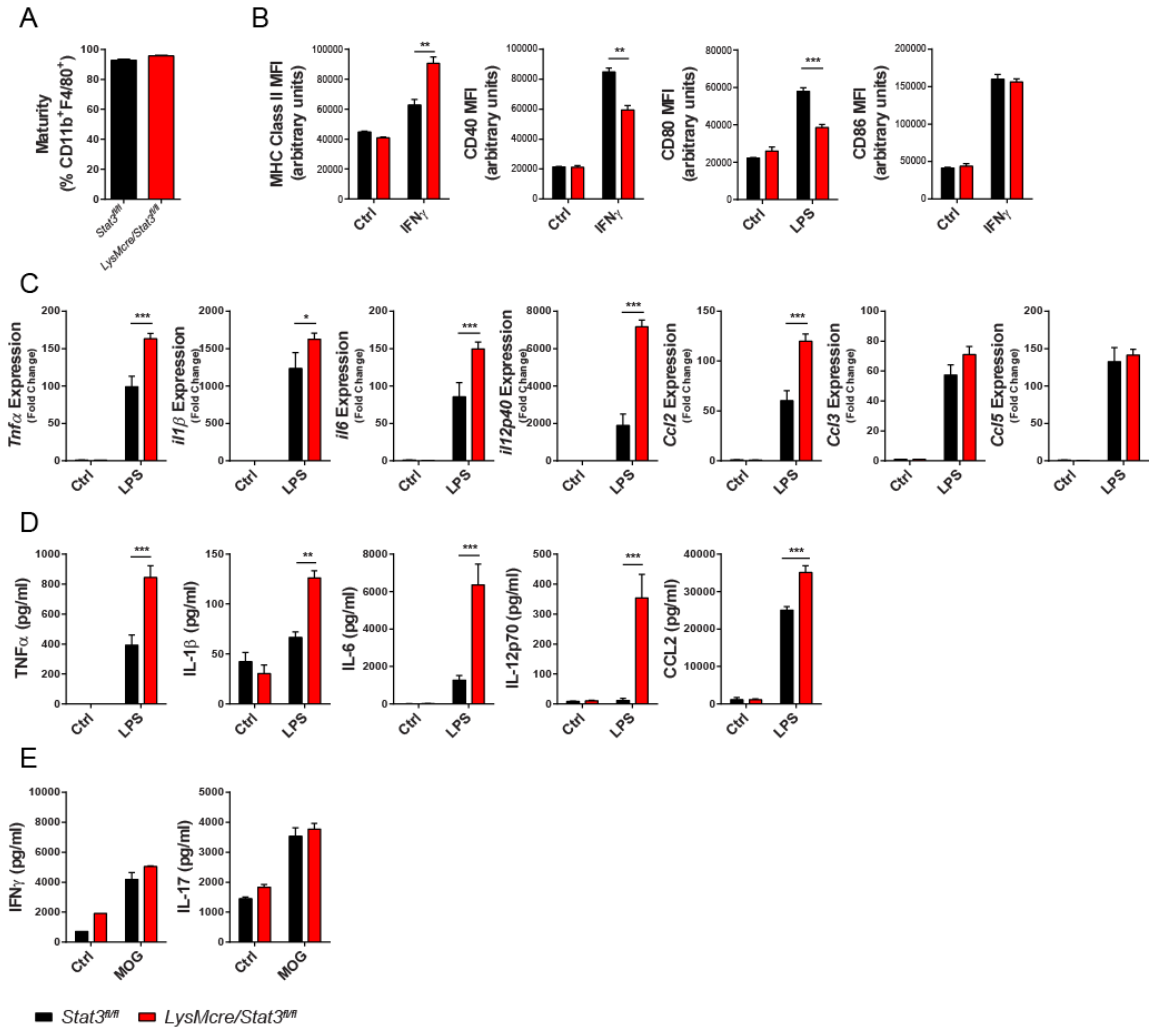

Figure 15. *LysMcre/Stat3$^{fl/fl}$* BMDMs exhibited enhanced proinflammatory responses. BMDMs were developed from bone marrow cells in the presence of L929 conditioned medium as described in the methods. **A**, Cell maturity was evaluated by staining with α-CD11b and α-F4/80 after 7 days of culturing. *Stat3$^{fl/fl}$*, *n* = 3. *LysMcre/Stat3$^{fl/fl}$*, *n* = 3. **B**, BMDMs were stimulated with 10 ng/ml IFNγ for 24 h, and then stained with α-MHC Class II, α-CD40, α-CD80, and α-CD86 and analyzed with flow cytometry. *Stat3$^{fl/fl}$*, *n* = 2. *LysMcre/Stat3$^{fl/fl}$*, *n* = 2. **C**, BMDMs were stimulated with 10 ng/ml LPS for 5 hr. Expression of cytokine mRNA was measured by quantitative RT-PCR. *Stat3$^{fl/fl}$*, *n* = 3. *LysMcre/Stat3$^{fl/fl}$*, *n* = 3. **D**, BMDMs were stimulated with 10 ng/ml LPS for 24 h. Cytokine secretion into the supernatant was measured by ELISA. *Stat3$^{fl/fl}$*, *n* = 3. *LysMcre/Stat3$^{fl/fl}$*, *n* = 3. **E**, BMDMs were co-cultured with *in vitro* pre-differentiated T_H1 or T_H17 cells for 1 d (T_H1) or 3 d (T_H17). Secretion of cytokines was measured by ELISA. *Stat3$^{fl/fl}$*, *n* = 2. *LysMcre/Stat3$^{fl/fl}$*, *n* = 2. Data represent mean ± SEM. **p* < 0.05, ***p* < 0.01, ****p* < 0.005.

2.3.7 LysMcre/Stat3$^{fl/fl}$ Mice Are Only Partially Resistant to Passive EAE by Adoptive Transfer

Our data so far suggest that impaired $CD4^+$ T-cell differentiation underlies the resistance of *Stat3*-mutant mice to MOG_{35-55}-induced active EAE. STAT3, however, is involved in many cellular processes. As such, in addition to facilitating T-cell differentiation, myeloid STAT3 activation could potentially contribute to the development of EAE through other mechanisms. To further investigate whether impaired T-cell differentiation is indeed the major contributing factor to the resistance of *LysMcre/Stat3$^{fl/fl}$* mice to active EAE, we induced EAE by adoptive transfer of lymphocytes isolated from C57BL/6 EAE mice, therefore bypassing the requirement of generating endogenous differentiated T-cells (Figure 16). After isolating and culturing the cells from draining LNs from donor mice for 4 days, the donor cell population is primarily B-cells, $CD4^+$ T-cells, and $CD8^+$ T-cells (Figure 17A). Of the $CD4^+$ T-cells, 46.6% and 32.4% were IFNγ-secreting T_H1 cells and IL-17A-secreting T_H17 cells, respectively (Figure 17B). In contrast to active EAE (Figure 6), two thirds of the *LysMcre/Stat3$^{fl/fl}$* mice developed passive EAE after receiving the encephalitogenic T-cells (Figure 18A). *LysMcre/Stat3$^{fl/fl}$* mice exhibited significantly lower clinical scores on average at the peak of disease (Figure 18B). The *LysMcre/Stat3$^{fl/fl}$* mice generally showed less CNS-infiltrating leukocytes in comparison to littermate controls. However, the differences were not statistically significant (Figure 18C). In addition, there was no significant difference in mRNA expression of any of the cytokines tested in the spinal cord (Figure 18D). *Stat3$^{fl/fl}$* and *LysMcre/Stat3$^{fl/fl}$* mice of comparable EAE clinical

scores also exhibited similar extent of inflammation as determined by immunofluorescence in the spinal cord sections (Figure 18E, F). Taken together, *LysMcre/Stat3*$^{fl/fl}$ mice developed less severe adoptive transfer EAE on average than *Stat3*$^{fl/fl}$ mice due to lower onset rate, but are nevertheless susceptible to EAE when passively induced by adoptive transfer of encephalitogenic T-cells.

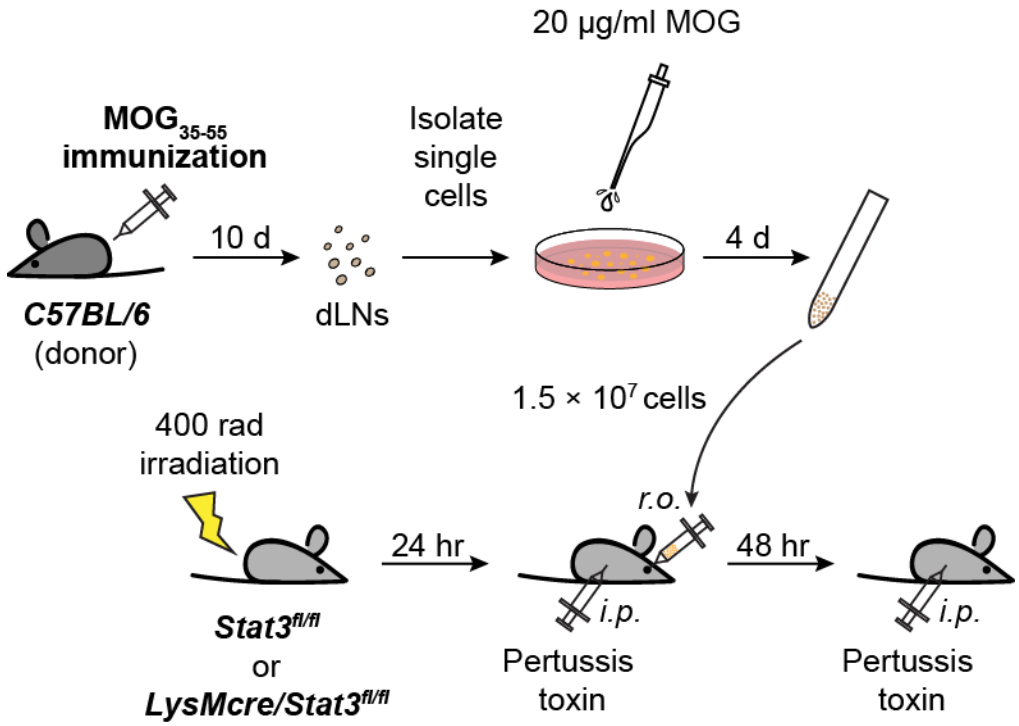

Figure 16. Schematic of passive induction of EAE by adoptive transfer of encephalitogenic lymphocytes.

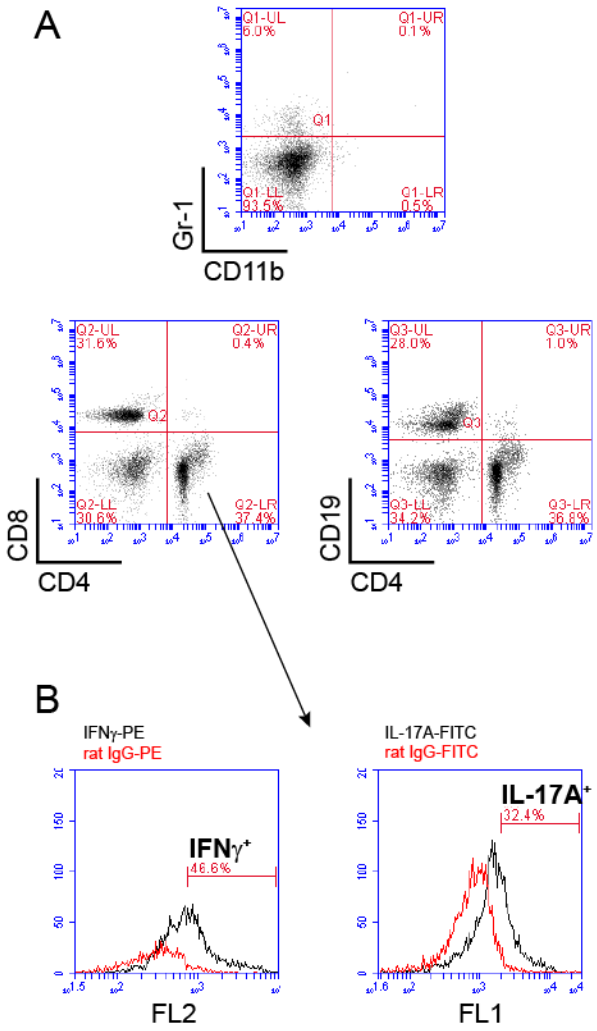

Figure 17. Donor cells for adoptive transfer EAE consist primarily of lymphocytes. Donor C57BL/6 mice were immunized with $MOG_{35.55}$. After 9-10 days, cells from the draining LNs were isolated from the mice and cultured in the presence of 20 µg/ml MOG_{35-55} for 4 d. **A**, Cell profile after 4 days of culturing was analyzed with flow cytometry. **B**, Protein transport was blocked with Brefeldin A for the last 5 h of culturing. the percentage of T_H1 and T_H17 cells was analyzed with flow cytometry using IgG control (rat IgG-PE and rat IgG-FITC) as baseline.

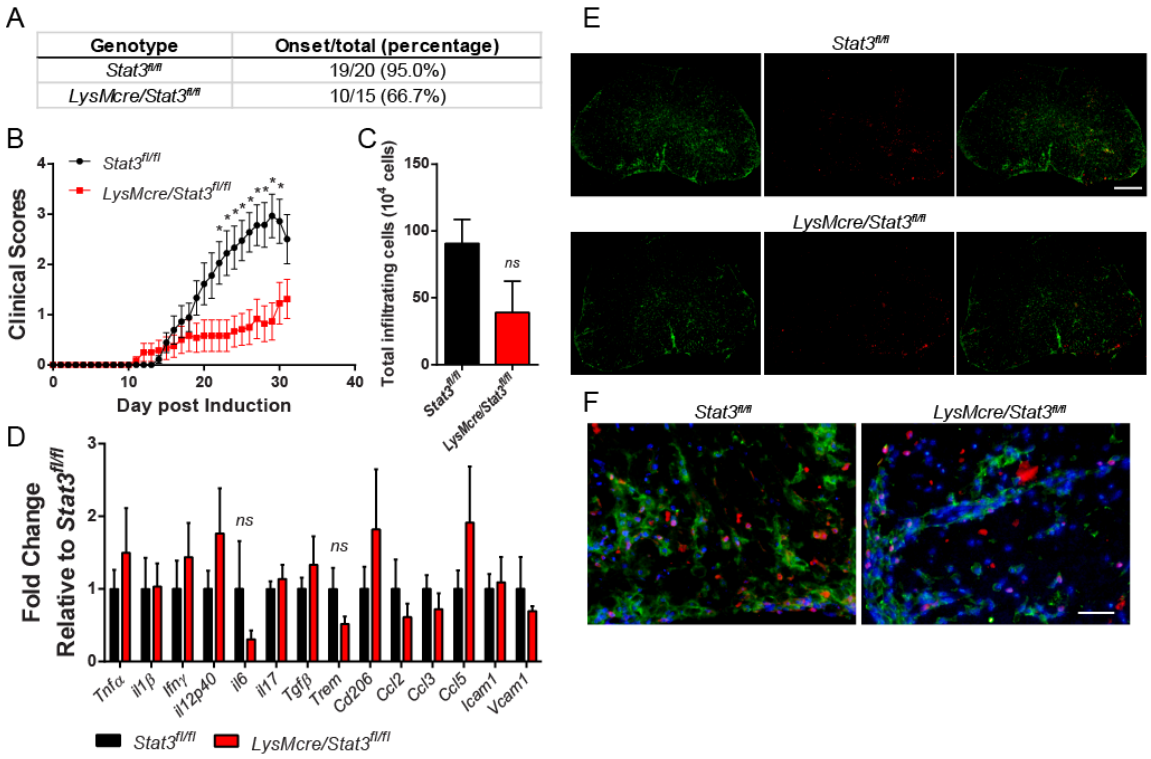

Figure 18. *LysMcre/Stat3$^{fl/fl}$* mice are partially resistant to passive induction of EAE by adoptive transfer. A, B, T-cell adoptive transfer EAE was induced in *Stat3$^{fl/fl}$* (n = 20) and *LysMcre/Stat3$^{fl/fl}$* (n = 15) mice, and the clinical score was assessed daily as described in the methods. **A**, Table of onset rate. **B**, Clinical scores up to 31 dpi. Data represent mean ± SEM. *$p < 0.05$. **C,** CNS infiltrating leukocytes were isolated from *Stat3$^{fl/fl}$* (n = 3) and *LysMcre/Stat3$^{fl/fl}$* (n = 3) mice at 30 dpi and counted with a hemacytometer. Data represent mean ± SEM. **D**, Expression of cytokine mRNA in SC from 35 dpi mice (*Stat3$^{fl/fl}$*, n = 6; *LysMcre/Stat3$^{fl/fl}$*, n = 5) were determined with quantitative RT-PCR. Data represent fold expression compared to *Stat3$^{fl/fl}$*. Data represent mean ± SEM. **E, F,** Spinal cord cryosections from mice at 36 dpi were stained with α-Iba-1 (green), α-CD3 (red), and Hoechst. Scale bar (**E**), 200 µm. Scale bar (**F**), 25 µm.

2.3.8 STAT3 in the Peripheral Myeloid Cells, but Not in Microglia, Is Important for the Development of Active EAE

It's been shown that microglia exhibit different accumulation kinetics and gene expression than infiltrating monocytes during EAE [141]. During the resolving phase of EAE, it has been reported that infiltrating monocytes gradually vanish, whereas microglia return to the quiescent state [142]. These findings suggest that microglia may function differently than monocytes during EAE. To investigate whether STAT3 in microglia contributed to the EAE resistance in *LysMcre/Stat3*$^{fl/fl}$ mice, we utilized the fact that microglia are radio-resistant and created BM chimeric mice by transferring donor BM into irradiated recipient mice (Figure 19A). We first tested the percent of engraftment using C57BL/6 CD45.2 mice receiving C57BL/6 CD45.1 congenic mouse BM (Figure 19B). 6 weeks after transplantation, roughly 85.7% splenocytes possess the donor CD45.1 marker (Figure 19B). Because irradiation may potentially damage the BBB, causing donor cells to move in the CNS and exhibit microglia-like phenotypes, we tested this by transferring *LysMcre/rosa26-Ai14* BM into irradiated C57BL/6 mice (Figure 19C). 6 weeks after transplantation, SC sections from the naïve mice contain a few red fluorescent donor cells at the meninges, but not in the CNS parenchyma (Figure 19C). These results demonstrated that the bone marrow chimeric mice exhibit high bone marrow replacement efficacy but minimal invasion of donor cells to the CNS after engraftment, making these mice suitable for investigation of CNS-only or periphery-only genetic effects.

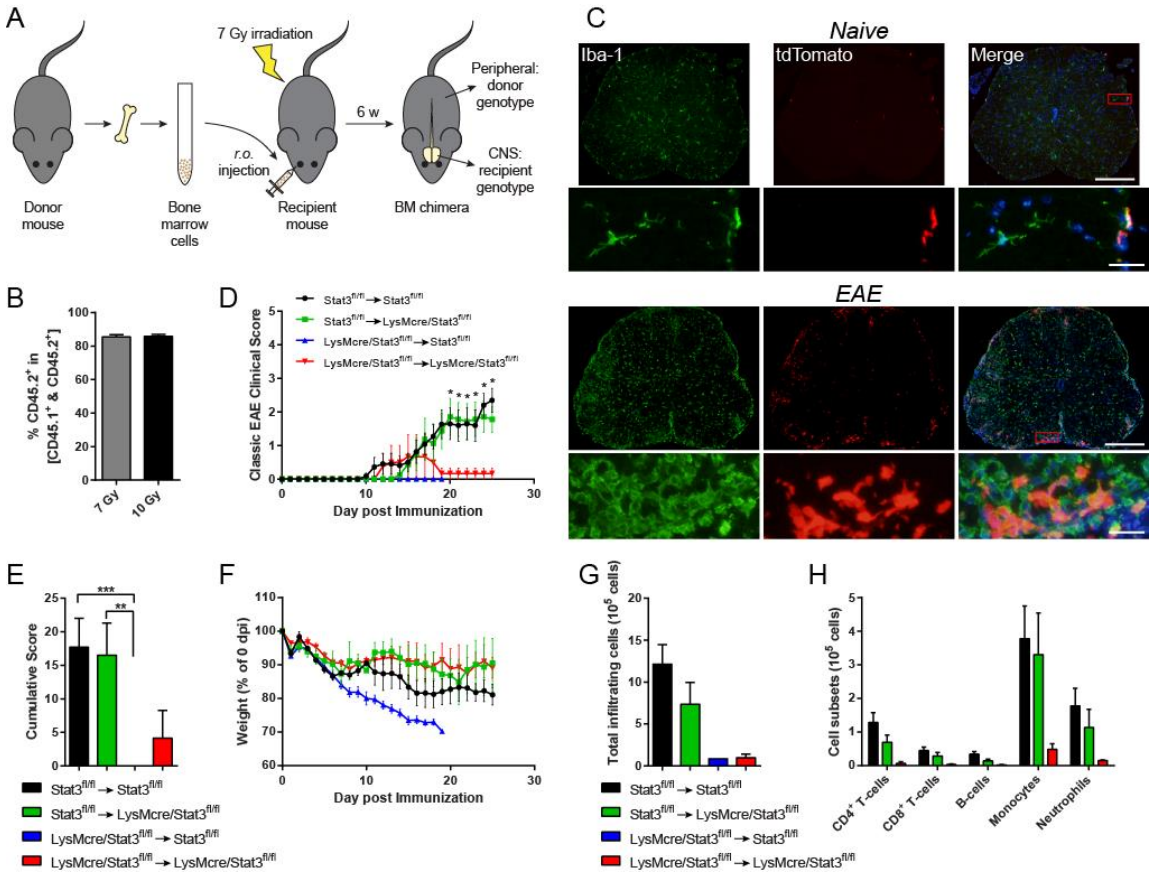

Figure 19. STAT3 in peripheral myeloid cells, but not microglia, is the major contributor to EAE pathogenesis. A, BM chimeric mice were generated by transferring BM cells from donor mice to lethally irradiated recipient mice. **B**, Engraftment efficiency was tested in CD45.2 mice that were irradiated with either 700 or 1000 rad and received BM from CD45.1 congenic mice (CD45.1 → CD45.2). 4 weeks after transplantation, splenocytes from CD45.1 → CD45.2 mice were stained with α-CD45.1 and α-CD45.2 and analyzed with flow cytometry. 700 rad, $n = 4$, 1000 rad, $n = 8$. **C**, C57BL/6 mice were subject to 1000 rad irradiation and received BM from *LysMcre/rosa26-Ai14* mice (*LysMcre/rosa26-Ai14* → C57BL/6). Active EAE was induced 6 weeks after transplantation. Spinal cord sections from EAE mice at 21 dpi (EAE) or unimmunized mice at 9-week post transplantation (naïve) were stained with α-Iba-1 (green). **D-H**, Active EAE was induced in BM chimeric mice 6-week post transplantation and assessed daily. *Stat3*$^{fl/fl}$ → *Stat3*$^{fl/fl}$, $n = 11$; *Stat3*$^{fl/fl}$ → *LysMcre/Stat3*$^{fl/fl}$, $n = 8$; *LysMcre/Stat3*$^{fl/fl}$ → *Stat3*$^{fl/fl}$, $n = 11$; *LysMcre/Stat3*$^{fl/fl}$ → *LysMcre/Stat3*$^{fl/fl}$, $n = 4$. **D**, Clinical scores. **E**, Cumulative scores up to 25 dpi. **F**, Weight change. **G, H**, CNS infiltrating leukocytes were isolated from mice at 26 dpi and analyzed with flow cytometry. Data represent mean ± SEM. $*p < 0.05$, $**p < 0.01$, $***p < 0.005$.

Next, we induced active EAE in the four groups of BM chimeric mice (Figure 19D-H). *Stat3*$^{fl/fl}$ mice that received *LysMcre/Stat3*$^{fl/fl}$ BM (*LysMcre/Stat3*$^{fl/fl}$ → *Stat3*$^{fl/fl}$), which possess normal microglia but STAT3-deficient peripheral myeloid cells, did not

develop EAE (Figure 19D, E), demonstrating the essential role of STAT3 activation in peripheral myeloid cells in the development of EAE. Conversely, *LysMcre/Stat3*$^{fl/fl}$ mice that received wildtype BM (*Stat3*$^{fl/fl}$ → *LysMcre/Stat3*$^{fl/fl}$), which possess STAT3-deficient microglia but normal peripheral myeloid cells, developed EAE with the severity indistinguishable from that of *Stat3*$^{fl/fl}$ → *Stat3*$^{fl/fl}$ mice (Figure 19D, E). The number of CNS-infiltrating leukocytes was comparable between wildtype mice that received wildtype BM (*Stat3*$^{fl/fl}$ → *Stat3*$^{fl/fl}$) and *Stat3*-mutant mice that received wildtype BM (*Stat3*$^{fl/fl}$ → *LysMcre/Stat3*$^{fl/fl}$), whereas wildtype mice that received *Stat3*-mutant BM (*LysMcre/Stat3*$^{fl/fl}$ → *Stat3*$^{fl/fl}$) had lower number of CNS-infiltrating cells than the other two groups (Figure 19G, H). These data suggest that STAT3 activation in the peripheral myeloid compartment, but not in the CNS compartment, is critical for the development of EAE.

Because *LysM*-driven Cre recombination occurs in roughly a third of the microglia population *in vivo* as determined by flow cytometric analysis of CNS mononuclear cells from reporter mice (Figure 5C), our above findings with BM chimeric mice (Figure 19) do not completely exclude the possible contribution of microglial STAT3. Therefore, we generated new *Stat3* conditional mice, employing a newly available line (*Cx3cr1creER*) that allows effective and selective gene targeting of microglial cells [137].

We first tested the efficiency of *Cx3cr1*-driven Cre recombination by crossing to *rosa26-Ai14* line (Figure 20A). One week after tamoxifen administration, 13.4% and 77.9% of circulating granulocytes and Ly6C^{hi} monocytes, respectively, were tdTomato

positive (Figure 20B, C). 4 weeks after administration, only microglia were mostly tdTomato^{+} (96.9%), whereas expression in circulating myeloid cells have significantly decreased (Figure 20B, C), making these mice a more suitable model to study microglia.

When we induced active EAE in *Stat3$^{fl/fl}$* and *Cx3cr1-creER/Stat3$^{fl/fl}$* mice 4 weeks after tamoxifen administration, the clinical scores did not significantly differ between the two groups (Figure 20D, E). There were also no major differences in the cytokine mRNA expression from SC from EAE mice (Figure 20F). We also attempted to characterize the immune functions of STAT3-deficient microglia *in vitro* (Figure 21). *LysMcre/Stat3$^{fl/fl}$* pure primary microglia did not differ in the secretion of TNFα (Figure 21A). There were also no differences in TNFα, IL-1β, IL-6, IL-12, CCL2, CCL3, or CCL5 in *LysMcre/Stat3$^{fl/fl}$* primary mixed glial culture (Figure 21B, C). *Cx3cr1-creER/Stat3$^{fl/fl}$* primary pure microglia did not differ in TNFα and IL-6 (Figure 21D). In *Cx3cr1-creER/Stat3$^{fl/fl}$* primary mixed glial culture, there was an increase in TNFα, but not other cytokines tested (Figure 21E, F). Taken together, STAT3 in microglia is unlikely to have an important role in EAE.

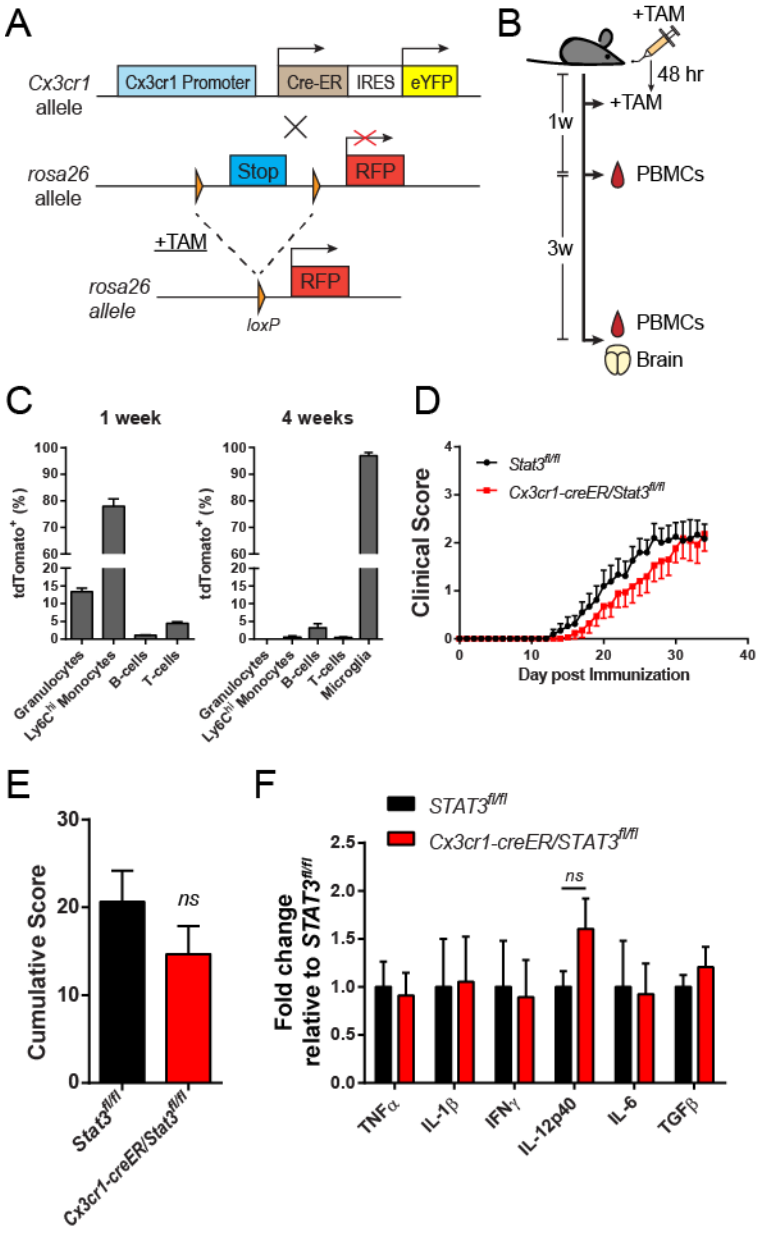

Figure 20. STAT3 in microglia is not critical in pathogenesis of EAE. A, Cx3cr1 -driven Cre recombination upon tamoxifen administration splices the Stop codon in the *rosa26-Ai14* construct, enabling the expression of RFP. **B, C**, *Cx3cr1-creER/rosa26-Ai14* mice (n = 3) were administered with two doses of tamoxifen by oral gavage 48 h apart at age of 5 weeks. Expression of tdTomato reporter from PBMCs 1 week and 4 weeks after as well as in CNS mononuclear cells 4 weeks after was analyzed with flow cytometry. Granulocytes, $CD11b^{+}Gr\text{-}1^{+}$; $Ly6C^{hi}$ monocytes, $CD11b^{+}Ly6C^{hi}$; T-cells, $CD3^{+}$; B-cells, $CD19^{+}$; Microglia, $CD11b^{+}CD45^{int}$. **C-E**, *Cx3cr1-creER/Stat3*$^{fl/fl}$ (n = 17) and littermate *Stat3*$^{fl/fl}$ mice (n = 21) were administered with tamoxifen at age of 5 weeks. Active EAE was induced 4 weeks after and assessed daily. **C**, Clinical scores. **D**, Cumulative scores up to 30 dpi. **E**, Cytokine mRNA expression from SC tissue at 30 dpi (*Stat3*$^{fl/fl}$, n = 8; *Cx3cr1-creER/Stat3*$^{fl/fl}$, n = 6) was analyzed with quantitative RT-PCR. Data represent fold expression compared to *Stat3*$^{fl/fl}$. Data represent mean ± SEM.

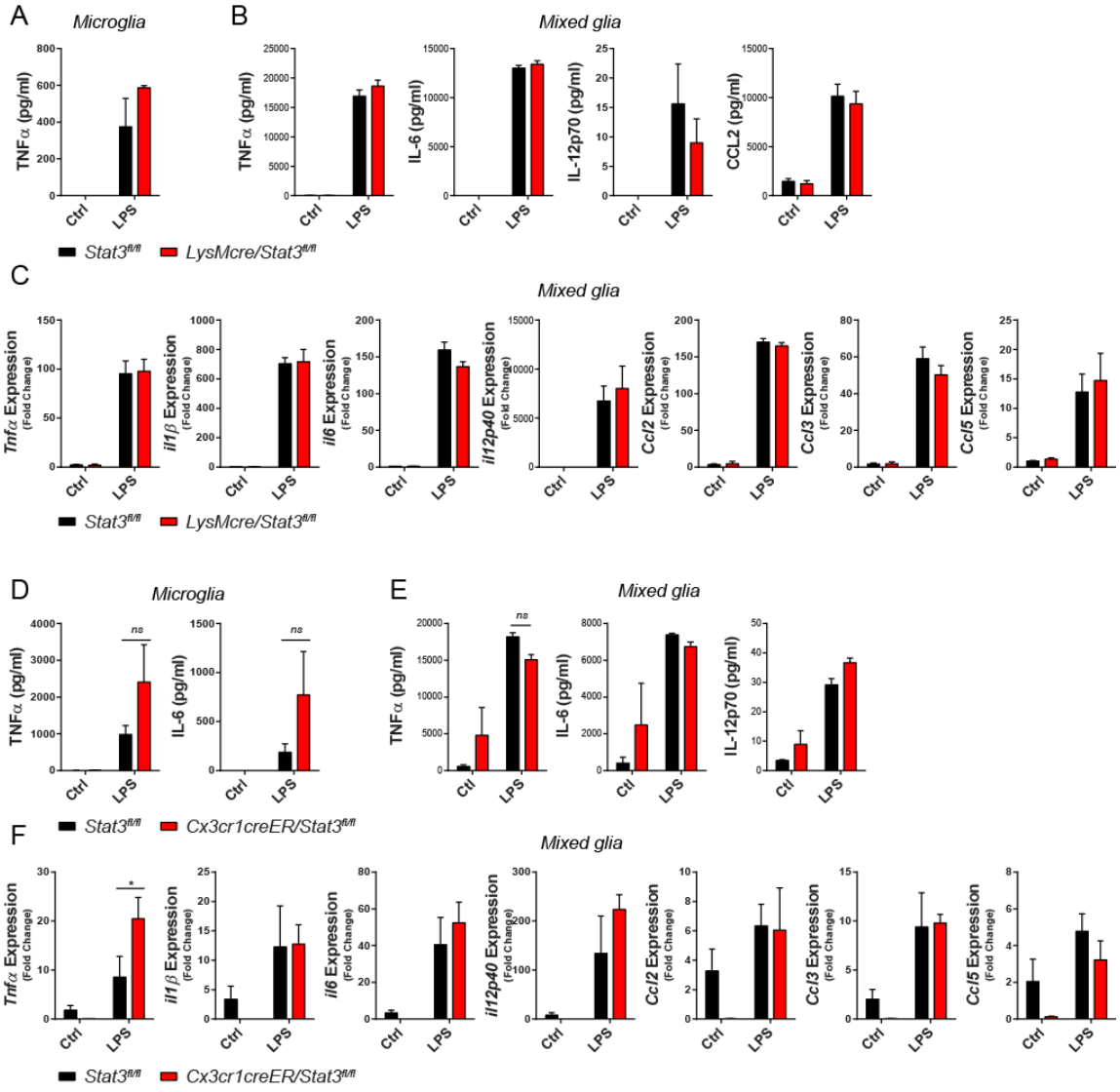

Figure 21. Innate immune responses in primary microglia and mixed glial cultures. A, Primary microglia from *Stat3*$^{fl/fl}$ (n = 2) and *LysMcre/Stat3*$^{fl/fl}$ (n = 2) was stimulated with 10 ng/ml LPS for 24 hr. TNFα secretion was measured by ELISA. **B, C**, Primary mixed glia from *Stat3*$^{fl/fl}$ (n = 5) and *LysMcre/Stat3*$^{fl/fl}$ (n = 4) was stimulated with 10 ng/ml LPS for 24 hr (**B**) or 5 hr (**C**). **B**, Cytokine secretion was measured by ELISA. **C**, Cytokine mRNA expression was determined by qRT-PCR. **D**, Primary microglia from *Stat3*$^{fl/fl}$ (n = 2) and *Cx3cr1creER/Stat3*$^{fl/fl}$ (n = 2) was stimulated with 10 ng/ml LPS for 24 hr. TNFα and IL-6 secretion was measured by ELISA. **E, F**, Primary mixed glia from *Stat3*$^{fl/fl}$ (n = 5) and *Cx3cr1creER/Stat3*$^{fl/fl}$ (n = 3) was stimulated with 10 ng/ml LPS for 24 hr (**E**) or 5 hr (**F**). **E**, Cytokine secretion was measured by ELISA. **F**, Cytokine mRNA expression was determined by quantitative RT-PCR. Data represent mean ± SEM. *$p < 0.05$.

2.4 Discussion

In this section, we demonstrate that STAT3 in peripheral myeloid cells is essential in the development of CNS pathologies in an animal model of MS. We show that conditional deletion of *Stat3* in myeloid cells using *LysMcre/Stat3*$^{fl/fl}$ mice results in resistance to MOG_{35-55}-induced EAE in C57BL/6 mice (Figure 6). *LysMcre/Stat3*$^{fl/fl}$ mice exhibit diminished helper T-cell immune functions during the pre-clinical and onset stages of the disease when compared to *Stat3*$^{fl/fl}$ mice (Figure 8). Myeloid cells isolated from immunized *LysMcre/Stat3*$^{fl/fl}$ mice fail to differentiate naïve 2D2 $CD4^+$ T-cells and expressed less antigen presenting and co-stimulatory molecules (Figure 12). Passively inducing EAE by adoptive transfer of autoreactive T-cells, thereby bypassing the need to differentiate endogenous $CD4^+$ T-cells, renders *LysMcre/Stat3*$^{fl/fl}$ mice partially susceptible (Figure 18). In contrast to peripheral STAT3, microglial STAT3 does not have a significant role in EAE pathogenesis (Figure 19, Figure 20).

Stat3 dys-regulation has been implicated in many cancer studies, and several of its inhibitors has been in use or on clinical trials [143, 144]. *Stat3* in monocytes is also shown to be up-regulated in rheumatoid arthritis [145], which is also an autoimmune disease and suggest its close relationship with autoimmunity. *LysMcre/Stat3*$^{fl/fl}$ BMDMs exhibited enhanced proinflammatory responses in our study, consistent with the finding that Stat3 signals IL-10 anti-inflammatory responses in myeloid cells [122, 146-148]. STAT3 has also been shown to be a negative regulator of DC functions and decrease MHC II expression in DCs [149, 150]. The enhanced proinflammatory response in the absence of its negative feedback could, in theory, cause more severe pathologies in

autoimmune diseases. Our results, however, indicated otherwise in autoimmune demyelination disease. Not only *LysMcre/Stat3*$^{fl/fl}$ mice are resistant to active EAE, the myeloid cells isolated from immunized *LysMcre/Stat3*$^{fl/fl}$ mice also failed to differentiate T-cells. It is possible that the *in vitro* derived BMDMs and BMDCs, albeit widely utilized by many studies, are intrinsically less relevant and the results from the experiments using these cells do not translate well in *in vivo* conditions, where the responses from the cells are the net result of many more stimulants and environmental factors.

In this study, we demonstrated that STAT3 is involved in the expression of antigen presenting and co-stimulatory molecules in the APCs, which participate in the differentiation of encephalitogenic T-cells during MOG-induced EAE (Figure 22). It is important to bear in mind, however, that *Stat3* is a gene with pleotropic functions [151]. It is possible that the resistance to EAE in *LysMcre/Stat3*$^{fl/fl}$ mice is a combined result from multiple pathways and in different cell types. When we induced EAE by adoptively transferring autoreactive $CD4^+$ T-cells, thereby bypassing the requirement to differentiate and activate endogenous $CD4^+$ T-cells, *LysMcre/Stat3*$^{fl/fl}$ mice developed EAE although with lower severity than *Stat3*$^{fl/fl}$ mice, strongly suggesting the involvement of additional mechanisms. Neutrophils have been shown to be essential in the onset phase of EAE [152] without affecting $CD4^+$ T-cell differentiation. Although STAT3 possesses modulatory roles in neutrophil immune functions [153], studies also show that STAT3 signals G-CSF-induced expression of CXCL2 [154], and that bone marrow STAT3-deficient mice show impaired neutrophil mobilization [155]. Moreover,

deletion of SOCS3, a STAT3 inhibitor, in myeloid cells causes a more severe form of atypical EAE, and that is mainly mediated by neutrophils [114, 127]. Although we did not find a consistent difference in the number of circulating neutrophils in *LysMcre/Stat3*$^{fl/fl}$ mice, possible changes in their functions that are relevant to autoimmunity remain to be investigated.

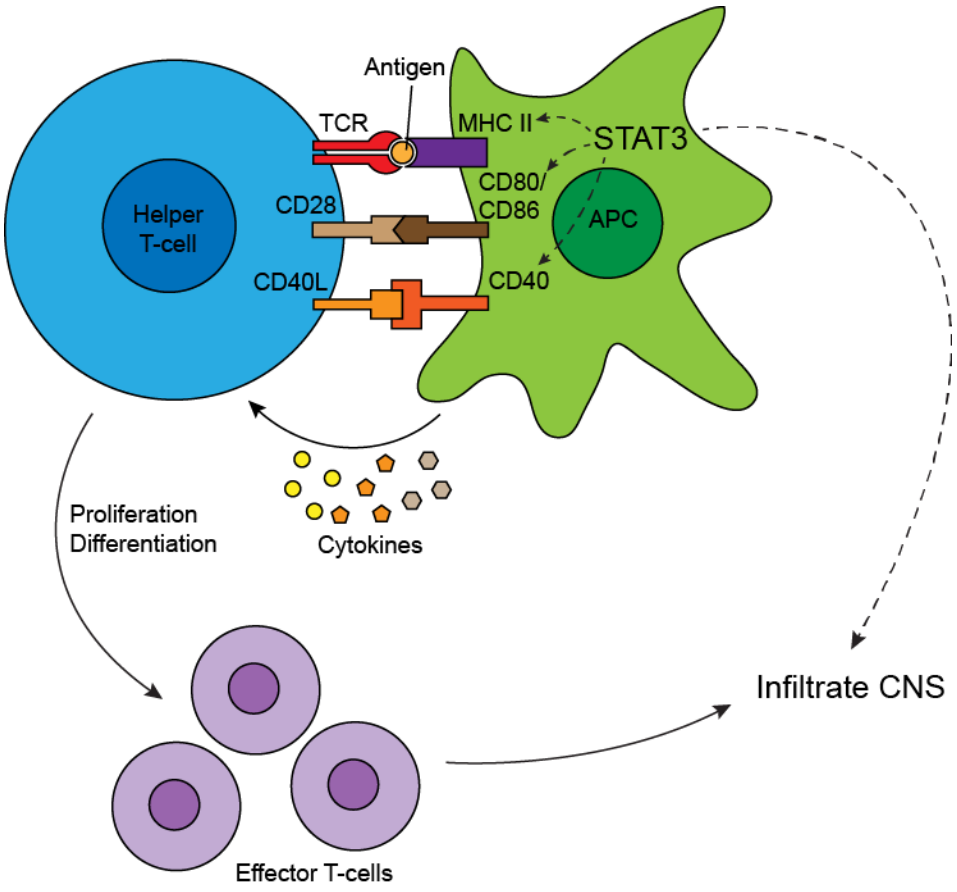

Figure 22. Proposed mechanism of myeloid STAT3 in EAE pathogenesis. Upon MOG_{35-55} immunization, STAT3 is involved in upregulation of MHC Class II, CD80, CD86, and CD40 on the cell surface of APCs. This facilitates the differentiation of encephalitogenic T-cells, leading to the development of EAE. Additionally, STAT3 may also be involved in myeloid cell functions independent of T-cell differentiation, thus contributing to EAE pathogenesis.

During EAE, leukocytes in the blood stream transmigrate across the blood-brain barrier into the CNS parenchyma to cause damage. Proteins of the matrix metalloproteinase (MMP) family, mainly secreted by myeloid cells [51], digest the extracellular matrix and facilitate the diapedesis [81, 82]. STAT3 is shown to be at least partially involved in MMP-2 and MMP-9 expression [128, 129], suggesting a possible role in facilitating cell diapedesis. However, studies investigating the effects of MMP knockouts yielded mixed results [83] presumably due to the fact that different MMPs can complement each other's functions. Therefore, the role of myeloid STAT3 in leukocyte transmigration requires further investigation.

We understand that most animal models with genetically modified mice are not perfect and ours is no exception. *LysMcre/Stat3*$^{fl/fl}$ mice and other similar lines were shown to develop spontaneous enterocolitis and the onset increases with age [124, 149, 156]. The inflamed gastrointestinal tract will likely disrupt the balance in commensal microbiota, which has been shown to have profound effects in EAE and other autoimmune diseases [157]. We induced EAE at relatively young age (6-7 weeks), and only a few of our *LysMcre/Stat3*$^{fl/fl}$ mice developed rectal prolapse during or before EAE induction (Table 3). Although the mice with rectal prolapse did not develop actively induced EAE, neither did most other *LysMcre/Stat3*$^{fl/fl}$ mice. Interestingly, all of our mice with rectal prolapse still developed passively induced EAE by adoptive transfer. Therefore, the EAE resistance conferred by myeloid STAT3 deletion cannot be solely explained by its effect on the commensal microbiota.

Table 3. Anal prolapse in the *LysMcre/Stat3$^{fl/fl}$* mice.

LysMcreStat3$^{fl/fl}$ mice	*EAE Onset/Total*	*EAE Onset/Anal Prolapse*
Active EAE	2/36	0/2
Adoptive EAE	10/15	2/2

In our EAE experiment involving bone marrow chimeric mice, we discovered that although *LysMcre/Stat3$^{fl/fl}$* → *Stat3$^{fl/fl}$* mice did not develop EAE (Figure 19D), they displayed sickness behaviors and appeared hunched and lethargic. They also lost a significant amount of body weight (Figure 19F). These mice, however, did not develop other symptoms associated with atypical EAE such as ataxia and axial rotation. We found one mouse exhibiting cerebellum inflammation (Figure 23A) but not in the other mice. We speculate that the enhanced innate immune response in their system elicited by the injection of CFA caused a septic shock in these mice, as we discovered that the serum from *LysMcre/Stat3$^{fl/fl}$* mice at pre-clinical stage contain elevated levels of TNFα (Figure 23B, C). This is supported by the fact that the *LysMcre/Stat3$^{fl/fl}$* → *Stat3$^{fl/fl}$* mice did not exhibit any apparent health problems or weight loss prior to immunization. Although we are uncertain as to why regular *LysMcre/Stat3$^{fl/fl}$* and chimeric *LysMcre/Stat3$^{fl/fl}$* → *LysMcre/Stat3$^{fl/fl}$* mice did not exhibit significant weight loss, we speculate that their system adapted to the enhanced response during development, whereas the heightened immune responses in *LysMcre/Stat3$^{fl/fl}$* → *Stat3$^{fl/fl}$* mice elicited sickness behaviors.

In summary, we found that Stat3 in myeloid cells is critically important in the development of EAE. Myeloid cells in *LysMcre/Stat3*$^{fl/fl}$ mice express less antigen presentation and co-stimulatory molecules, and exhibit impaired capability to differentiate $CD4^+$ T-cells. We provide evidence that *Stat3* may be a therapeutic target in autoimmune diseases in the CNS. Our future direction would be to investigate the cellular mechanisms in which Stat3 influences expression of antigen presentation and co-stimulatory molecules, and their possible specific functions in different subsets of myeloid cells.

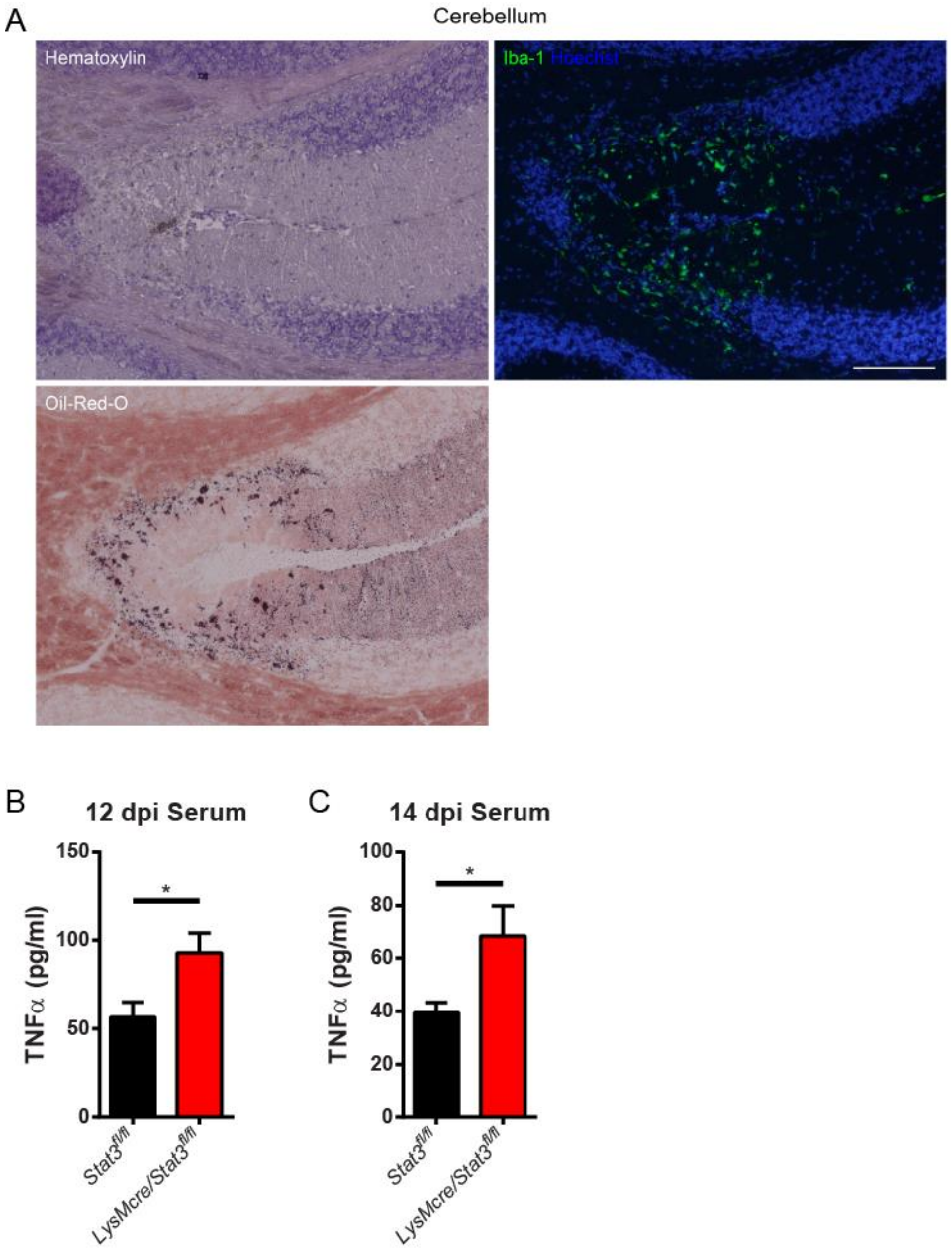

Figure 23. Bone marrow chimeric mouse cerebellum and preclinical mouse serum. A, *LysMcre/Stat3*$^{fl/fl}$ → *Stat3*$^{fl/fl}$ mice were induced with active EAE. At 17 dpi, 2 mice were sacrificed due to moribundity. Brain tissue was cryosectioned and stained with hematoxylin, α-Iba-1, Hoechst, and oil-red-O. Representative pictures were shown. **B**, *Stat3*$^{fl/fl}$ (n = 6) and *LysMcre/Stat3*$^{fl/fl}$ mice (n = 5) were induced with active EAE. At 12 dpi, serum samples were obtained from mouse blood. Level of TNFα in the serum was measured by ELISA. **C**, *Stat3*$^{fl/fl}$ (n = 4) and *LysMcre/Stat3*$^{fl/fl}$ mice (n = 3) were induced with active EAE. At 14 dpi, serum samples were obtained from mouse blood. Level of TNFα in the serum was measured by ELISA. Data represent mean ± SEM. *$p < 0.05$.

3. THE ROLE OF MICROGLIAL STAT3 IN BRAIN DEVELOPMENT

3.1 Introduction

Microglia are the tissue-resident macrophages of the CNS and consist roughly 10-15% of CNS cell population. Microglia arise from a process called primitive hematopoiesis that occurs in the yolk sac and migrate towards the CNS from E7.5 in mice [64-67], a process distinct from the adult hematopoiesis, in which the blood cells are formed from the hematopoietic stem cells. Studies that utilize techniques such as parabiosis [158] and *Cx3cr1creER*/iDTR mice [159] have demonstrated that microglia are replenished by self-renewal, unlike the bone marrow-derived leukocytes. Microglia exhibit different accumulation kinetics and gene expression than infiltrating monocytes during EAE [141]. Moreover, it's also shown that although bone marrow-derived monocytes can enter the CNS lesion sites during EAE, they do not stay in the CNS and contribute to the microglia population after disease resolution [142], further indicating the difference between microglia and monocytes. As the tissue-resident macrophage, microglia can become activated via pattern recognition receptors and carry out immune functions such as proinflammatory mediator secretion, phagocytosis, antigen presentation and more [160]. In their resting state, microglia exhibit a non-overlapping distribution in the CNS [161] and remain highly dynamic and are actively surveying the environment by constantly sending out and retrieving processes [162].

Despite having an immune cell origin, microglia have many functions related to the development of the nervous system, some of which utilizing their immune cell

functions. During early development, more neurons than needed are initially formed, and the number is subsequently reduced via programmed cell death [163, 164]. For example, most newborn neurons in the subgranular zone of the dentate gyrus undergo apoptosis, and are quickly cleared by phagocytosis [165]. Microglia use their phagocytic capability to clear up the dead cells [166], creating space for the nervous system to continue to develop. Microglia are also shown to be able to actively induce programmed cell death in neurons [167-170]. Using retinal cultures with or without microglia, it was shown that microglial-derived nerve growth factor (NGF) induces neuronal death in developing retina [167]. Microglia and their secretion of TNFα enhanced the programmed cell death "competence" in motoneurons from rat E13 embryo explants [168]. In TNFα- or TNFR-deficient mice, programmed cell death in E11 explants were reduced in half compared to WT [168]. Other microglial-derived factors such as nitric oxide (NO) [169] and reactive oxygen species (ROS) [170] on neuronal cell death have also been reported. Microglia have also been shown to regulate the number of neural precursor cells (NPCs) in the developing embryo. Microglial activation by LPS injection in the pregnant mice at E15 decreased number of NPCs, whereas inhibition of microglia with doxycycline increased the number of NPCs [171]. Microglia are also shown to influence neurogenesis through secretion of growth factors. Macrophages and microglia are the major sources of insulin-like growth factor-1 (IGF-1) [172]. IGF-1 secretion from the microglia that are stimulated with IL-4 can induce neurogenesis in neural progenitor cells [173]. Microglia-derived IGF-1 was also shown to promote the survival of neurons in layer V

cerebral cortex [174]. Together, these studies strongly suggest that microglia are actively involved in regulating neuronal cell number in the developing brain.

During development, synaptic connections are initially formed excessively, and subsequently undergo remodeling and elimination in a neuronal activity-dependent fashion [175]. It has been found that neurons in the developing brain express the complement protein C1q at the synapses [176]. Normally, the lateral geniculate nucleus (LGN) segregates into regions containing neurons that respond to either the left eye or the right eye, but not both. In C1q-KO mice, the LGN was not segregated, and the neurons remained innervated by both eyes [176]. The same group also found that microglia were located at the synapses and phagocytosing the inputs from the retinal ganglion cells (RGC). Using tetrodotoxin and CR3-KO mice, they also found that the phagocytosis of RGC inputs was dependent on neuronal activity and the complement receptor CR3 on microglia [177]. Consistent with this, CX3CR1 KO mice showed increased number of immature dendritic spines in the first two postnatal weeks [178]. These studies indicate that microglia are actively involved in remodeling of synaptic connections during development. In addition to synaptic remodeling, developing axons undergo an elimination process during development, and microglia with vacuoles containing inclusions were observed under electron microscopy, suggesting its phagocytic activity during axonal pruning [179]. It's also found that dopaminergic axons in the forebrain during development "over-extend" in microglia-deficient (Pu.1-KO) or -depleted (CSF1R Ab) mice [180], suggesting the involvement of microglia in axonal pruning.

Many behavioral disorders such as stress related disorders and autism spectrum disorders are connected to abnormal neural circuits in various brain regions [181, 182]. Since microglia arrive at the CNS early during development and are involved multiple aspects of neuronal development, abnormalities in microglia could lead to abnormal brain circuitry, which could then translate to behavioral deficits. CX3CR1 is a fractalkine receptor that is highly expressed in microglia, and the CX3CR1-fractalkine interaction modulates microglial activation [183]. Cx3cr1-KO mice showed a transient decrease of microglia during early postnatal development and consequent deficit in synaptic multiplicity and functions connectivity across multiple brain regions [184]. These mice also showed reduced social behaviors and increased repetitive behaviors such as self-grooming. Depleting microglia with the *Cx3cr1creER*/iDTR mice caused altered synaptic protein levels and reduced performance improvement in the rotarod test [137]. M-CSFR signaling is required for macrophage and microglial survival. M-CSFR KO mice showed nearly complete deletion of microglia, had enlarged ventricles and compressed CNS parenchyma, and exhibited impaired olfactory functions in a food-finding test [185]. Depleting microglia with clodronate liposome at P1 and P4 in rats leads to reduced anxiety in elevated maze and open field tests, increased locomotor activity, decreased chasing behaviors during social play, and decreased despair, i.e. immobile time, in forced swim test [186]. Similarly, depleting microglia with clodronate liposome at P0, 2, 4 in rats leads to reduced anxiety, increased locomotion, and deficits in male sex behaviors [187]. Besides microglial cell depletion, changing the activation state of microglia has also been shown to have behavioral effects. *s.c.* injection of *E. coli*

in P4 rat pups caused a memory forming deficit in the fear conditioning test in the adults (P60-63) when followed by peripheral immune challenge with *i.p.* injection of LPS [188]. The offspring of mice subjected to maternal immune activation mothers by *i.p.* injection of poly(I:C) at E10.5, 12.5, and 14.5 exhibited decreased sociability and increased compulsive behaviors in both marble burying and self-grooming [189]. These studies indicate that manipulations in microglia can lead to profound behavioral abnormalities.

While studies indicate that STAT3 is involved in neurogenesis and astrogliogenesis [97-99], whether STAT3 is involved in microglial formation is not clearly understood. Microglia arise from primitive hematopoiesis beginning with embryonic stem cells (ESCs). Many key factors controlling microglia development were identified, and include Runx1, C/EBPα, PU.1, IRF-8, M-CSFR, miR-124, and more [190-192]. Adult definitive hematopoiesis begins with hematopoietic stem cells (HSCs). The development of bone marrow derived monocytes involves multiple stages. Briefly, C/EBPα is required for developing from multipotent progenitors (MP) to common myeloid progenitors (CMP); PU.1 is required for developing from CMP to granulocyte-macrophage progenitors (GMP); M-CSFR is required from GMP to monocytic progenitors (MP) [191]. Although the discovery of microglial origin is relatively new and the detailed stages involved are not as clear, the overlapping of several key factors, namely C/EBPα, PU.1, and M-CSFR, suggests that the two hematopoietic processes may share similar developmental stages. Between these factors, C/EBPα can directly induce PU.1, which induces M-CSFR [191, 193]. M-CSFR signals mainly through PI3-

kinase and MAPK pathways [194-196]. However, an early report showed M-CSFR induces STAT3 activation [197]. Interestingly, IL-34, a cytokine with overlapping functions with M-CSF, also signals through M-CSFR and was shown to be important in microglial development [198]. IL-34 was shown to activate STAT3 and to induce expression of osteoclast-related genes in the bone marrow macrophages during osteoclastogenesis, which can be blocked by AG490 [199]. IL-34 was also shown to activate STAT3 in the fibroblast-like synovial cells from rheumatoid arthritis patients [200]. Therefore, JAK/STAT pathway might be involved in microglia formation through M-CSFR signaling.

Another possibility of JAK/STAT involvement is through GM-CSF. GM-CSF is implicated in myelopoiesis, and its receptor GM-CSFRα signals through JAK2/STAT3 and STAT5 pathways [201]. Stimulation of GM-CSF is involved in transition from CMP to GMP, the step in which PU.1 is required. It has also been shown that PU.1 mediates GM-CSF in alveolar macrophage differentiation [202], and that STAT3 induces PU.1 expression [203, 204]. Therefore, GM-CSF might signal through STAT3 and induce PU.1, thereby contributing to the differentiation from CMP to GMP. It's also reported that high level of PU.1 skews the development towards MP [193], thus the GM-CSF signaling may contribute to such high level of PU.1. It is to be noted that myelopoiesis in GM-CSF knockout mice appears normal. Therefore, GM-CSF and its signaling through JAK/STAT pathways may play a modulatory role for myeloid function, rather than being essential in myeloid development.

STAT3 was reported to become activated in a microglial cell line after radiofrequency (RF) electromagnetic field exposure, and the STAT3 inhibitor Stattic reduced RF field-induced expression of pro-inflammatory cytokines such as TNFα, IL-1β, IL-6, and NO [205]. STAT3 and STAT1 together were also shown to target Jmjd3, which in turn drives other pro-inflammatory cytokines in response to LPS in microglia [206]. These studies suggest that STAT3 may have a pro-inflammatory effect in microglia, although these studies utilized cell lines, so the applicability requires further testing.

Strong evidence of STAT3 in microglia development and/or activation is still sparse. However, STAT3 is a regulatory gene that is involved in many functions across different cell types. In this section, we attempted to study the role of STAT3 in microglia development and possible effects on behavioral changes in mice with inducible ablation of microglial STAT3.

3.2 Materials and Methods

3.2.1 Animals

STAT3$^{fl/fl}$ mice contain two loxP sites that flank exon 22 of *Stat3* gene [135], were a generous gift from Dr. Shizuo Akira (Hyogo College of Medicine, Nishinomiya, Japan), and were backcrossed to C57BL/6 mice for 8 generations. *Cx3cr1creER* mice express an enhanced yellow fluorescent protein (EYFP) and a Cre recombinase linked to a mutated estrogen receptor that binds to tamoxifen under control of *Cx3cr1* promoter [137]. Conditional mutant mice were generated by crossbreeding *Stat3$^{fl/fl}$* mice to

Cx3cr1creER mice. *Stat3$^{fl/fl}$;Cx3cr1-creER$^{+/-}$* and *Stat3$^{fl/fl}$;Cx3cr1-creER$^{-/-}$* littermates were used in the experiments. B6.129P2(Cg)-Cx3cr1$^{tm2.1(cre/ERT2)Litt}$/WganJ mice (*Cx3cr1creER*) and B6;129S6-Gt(ROSA)26Sor$^{tm14(CAG-tdTomato)Hze}$/J mice (*rosa26-Ai14*) were obtained from Jackson Laboratory (Bar Harbor, ME). Mice were under husbandry and bred in the animal facility in Texas A&M University Comparative Medicine Program. All animal use was approved by Institutional Animal Care and Use Committee in Texas A&M University.

3.2.2 Administration of Tamoxifen

Tamoxifen (T5648, Sigma-Aldrich) was administered in either adults or neonatal *Cx3cr1-creER/Stat3$^{fl/fl}$* mice. For the adults, tamoxifen was first dissolved in corn oil (C8267, Sigma-Aldrich) at 40 mg/ml by incubating while shaking at 37°C for 30 min followed by pulse sonication. Each mouse at age of 5 weeks received 2 doses of 8 mg tamoxifen (in 200 µl corn oil) by oral gavage, 48 hr apart. For the neonatal mice, 10 mg tamoxifen was first dissolved in 250 µl ethanol by vortexing. 750 µl corn oil was then added to achieve 10 mg/ml (10x). The solution was stored at 4°C and used for one experiment before disposal. Each day for P1-P3, the 10x solution was diluted 1:10 in corn oil to achieve 1 mg/ml. Each pup received intragastric injection of 50 µg tamoxifen (in 50 µl volume) daily for P1-P3.

3.2.3 Behavioral Tests

In all animal behavioral tests, the mice were housed in groups and in a 12-hr light/dark cycle. The mice were transferred in their home cage to the test room and left undisturbed for 30 min before the experiments were conducted. All behavioral tests were

conducted during the light phase of the day cycle. The same behavioral test was conducted at the same time of a day for all animals. Other than the Morris Water Maze test, the lighting conditions in the test rooms were approximately the same as the regular housing room, and the room temperature was set at 21°C.

Open Field. The open field test to measure anxiety and explorative behavior was described previously [207, 208] and was performed using the Tru Scan Activity System (Coulbourn Instruments, Holliston, MA). Before the experiment, all the equipment was sprayed and wiped with 70% ethanol. Each mouse was placed in the center of an open field arena of size 26 cm × 26 cm to allow exploration for 30 min. Mouse activity during the 30 min was recorded by two infrared sensor rings, one for the floor plane and the other for the vertical plane. After each test, the mouse was returned to its home cage, the feces were removed from the arena, and the arena was cleaned with 70% ethanol and let dry before subsequent tests. Perimeters including total movements, movement time, movement distance, average distance per move, mean velocity, number of jumps, rest time, margin distance, margin time, center distance, center time, center entries, vertical plane entries, and vertical plane time were collected on the Tru Scan 2.0 software. The data was collected in 2-min intervals.

Marble Burying. The mice were first translocated in their home cage to the test room and habituated for 30 min. A clean mouse cage of approximate size 28 cm × 17 cm was prepared for each mouse and contains 5-cm deep SANI-CHIP bedding. The bedding was pressed by hand to create a flattened surface. 10 white marbles of size 1.45 cm in diameter were placed in a "3 by 3 plus 1" pattern on the bedding (Figure 24). Food and

water were withheld from the testing cages. Each mouse was placed in the center of one testing cage. The cages were covered with cage tops and left undisturbed for 30 min. After the test, the mice were returned to the home cage, and the number of marbles that were at least 70% buried in bedding was recorded.

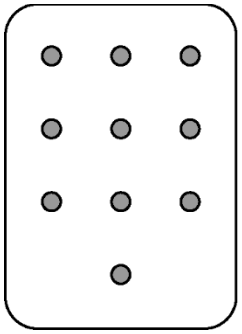

Figure 24. Placement of marbles for the marble burying test.

Social Interaction. The social interaction test to assess sociability was described previously [209]. In a 3-chamber apparatus of approximate size 60 cm × 40 cm (Figure 25), a mouse was placed in the center chamber for habituation for 10 min while the doors to the other chambers were closed. An inverted empty metal wire pencil cup was placed in one of the side chambers, and another inverted empty metal wire pencil cup holding a stranger male mouse was placed in the chamber on the opposite side. After 10 min of habituation, the doors connecting the 3 chambers were removed. The mouse activity was recorded for another 10 min. The time spent in the novel stranger chamber ("Stranger"), the time in the novel object chamber ("Opposite"), and the time interacting

with the stranger mouse was noted. The interaction was defined as when the tested mouse was sniffing with its nose within 1 cm of the stranger cup.

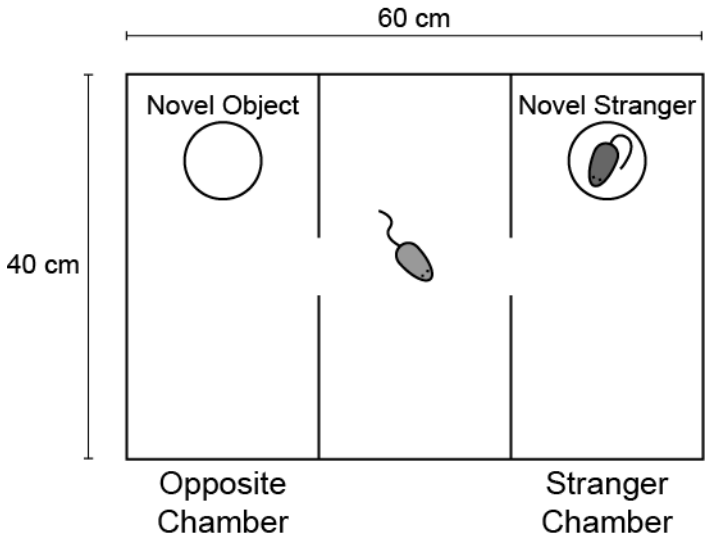

Figure 25. Illustration of the three-chamber social interaction device.

Rotarod. The rotarod test to assess motor coordination was carried out following the Standard Operating Procedures on EUMORPHIA and using a Rota-rod Treadmill apparatus (#7650; Ugo Basile Biological Research Apparatus, Varese, Italy). The mice were first translocated in their home cage to the test room and let accommodate for 30 min. Meanwhile, the rotarod apparatus was thoroughly cleaned and dried with 70% ethanol and paper towels. For each trial, the apparatus was initially set at a constant 4 rpm speed, while up to 3 mice were placed onto separate lanes on the apparatus, facing forward. After all mice were correctly positioned and oriented, the apparatus was switched to the accelerating mode, in which the rotating speed increases from 4 rpm to

40 rpm in 300 sec. The latency until each mouse fell from the treadmill was recorded. Mice that clung on the rod for a full passive rotation counted as a "fall" and were returned to the cage. Mice that stayed on the treadmill for the whole 300-sec duration had the latency to fall value recorded as 300. The apparatus was cleaned with 70% ethanol, and the procedure was repeated for all other mice to complete the first trial. Each day consisted of 3 trials, with 15 min inter-trial interval between each trial. The procedure was repeated for a total of 3 consecutive days.

Morris Water Maze. The MWM to test spatial learning was performed as described previously [210, 211] with modifications. A water bucket of size 120 cm in diameter was filled with tap water in the test room in which the room temperature was set at 78°F (25.6°C). The water was left for a day in order for its temperature to reach the corresponding room temperature. The mice underwent 6 trials per day, 3 days of visible platform training (day 1-3). During the visible platform training, the water bucket was surrounded by white curtain, but no visual cues were present. A platform of size 15.5 cm in diameter was place 1 cm above the water level. For each trial, each mouse was allowed to swim in the pool for up to 2 min. If the mouse reaches the platform, it is allowed to sit on the platform for 20 s before returning to its home cage. If the mouse does not reach to platform within 2 min, it is guided to the platform and allowed to sit for 20 s before returning to its home cage. After the visible platform training, the mouse underwent 3 trials per day, 6 days of hidden platform training (day 4-9). During the hidden platform training, the water was made opaque by adding non-toxic white tempera paint. The platform was placed 5 mm below water level. Three high-contrast visual cues

were placed on the surrounding curtain. During each trial, a mouse was allowed to swim for up to 60 s. If the mouse reaches the platform, it is allowed to sit on the platform for 15 s before returning to its home cage. If the mouse does not reach to platform within 60 s, it is guided to the platform and allowed to sit for 15 s before returning to its home cage. The mouse' swimming trail was captured and analyzed on the WaterMaze software (Coulbourn Instruments, Holliston, MA). On day 4 before the hidden platform training, day 9 two hours after the hidden platform training, and day 10, three trials of probe tests were performed for each mouse. During the probe test, the setup remained the same as the hidden platform training except that the platform was absent. The software captures the swimming trail during the 60 s and computes average proximity and percent time spent in the platform quadrant.

3.2.4 Isolation of Fresh Neonatal Microglia for RNA Sequencing

Neonatal mice were administered with tamoxifen daily from P1-P3. At P6, toe clips were obtained for determining the genotypes. At P8, the mice were anesthetized with ketamine and xylazine, and transcardially perfused with 10 ml PBS. The skin around the head was removed. The skull was cut open along the midline from the posterior end, and the brain was removed with a scoop. The brain was disrupted with scissors and digested in 5 ml Stempro Accutase (A11105-01; Life Technologies, Carlsbad, CA) at 37°C for 30 min. Every 5 min during the incubation, the tube was inversed several times to mix the content. After the 30-min incubation, the enzyme activity of Accutase was blocked by addition of 2 ml FBS. The digested tissue was then filtered through a 70-μm cell strainer with the help of a 3-ml syringe plunger to make

single cell suspension. Cells were centrifuged and resuspended in 5 ml 35% Percoll (P4937; Sigma-Aldrich) in PBS. 3 ml 70% Percoll was slowly added to the bottom with a Pasteur pipette attached to a rubber bulb. The tubes were then centrifuged at 2,000 × *g* for 20 min at 18°C with the brake set to 0. The top lipid/myelin layer was quickly removed using a pipette. Cells in the interphase between the 35% and 70% Percoll layers were harvested with a Pasteur pipette, washed by centrifugation and resuspended in ice-cold PBS. The cells were stained with α-ms CD11b APC (#17-0112; eBioscience), washed and resuspended in PBS containing propidium iodide and 1 mM EDTA. $CD11b^{+}PI^{-}$ cells were FACS-sorted and resuspended in 500 µl Tri Reagent, flash frozen and stored at -80°C until use. RNA was isolated using Direct-zol RNA MiniPrep kit (R2052; Zymo Research) following the instruction manual.

3.2.5 Histological Analysis of P10 and P32 Mouse Brains

Mice were administered with tamoxifen daily from P1-P3. At P10 or P32, the mice were transcardially perfused with PBS. The brains were removed and fixed in 4% PFA in PBS at 4°C overnight. The next day, the tissues were changed to 30% sucrose in PBS for cryoprotection for roughly two days until they sank. The tissues were embedded in Tissue-Tek O.C.T. Compound (#4583, Sakura Finetek USA, Inc., Torrance, CA) and frozen-sectioned into 10 µm sagittal sections on Leica CM1950 cryostat (Leica, Nusslock, Germany). The sections were adhered onto Superfrost Plus Microscope Slides (Fisher Scientific, Waltham, MA) and stored at -20°C until use.

The slides were thawed and dried for 30 min to 1 hr at 37°C prior to staining. For immunofluorescence, appropriate regions of the slides were marked with an ImmEdge

hydrophobic barrier pen (Vector Lab, Inc. Burlingame, CA) to separate different sections. The sections were rinsed in PBS twice for 5 min each to remove the O.C.T. Compound. Sections were blocked for unspecific binding and permeabilized with PBS containing 5% goat serum and 0.3% Triton X-100 (T9284, Sigma Aldrich) for 1 hr at room temperature, and incubated with rabbit α-Iba-1 (1:400; #019-19741, Wako, Richmond, VA), chicken α-GFP (A10262, Invitrogen), or mouse anti-NeuN (1:200; MAB377, Millipore) diluted in PBS containing 5% goat serum and 0.1% Triton X-100 at 4°C overnight. The next day, tissue sections were washed in PBS three times for 5 min each, and incubated with Alexa Fluor 488 goat α-rb IgG (A11034, Invitrogen, Eugene, OR), Alexa Fluor 488 goat α-ms IgG (A11029, Invitrogen, Eugene, OR), or Alexa Fluor 488 goat α-rat IgG (A11006, Invitrogen, Eugene, OR), diluted 1:1000 in PBS containing 5% goat serum and 0.3% Triton X-100 for 1 hr in dark at room temperature, followed by three washes in PBS. Cell nuclei were stained with Hoechst 33342 (Invitrogen) at 1:1000 dilution in PBS for 2 min. Images of sections were obtained under an Olympus IX71 microscope (Olympus, Tokyo, Japan) and its proprietary imaging software at constant settings across different sections/samples. Post-processing (image merging and background removal) was performed in a uniform fashion in Adobe Photoshop software. Number of cells was counted and divided by the counting area to obtain the cells density from multiple fields in the cerebral cortex using ImageJ software.

3.3 Results

3.3.1 Neonatal Deletion of Microglial STAT3 Causes a Transient Reduction of Microglial Number in the Cerebral Cortex

To investigate the role of STAT3 in microglial development and functions, tamoxifen was administered daily from P1-P3 in *Cx3cr1creER/Stat3$^{fl/fl}$* mice and *Stat3$^{fl/fl}$* littermates (Figure 26). The efficiency of Cre recombinase expression was first assessed using the *rosa26-Ai14* reporter line. At P6, most YFP-expressing microglia are also tdTomato positive in the brain (Figure 27A), indicating high efficiency of recombination. Granulocytes and Ly6C^{hi} monocytes in the spleen at P6 are 98.0% and 97.0% tdTomato positive, respectively, whereas little expression was found in B-cells and T-cells (Figure 27B).

After establishing the efficacy of tamoxifen-induced recombination in CX3CR1^{+} myeloid cells in the CNS, we then assessed number of microglia and neurons in the CNS in *Cx3cr1creER/Stat3$^{fl/fl}$* and *Stat3$^{fl/fl}$* mice at two different ages with immunohistochemistry (Figure 28). At P10 in the frontal cortex, a dense Iba-1^{+} microglia population was observed in the *Stat3$^{fl/fl}$* mice (Figure 28A), whereas the microglia distribution in the *Cx3cr1creER/Stat3$^{fl/fl}$* mice was rather sparse (Figure 28B). Further analysis by cell counting revealed a significant reduction in the number of microglia in the *Cx3cr1creER/Stat3$^{fl/fl}$* mice as compared to *Stat3$^{fl/fl}$* controls (Figure 28D). Preliminary histological analysis of Nissl staining suggested that the number of neurons in the cortex was modestly increased in *Cx3cr1creER/Stat3$^{fl/fl}$* mice in comparison to *Stat3$^{fl/fl}$* controls (Figure 28C, E). In contrast to P10, the number of

microglia or neurons were not significantly different at 4 weeks of age (P32; Figure 28F, G). Taken together, these results indicate a transient reduction of microglia in the second postnatal week of *Cx3cr1creER/Stat3*$^{fl/fl}$ mouse brain, but the microglial number recovered by one month of age.

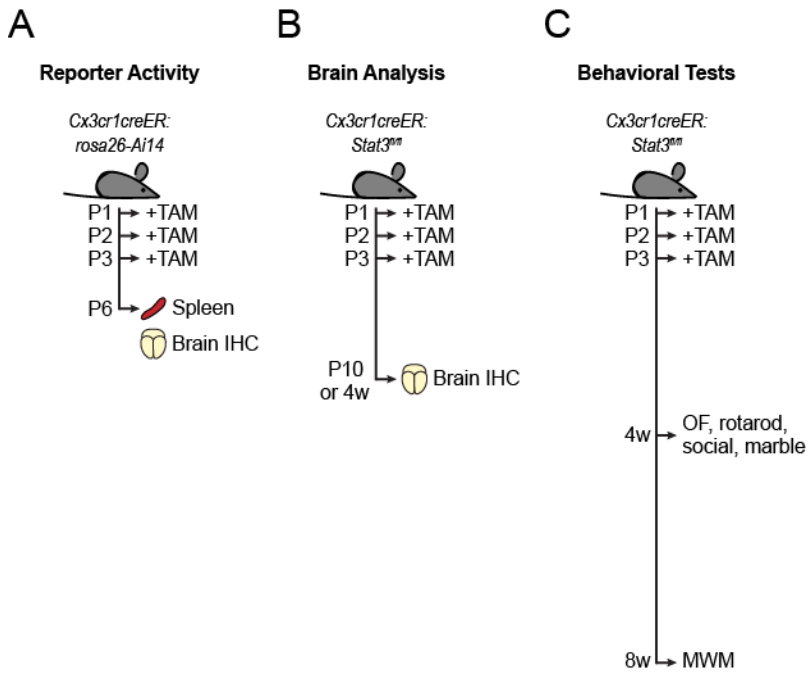

Figure 26. Schematic of developmental and behavioral experiments in the microglial STAT3-mutant mice.

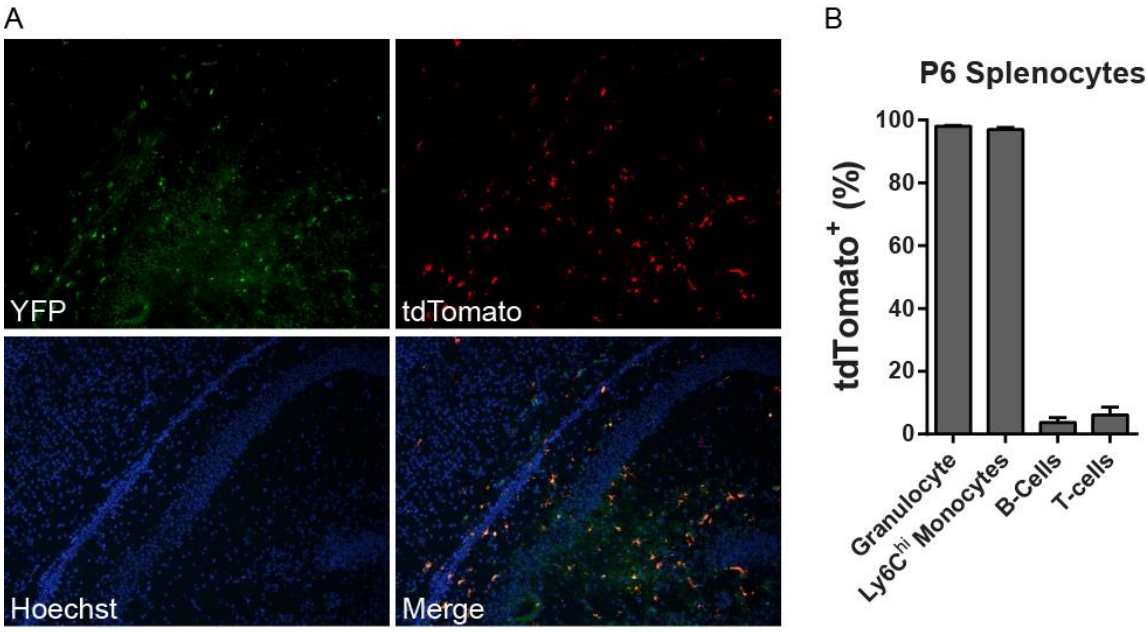

Figure 27. *Cx3cr1*-driven Cre recombination upon neonatal administration of tamoxifen. *Cx3cr1creER/rosa26-Ai14* mice (n = 8) received daily intragastric injection of 50 µg tamoxifen from P1-P3. The mice were sacrificed at P6. **A**, Coronal brain sections were stained with α-YFP (green) and Hoechst. A representative picture is shown. **B**, Splenocytes were isolated and stained with antibodies for cell surface markers and analyzed with flow cytometry. Granulocytes, $CD11b^{+}Gr\text{-}1^{+}$; $Ly6C^{hi}$ monocytes, $CD45^{+}Ly6C^{hi}$; B-cells, $CD19^{+}$; T-cells, $CD3^{+}$. Data represent mean ± SEM.

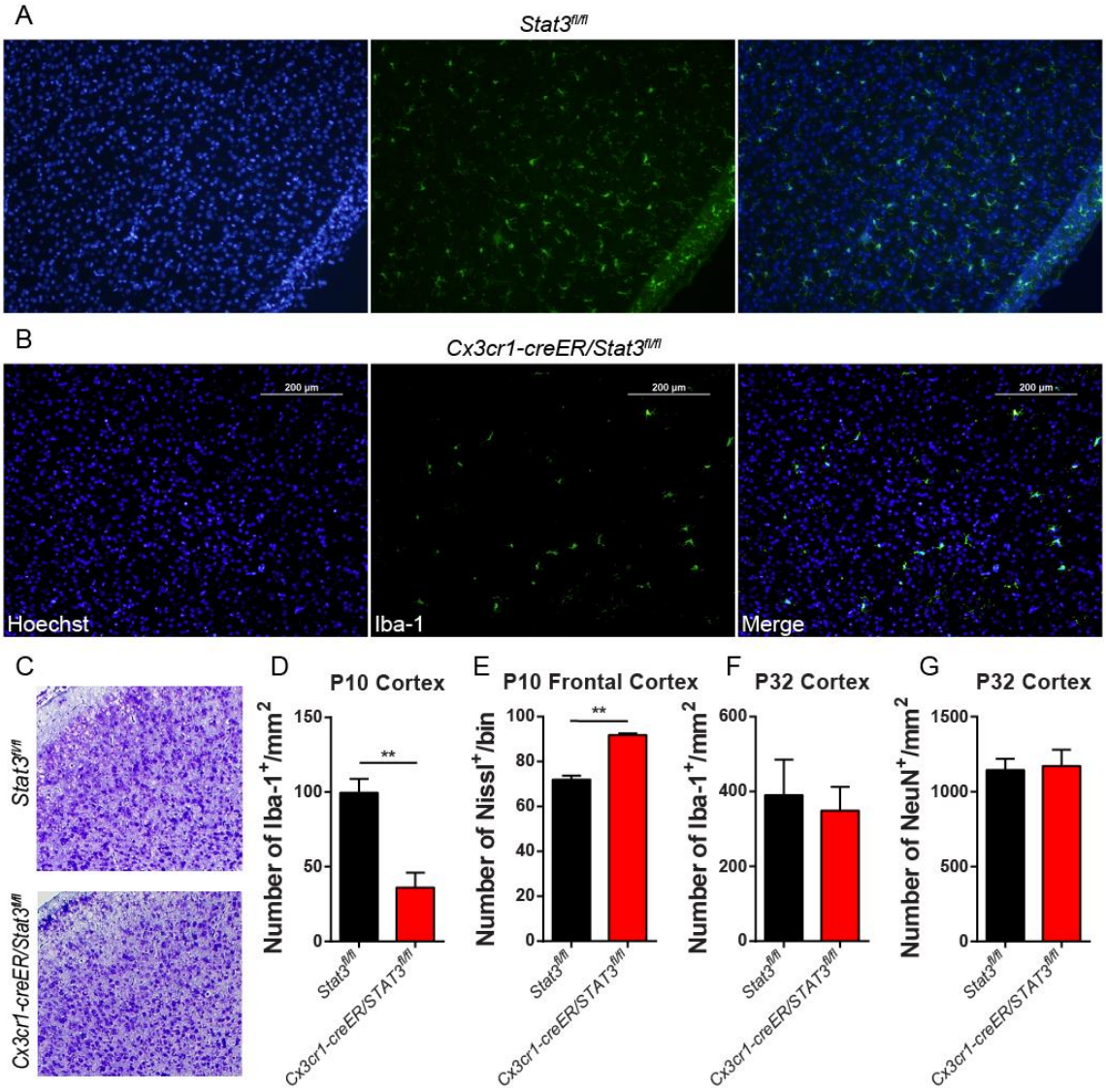

Figure 28. Number of microglia is transiently reduced in the *Cx3cr1creER/Stat3$^{fl/fl}$* mice. *Stat3$^{fl/fl}$* and *Cx3cr1creER/Stat3$^{fl/fl}$* mice received daily intragastric injection of 50 µg tamoxifen from P1-P3. **A, B, D**, Sagittal sections of P10 brain were stained with Hoechst and α-Iba-1 (green). Representative pictures are shown. Iba-1^{+} cells in the cerebral cortex were counted. Scale bar, 200 µm. *Stat3$^{fl/fl}$*, $n = 4$; *Cx3cr1creER/Stat3$^{fl/fl}$*, $n = 3$. **C, E**, P10 sagittal sections were stained with Nissl staining. *Stat3$^{fl/fl}$*, $n = 2$. *Cx3cr1creER/Stat3$^{fl/fl}$*, $n = 2$. **F, G**, P32 brain sagittal sections were stained with Hoechst and α-Iba-1 (**F**) or α-NeuN (**G**). *Stat3$^{fl/fl}$*, $n = 3$. *Cx3cr1creER/Stat3$^{fl/fl}$*, $n = 3$. Data represent mean ± SEM. $^{**}p < 0.01$.

3.3.2 Behavioral Assessment of Mice with Neonatal Deletion of Microglial STAT3

To assess possible behavioral changes resulting from the transient reduction of microglial number in neonatal *Cx3cr1creER/Stat3*$^{fl/fl}$ mice, multiple types of behavioral tests were performed at 4 weeks of age as well as Morris Water Maze (MWM) at 8 weeks of age. The body weight was first measured at 4 weeks of age prior to the behavioral tests. No significant difference in the body weight was found between the *Cx3cr1creER/Stat3*$^{fl/fl}$ mice and *Stat3*$^{fl/fl}$ littermates (Figure 29A), indicating no major deficit in overall growth that could potentially be accountable for differences in behavioral performances. In the social interaction test, *Cx3cr1creER/Stat3*$^{fl/fl}$ and *Stat3*$^{fl/fl}$ mice spent roughly the same amount of time in the chamber with a novel stranger mouse ("Stranger"), in the opposite chamber ("Opposite"), as well as time spent in interacting with the novel stranger mouse (Figure 29B). In the marble burying test, the *Cx3cr1creER/Stat3*$^{fl/fl}$ mice buried significantly fewer marbles than *Stat3*$^{fl/fl}$ mice during the 30-minute testing period (Figure 29C). In the rotarod test, the *Cx3cr1creER/Stat3*$^{fl/fl}$ mice showed a trend of decreased ability to stay on the rod for all three days of testing, although no significant differences were found (Figure 29D). The *Cx3cr1creER/Stat3*$^{fl/fl}$ mice showed greater improvement in performance when compared to the *Stat3*$^{fl/fl}$ mice (Figure 29E), although this is likely due to a ceiling effect.

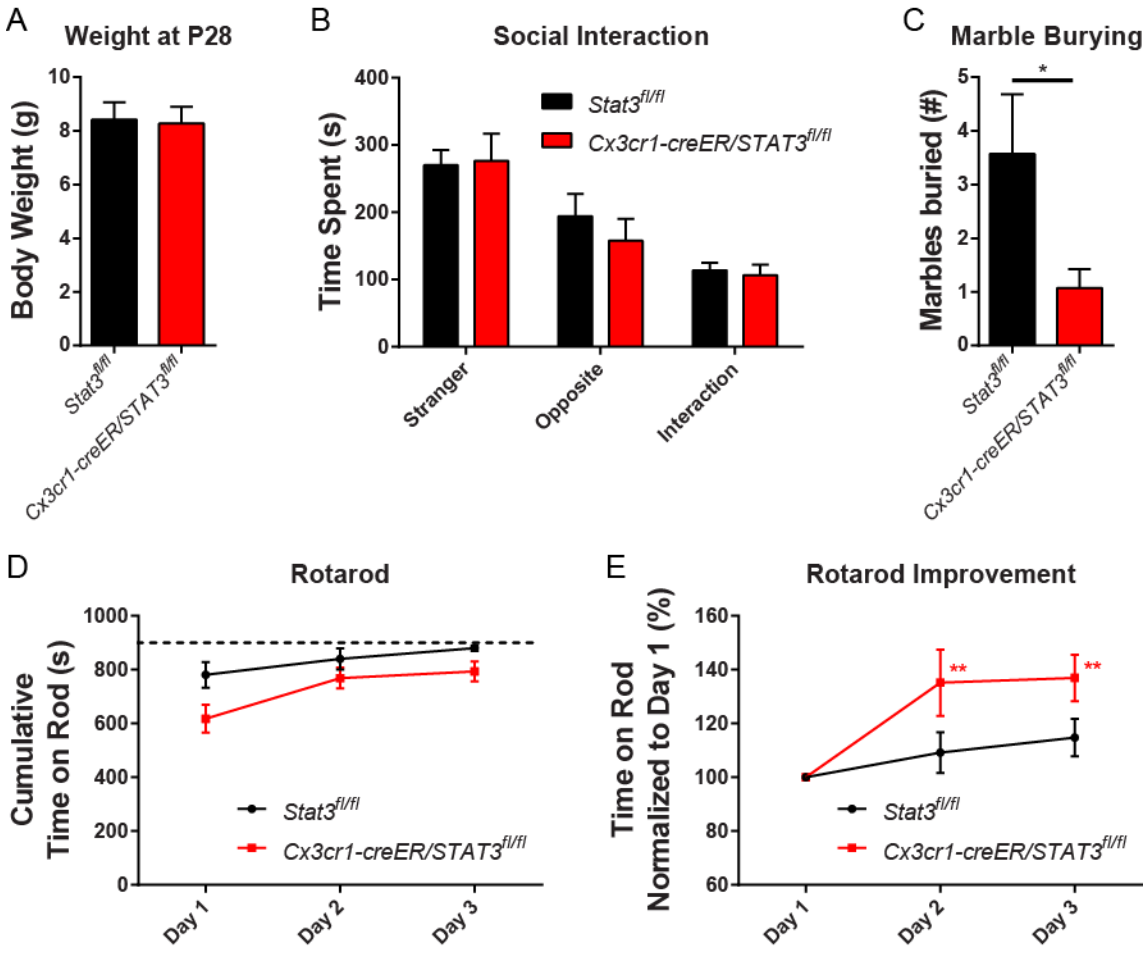

Figure 29. Behavioral tests in the *Cx3cr1creER/Stat3$^{fl/fl}$* mice. P28 *Stat3$^{fl/fl}$* (n = 7) and *Cx3cr1creER/Stat3$^{fl/fl}$* mice (n = 14) were weighed (**A**) and tested for social interaction (**B**), marble burying (**C**), and rotarod (**D, E**). **B**, Mice were tested in the three-chamber device for 10 min. Stranger, total time spent in the chamber that contained a stranger mouse. Opposite, total time spent in the opposite chamber that contained an inversed metal mesh pencil holder. Interaction, total time spent sniffing the stranger mouse. **C**, Mice were placed in a cage with 2-inch deep of SANI-CHIP bedding and 10 marbles for 30 min. Total number of marbles that are at least 70% buried after the test was counted. **D**, Mice were placed in the rotarod device for 5 min per trial, 3 trials per day for 3 consecutive days. Cumulative time staying on the rod was graphed. Dashed line indicates maximum performance (900 s). **E**, Time spent on rod normalized to day 1 as an indication of improvement. Red **, performance of day 2 and day 3 *Cx3cr1creER/Stat3$^{fl/fl}$* mice compared to day 1 *Cx3cr1creER/Stat3$^{fl/fl}$* mice. Data represent mean ± SEM. *p < 0.05. **p < 0.01.

To evaluate the general activity and anxiety level of the *Cx3cr1creER/Stat3$^{fl/fl}$* mice, multiple parameters of activity were analyzed during the 30-minute open field test

(Figure 30). *Cx3cr1creER/Stat3*$^{fl/fl}$ mice exhibited a very slight trend of decreased general activity, including the number of moves (Figure 30A) and jumps (Figure 30B), moving velocity (Figure 30D), total distance traveled (Figure 30E), time spent moving (Figure 30F), number of entries into the vertical plan (Figure 30H), and the time spent in the vertical plan (Figure 30I). However, the differences are modest and none is statistically significant. The mice of both genotypes also spent roughly the same amount of time in the margin versus the center (Figure 30F), and left the same amount of droppings during the test duration (Figure 30J), indicating no major difference in the level of anxiety in an open area. We also attempted separating the analysis by sex (male *Stat3*$^{fl/fl}$, n = 4; male *Cx3cr1creER/Stat3*$^{fl/fl}$, n = 9; female *Stat3*$^{fl/fl}$, n = 9; female *Cx3cr1creER/Stat3*$^{fl/fl}$, n = 14), and in both sexes we observed the same trend.

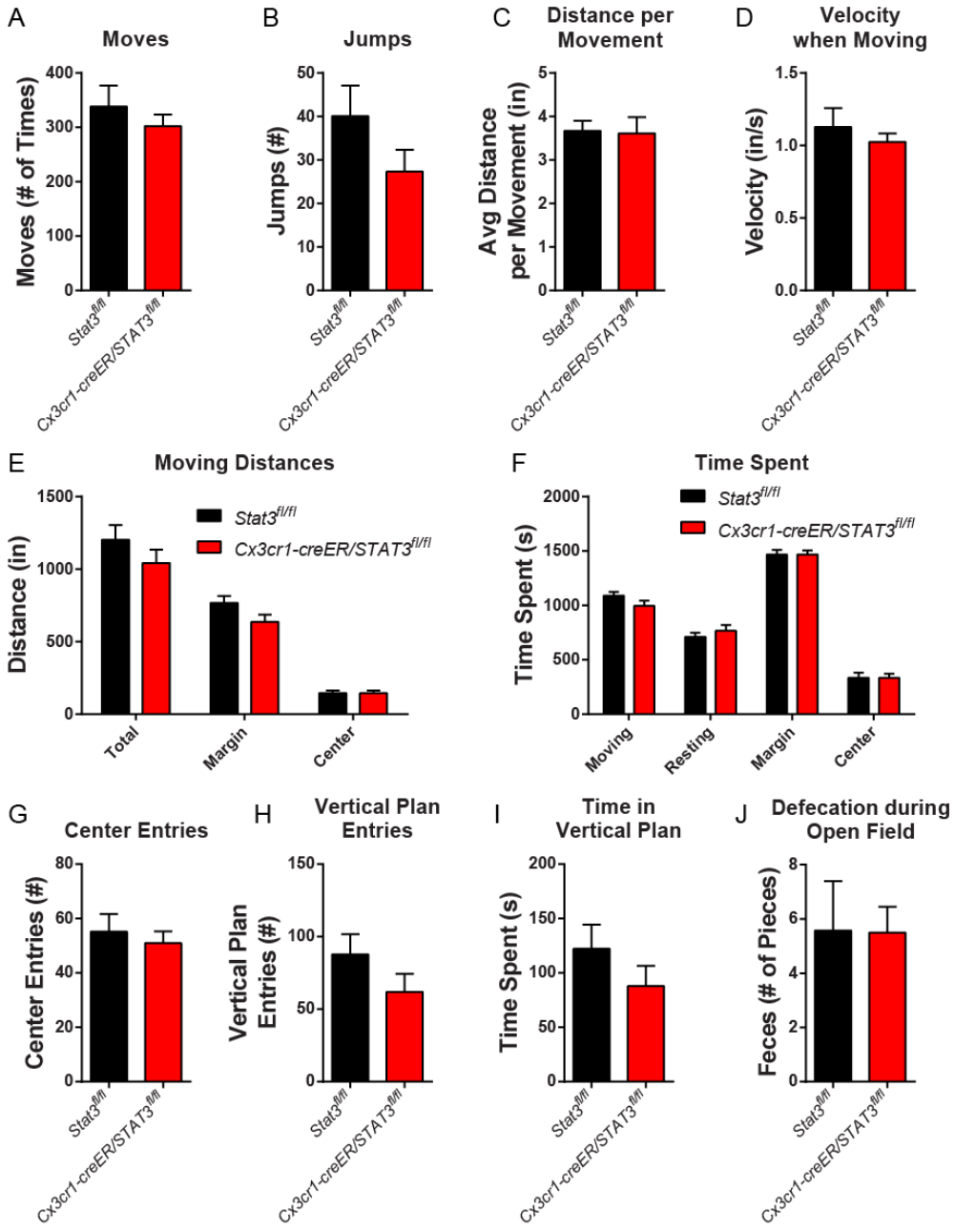

Figure 30. Open field test in the *Cx3cr1creER/Stat3$^{fl/fl}$* mice. P28 *Stat3$^{fl/fl}$* (*n* = 13) and *Cx3cr1creER/Stat3$^{fl/fl}$* mice (*n* = 23) were placed in the open field device for 30 min. Parameters of measurements during the whole test period were computed. **A**, Number of moves. **B**, Number of jumps. **C**, Average distance per move. **D**, Speed when moving. **E**, Total, total moving distance. Margin, total moving distance while being in the margin area. Center, total moving distance while being in the center area, defined as being farther than 2.5 beams to the wall. **F**, Moving, total time spent moving. Resting, total time the coordination remain unchanged. Margin and center, total time spent in the margin or center area. **G**, Number of times the mouse crossed into the center area. **H,** Number of time the mouse raised its body to reach the upper sensor bar. **I**, Total time the mouse spent raising its body. **J**, Number of droppings was counted after the open field test. Data represent mean ± SEM.

To evaluate the spatial learning ability of the *Cx3cr1creER/Stat3*$^{fl/fl}$ mice, MWM was performed at 8 weeks of age (Figure 31). During the 6-day period for hidden platform training, the *Stat3*$^{fl/fl}$ mice improved performance from day 3 to day 5, as evidenced by the decrease in the time spent and distance traveled before locating the platform (Figure 31A, B). However, the performance drastically worsened on the last day of training (day 6). Moreover, the performance on day 5 was not necessarily better than day 1. Therefore, the training results may be due to natural variations, or the mice may not have been sufficiently trained. During the 6-day training period, there was a trend of the *Cx3cr1creER/Stat3*$^{fl/fl}$ mice spending longer time to locate the platform (Figure 31A). However, since the presence of a learning effect is questionable in the *Stat3*$^{fl/fl}$ mice, it cannot be concluded that *Cx3cr1creER/Stat3*$^{fl/fl}$ mice located the platform more slowly due to impaired spatial learning. Instead, this could be due to the trend that *Cx3cr1creER/Stat3*$^{fl/fl}$ mice swam more slowly (Figure 31C), thereby spending more time to locate the platform by chance. Two hours and a day after the last training, a probe test was performed in which the mice were placed back in the pool without the platform (Figure 31D, E). No significant difference was found in the proximity of the mouse to the now-absent platform during either of the probe tests (Figure 31D). Although the *Cx3cr1creER/Stat3*$^{fl/fl}$ mice spent significantly less time in the target quadrant, *i.e.*, the quadrant of the pool where the platform used to be, the *Stat3*$^{fl/fl}$ mice only spent roughly 25% of the test time in the target quadrant (Figure 31E), indicating that no actual learning had occurred.

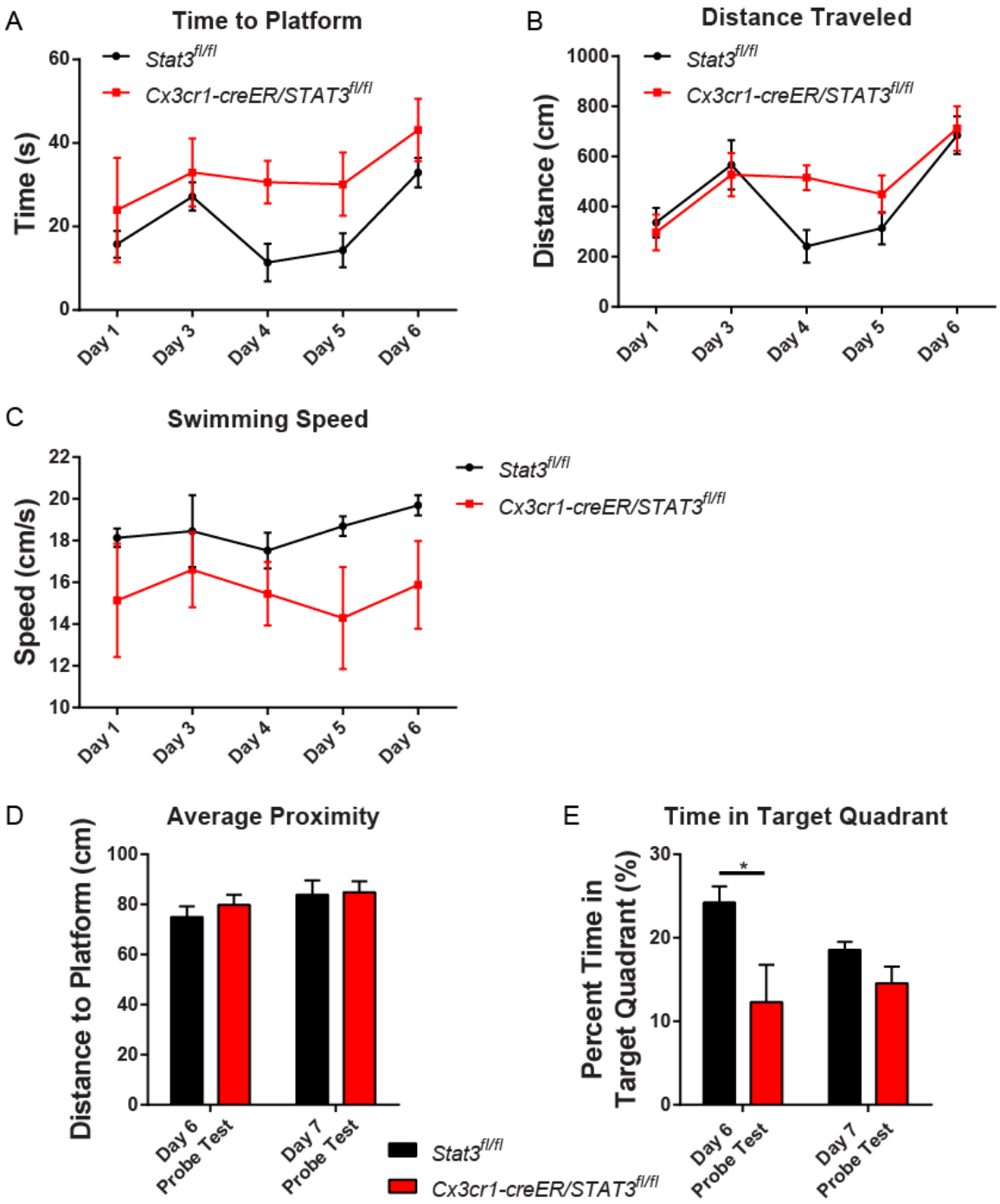

Figure 31. MWM test in the *Cx3cr1creER/Stat3$^{fl/fl}$* mice. **A-C**, 8-week old *Stat3$^{fl/fl}$* (n = 4) and *Cx3cr1creER/Stat3$^{fl/fl}$* mice (n = 3) undertook 6 consecutive days of hidden platform training. **A**, Average time spent before locating the platform. **B**, Distance traveled before locating the platform. **C**, Swimming speed. **D, E**, 2 hr and 24 hr after the last hidden platform training, the mice undertook a probe test. **D**, The average distance to the platform within the first 5 s of the probe test. **E**, Percent time spent in the quadrant where the platform was previously placed. Data represent mean ± SEM. *p < 0.05.

3.4 Discussion

In this section, the role of microglial STAT3 in the developing brain and behavioral consequences were investigated. First, *Cx3cr1* promoter-driven Cre recombination upon P1-P3 administration of tamoxifen was determined to be highly efficient in the microglia, granulocytes, and Ly6C^{hi} monocytes at P6 (Figure 27). Using this paradigm, *Cx3cr1*-mediated *Stat3* ablation at P1-3 resulted in significant loss of microglial cells as determined by immunofluorescence microscopy and cell counting analysis (Figure 28). The mutant microglia also morphologically appeared to be in a more activated state than that of wildtype microglia at P10. Although the decreased microglial population at the second postnatal week essentially recovered and were morphologically similar to that of wildtype littermates in one-month old mice, the transient alterations of microglia in the *Stat3* mutant mice during the early postnatal period appeared to have long term functional effects on certain behaviors. The innate marble burying activity was significantly impaired in the mutant mice, while social activity and locomotor functions remained unaffected (Figure 29, Figure 30). Although our pilot MWM test indicated that *Stat3* mutant mice may have deficits in spatial learning and memory, due to insufficient training trials in this experiment, we consider these results inconclusive and require further investigation (Figure 31). Our study demonstrated that STAT3 activation is necessary for the normal development and function of microglia in the first two postnatal weeks, and that disruption of STAT3 signaling pathway in the microglia may have persistent functional consequences.

Initially regarded as one type of glial cells that "fill in the space" in the CNS when first described, microglia have now been found to possess functions in multiple aspects of immunity and neural development. Specifically, loss of microglia during early postnatal stage has been shown to cause many behavioral deficits [137, 184, 186, 187]. In this study, disruption of STAT3 during neonatal stage caused a drastic reduction of microglial number in the cerebral cortex at P10 (Figure 32). Due to the pleotropic functions of STAT3, the mechanisms that cause the loss of microglia in the *Cx3cr1creER/Stat3*$^{fl/fl}$ mice require further investigation. STAT3 is known for its function in regulating genes related to promoting cell cycle. Specifically, STAT3 can promote cell proliferation as well as prevent programmed cell death [96, 97, 100-103]. It is possible that STAT3 promotes the proliferation and expansion of microglial population during the first postnatal week. Alternatively, STAT3 may contribute to microglia homeostasis by reducing programmed cell death in the microglia. It is also possible that STAT3 mediates M-CSF and/or IL-34 signaling, both of which have been shown to be important in microglial differentiation and survival [161, 200]. Since microglia become activated during the first two postnatal weeks, it is also possible that STAT3-mediated IL-10 anti-inflammatory responses prevent microglial cell death caused by overactivation. A logical next step of this study would be to investigate proliferation and programmed cell death in the microglia at various developmental stages. Alternatively, proliferation, programmed cell death, and activation status can also be tested using primary glial cultures prepared from *Cx3cr1creER/Stat3*$^{fl/fl}$ mice and wildtype controls.

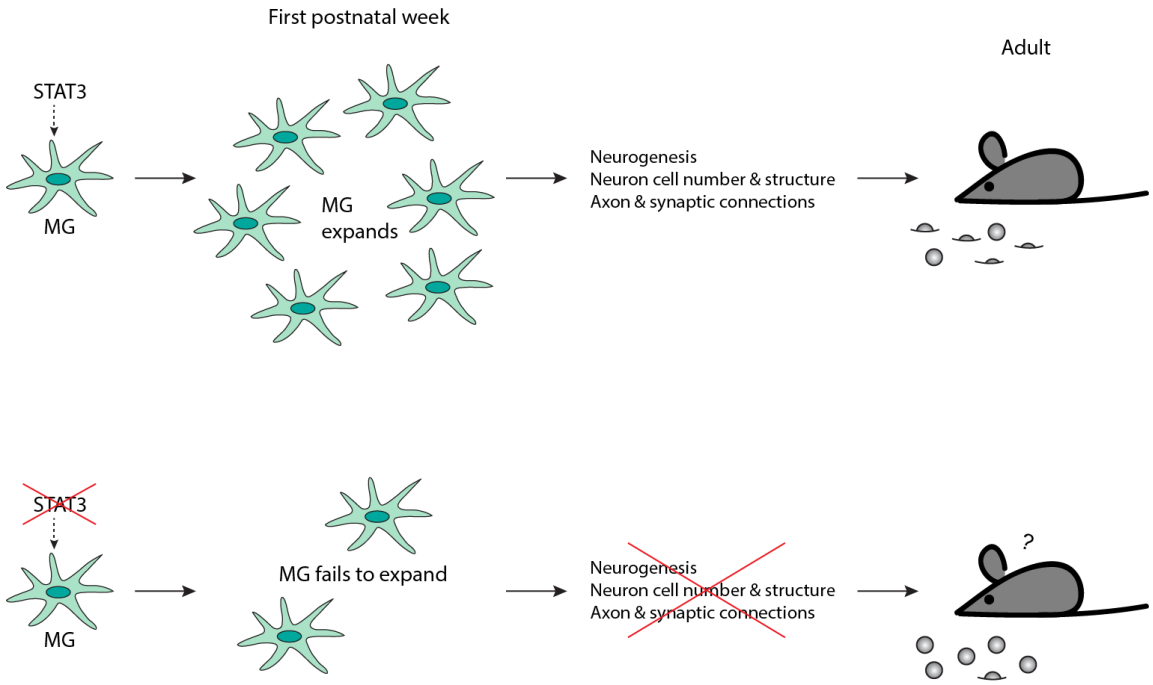

Figure 32. Summary of targeted deletion of Stat3 in the microglia.

In this study, our preliminary data indicate an increased neuronal cell number in the cortex. We also found that the mice deficient of microglial STAT3 exhibited impaired natural burying behavior. Since microglia are involved in regulating neuronal cell number, phagocytosis of cell debris, secretion of growth factors, refinement of synaptic connections and more, experimental depletion of microglia can cause a wide variety of developmental and behavioral abnormalities (reviewed by Frost and Schafer [212]). The reduction of microglial number in the STAT3-mutant mice could cause insufficient synaptic refinement and/or neural circuit maturation, which could then lead to impaired memory forming and natural behaviors. As a future direction, we plan to reveal neuronal structures including morphology of dendrites and axons with Golgi

staining at various developmental stages. In addition, cocultures with neurons and STAT3-mutant or wildtype microglia can help to investigate how neurons develop under the influence of mutant or wildtype microglia. These would help elucidate the underlying mechanisms of the abnormal natural behaviors in the microglial STAT3-mutant mice.

We utilized several types of behavioral tests were utilized to detect potential behavioral deficits in the *Cx3cr1creER/Stat3*$^{fl/fl}$ mice. Social interaction and marble burying tests are commonly used to test behaviors relevant to autism spectrum disorders and compulsive behaviors [209, 213]. The *Cx3cr1creER/Stat3*$^{fl/fl}$ mice did not show abnormalities in their social preferences in the social interaction test in this study. However, it is worth noting that different types of social interaction tests exist [214]. While the three-chamber social approach test utilized in this study is a standardized and well-established procedure, it offers fewer types of interaction measurement and is set in an environment unnatural to the tested mice. While a mouse under testing may be able to recognize and approach a novel mouse, this does not necessarily mean other social interactions, for example, following, pushing, or crawling over each other, are also unchanged. The chamber is transparent, has no food, water, bedding or smell of the home cage. It is thus possible that the mouse is stressed in such environment and is not ready to interact with a stranger yet. A refined social test with more natural settings will help to determine whether the *Cx3cr1creER/Stat3*$^{fl/fl}$ mice have altered social behaviors in relation to wildtype mice.

The *Cx3cr1creER/Stat3*$^{fl/fl}$ mice buried significantly fewer marbles during the marble burying test, suggesting that the mice are, if anything, displaying less compulsive behaviors. Although it would be tempting to speculate that the *Cx3cr1creER/Stat3*$^{fl/fl}$ mice display less anxiety-induced marble burying behavior, the interpretation of marble burying in terms of anxiety is controversial. Thomas and others [215] found that the marble burying test does not correlate with other anxiety related assays. If the marbles induce anxiety in the mouse, it may remain immobile rather than attempting to bury them. Therefore, other tests such as the open field or elevated maze test may be more suitable to assess anxiety.

In the open field test, the *Cx3cr1creER/Stat3*$^{fl/fl}$ mice spent roughly 83% of the testing period in the margin area of the test chamber, similar to the *Stat3*$^{fl/fl}$ mice. While this may suggest that the mice do not have anxiety-related disorders, it is worth noting that the chamber size might not be ideal as an anxiety test. Indeed, several early reports utilized much larger chambers in their studies, *i.e.*, 60 by 60 cm or 80 by 80 cm [216, 217]. If the chamber is not large enough, the mouse may not interpret the margin as "safer" than the center and may instead think that it is trapped in the chamber. This is consistent with the observation in this study that during the test, some mice repetitively jumped as if trying to escape the chamber. Therefore, a future direction of this study would be to incorporate the elevated plus maze test, in which the mouse can either stay in the closed arm or explore into the open arm.

The open field test is also used to measure locomotor activity [218]. The *Cx3cr1creER/Stat3*$^{fl/fl}$ mice only showed a slight trend towards fewer movements and

moving distance, indicating that their locomotor activity was not impaired. Similarly, no significant differences were found in the rotarod test, suggesting that the motor coordination was rather normal. However, during the rotarod test, a ceiling effect was observed in which most of the *Stat3*$^{fl/fl}$ mice were able to stay on the rod for the whole 15-min duration on the third day of training, potentially impeding a difference to be found. Therefore, it would be best to repeat the rotarod test with increased maximum speed.

In the MWM test, the *Cx3cr1creER/Stat3*$^{fl/fl}$ mice spent significantly less time in the target quadrant during the probe test. Unfortunately, the *Stat3*$^{fl/fl}$ mice did not even spend more than 25% of the testing period in the target quadrant, and over the six training days the mice had not improved their performance. Therefore, it is not possible to draw conclusions to this experiment. MWM is a complex test in which many factors, such as even changing the testing room can drastically affect the performance [210]. As such, our MWM test needs to be improved so that the spatial learning behaviors could be observed. For example, a more extensive visible platform training prior to the hidden platform training period could help the mice learn that once in water, there is a platform to look for. Because the MWM is a stressful test and the mice could give up when too stressed, it is important to maintain a sufficiently intensive training schedule while minimizing other stress-inducing factors. Gentle handling and the use of temperature controlled water should help to reduce stress. It is also important that the visual cues are large enough, have enough contrast, and are situated at a height that can be seen by the mice. Last but not the least, a probe test should be carried out prior to the first day of

hidden platform training, so there is a baseline performance to compare the before-and-after effect.

4. CONCLUSIONS

4.1 The Role of Myeloid STAT3 in EAE

MS is a CNS demyelinating and neurodegenerative disease that involves unknown etiology. Although MS likely involves both genetic and environmental factors, it is not attributable to one single gene, and to date no one infectious agent has been identified that can cause the disease. Furthermore, although MS likely involves autoimmunity, it is yet to be proven as a purely autoimmune-driven disease, and no single self-antigen has been identified. Various animal models exist to help study different aspects of MS. EAE is an autoimmune-driven model and due to its reliability of induction, relatively short experimental period, and availability in the C57BL/6 background in which many transgenic lines are, EAE is the most widely used model for MS. Although EAE has been criticized for its limited applicability to MS etiology, studies in EAE have greatly advanced our knowledge in autoimmune demyelination. *Stat3* gene is a risk factor for MS, and its role in differentiation of T_H17 cells, one of the most important cell types in EAE pathogenesis, has been established. Myeloid cells are also important in the development of EAE, and STAT3 activation has been shown to be increased in the monocytes of relapsing MS patients. However, the specific functions of STAT3 in the myeloid cells in EAE remains to be elucidated. To address this gap in knowledge, we set out to study the functions of myeloid STAT3 by generating conditional deletion of STAT3 using the *LysMcre/Stat3*$^{fl/fl}$ mice.

We first demonstrated that myeloid-specific STAT3 deletion confers a strong resistance to EAE. Most of the *LysMcre/Stat3*$^{fl/fl}$ mice did not show signs of classic EAE clinical symptoms, demyelination, or leukocyte infiltration. We also found that the helper T-cell responses in the peripheral lymphoid organs were decreased. Since helper T-cell responses are critically important in EAE such that they are not only necessary, but sufficient to induce EAE alone, we hypothesized that STAT3-deficient myeloid cells show impaired capability to differentiate helper T-cells.

Next, to test the capability of the STAT3-deficient myeloid cells to help differentiate helper T-cells into effector T-cell subsets, we took an *ex vivo* approach and co-cultured the myeloid cells with naïve 2D2 T-cells in the presence of the antigen MOG. We found that STAT3-deficient myeloid cells did not sufficiently differentiate the T-cells. We also found that the myeloid cells expressed less antigen-presenting and co-stimulatory molecules, likely resulting in the deficit in T-cell differentiation.

To test whether the deficit in generating effector T-cells is indeed accountable to the EAE resistance in the *LysMcre/Stat3*$^{fl/fl}$ mice, we conducted passive EAE induction by adoptive transfer of autoreactive T-cells, thereby bypassing the need to generate the host' own effector T-cells upon immunization. We found that two thirds of the *LysMcre/Stat3*$^{fl/fl}$ mice developed adoptive transfer EAE, indicating that the impaired T-cell responses are at least partially responsible to the EAE resistance.

Last, since it's been reported that microglia exhibit differential responses than infiltrating myeloid cells during EAE, we generated a more specific microglial STAT3 deletion by utilizing the *Cx3cr1creER* mice. We observed a trend towards decreased

average clinical scores in the *Cx3cr1creER/Stat3*$^{fl/fl}$ mice. However, the difference was not statistically significant.

Our study sheds light on the role of myeloid STAT3 in generation of autoimmune T-cell responses. Particularly, the impaired capability of STAT3-deficient myeloid cells to differentiate helper T-cells into effector subsets resulted in greatly reduced susceptibility to EAE. Future studies will be required to determine the downstream genes regulated by STAT3 that are important in the myeloid cell functions, as well as the potential differential functions of STAT3 in different subtypes of myeloid cells, such as neutrophils, dendritic cells, or monocytes. Additionally, since the partial susceptibility to adoptive transfer EAE suggests alternative mechanisms, another future direction would be to investigate other potential influences STAT3 has in the myeloid cells, such as the transmigrating capability.

4.2 The Role of Microglial STAT3 in Early Postnatal Development

Microglia are one of the tissue-resident macrophages that emerge from the yolk sac during primitive hematopoiesis. Since their initial discovering, microglia have been increasingly appreciated for their diverse roles in the neural development in the CNS. Studies that depleted microglia in the early postnatal period discovered abnormal brain structures as well as behavioral deficits in the animals. STAT3 is a transcription factor that are involved in genes that regulate cell cycle and inflammation. To investigate whether microglial STAT3 has a role in microglial cell survival and/or activation status and how this would translate to neural development, we set out to study microglial

STAT3 functions by inducing neonatal deletion of STAT3 in microglia in the *Cx3cr1creER/Stat3*$^{fl/fl}$ mice.

We discovered that neonatal deletion of microglial STAT3 results in a transient reduction of microglial number at P8-P10. In our limited analysis, we also found moderately increased number of cortical neuron cells. Although such difference was no longer observed at P32, the transient reduction in microglial number during the first two postnatal weeks likely have caused developmental abnormalities, which could then lead to persistent functional consequences. Indeed, we also found that the mice with microglial STAT3 deletion at neonatal age exhibited impaired marble burying behavior in young adulthood, indicating altered anxiety level and/or repetitive behaviors. Although so far we found a difference only in the marble burying test, some of the behavioral tests we employed, *e.g.,* the Morris' Water Maze, had not been sufficiently optimized to be able to test the intended behaviors. We plan to refine these behavioral tests as well as incorporating more tests, such as the elevated plus maze, so that other potential behavioral consequences in the disruption of neonatal microglial STAT3 activation can be identified.

Our study highlights the importance of STAT3 activation during the normal development and function of microglia in the first two postnatal weeks, and that disruption of STAT3 signaling pathway in the microglia may have persistent functional consequences. Future studies would be required to investigate the mechanism that STAT3 is involved in maintaining microglia homeostasis during development, as well as

to identify the developmental and structural abnormalities in the neurons caused by neonatal microglial STAT3 inactivation.

REFERENCES

1. Kumar, D.R., et al., *Jean-Martin Charcot: the father of neurology.* Clin Med Res, 2011. **9**(1): p. 46-9.
2. Hirtz, D., et al., *How common are the "common" neurologic disorders?* Neurology, 2007. **68**(5): p. 326-37.
3. Norman, J.E., Jr., J.F. Kurtzke, and G.W. Beebe, *Epidemiology of multiple sclerosis in U.S. veterans: 2. Latitude, climate and the risk of multiple sclerosis.* J Chronic Dis, 1983. **36**(8): p. 551-9.
4. Sospedra, M. and R. Martin, *Immunology of multiple sclerosis.* Annu Rev Immunol, 2005. **23**: p. 683-747.
5. McFarlin, D.E. and H.F. McFarland, *Multiple sclerosis (first of two parts).* N Engl J Med, 1982. **307**(19): p. 1183-8.
6. Kantarci, O.H. and B.G. Weinshenker, *Natural history of multiple sclerosis.* Neurol Clin, 2005. **23**(1): p. 17-38, v.
7. Miller, D.H. and S.M. Leary, *Primary-progressive multiple sclerosis.* Lancet Neurol, 2007. **6**(10): p. 903-12.
8. Neema, M., et al., *MRI in multiple sclerosis: what's inside the toolbox?* Neurotherapeutics, 2007. **4**(4): p. 602-17.
9. Lucchinetti, C., et al., *Heterogeneity of multiple sclerosis lesions: implications for the pathogenesis of demyelination.* Ann Neurol, 2000. **47**(6): p. 707-17.
10. Westerlind, H., et al., *Modest familial risks for multiple sclerosis: a registry-based study of the population of Sweden.* Brain, 2014. **137**(Pt 3): p. 770-8.

11. Dyment, D.A., G.C. Ebers, and A.D. Sadovnick, *Genetics of multiple sclerosis.* Lancet Neurol, 2004. **3**(2): p. 104-10.

12. Jakkula, E., et al., *Genome-wide association study in a high-risk isolate for multiple sclerosis reveals associated variants in STAT3 gene.* Am J Hum Genet, 2010. **86**(2): p. 285-91.

13. International Multiple Sclerosis Genetics, C., et al., *Risk alleles for multiple sclerosis identified by a genomewide study.* N Engl J Med, 2007. **357**(9): p. 851-62.

14. Madsen, L.S., et al., *A humanized model for multiple sclerosis using HLA-DR2 and a human T-cell receptor.* Nat Genet, 1999. **23**(3): p. 343-7.

15. Quandt, J.A., et al., *Unique clinical and pathological features in HLA-DRB1*0401-restricted MBP 111-129-specific humanized TCR transgenic mice.* J Exp Med, 2004. **200**(2): p. 223-34.

16. Witebsky, E., et al., *Chronic thyroiditis and autoimmunization.* J Am Med Assoc, 1957. **164**(13): p. 1439-47.

17. Rose, N.R. and C. Bona, *Defining criteria for autoimmune diseases (Witebsky's postulates revisited).* Immunol Today, 1993. **14**(9): p. 426-30.

18. Bielekova, B., et al., *Expansion and functional relevance of high-avidity myelin-specific CD4+ T cells in multiple sclerosis.* J Immunol, 2004. **172**(6): p. 3893-904.

19. Henderson, A.P., et al., *Multiple sclerosis: distribution of inflammatory cells in newly forming lesions.* Ann Neurol, 2009. **66**(6): p. 739-53.

20. Schrempf, W. and T. Ziemssen, *Glatiramer acetate: mechanisms of action in multiple sclerosis.* Autoimmun Rev, 2007. **6**(7): p. 469-75.

21. Fox, E.J., *Mechanism of action of mitoxantrone.* Neurology, 2004. **63**(12 Suppl 6): p. S15-8.

22. Chun, J. and H.P. Hartung, *Mechanism of action of oral fingolimod (FTY720) in multiple sclerosis.* Clin Neuropharmacol, 2010. **33**(2): p. 91-101.

23. Kappos, L., et al., *Natalizumab treatment for multiple sclerosis: updated recommendations for patient selection and monitoring.* Lancet Neurol, 2011. **10**(8): p. 745-58.

24. Kurtzke, J.F., *Epidemiology and etiology of multiple sclerosis.* Phys Med Rehabil Clin N Am, 2005. **16**(2): p. 327-49.

25. Matsushima, G.K. and P. Morell, *The neurotoxicant, cuprizone, as a model to study demyelination and remyelination in the central nervous system.* Brain Pathol, 2001. **11**(1): p. 107-16.

26. Denic, A., et al., *The relevance of animal models in multiple sclerosis research.* Pathophysiology, 2011. **18**(1): p. 21-9.

27. Olson, J.K., J.L. Croxford, and S.D. Miller, *Virus-induced autoimmunity: potential role of viruses in initiation, perpetuation, and progression of T-cell-mediated autoimmune disease.* Viral Immunol, 2001. **14**(3): p. 227-50.

28. Rivers, T.M., D.H. Sprunt, and G.P. Berry, *Observations on attempts to produce acute disseminated encephalomyelitis in monkeys.* J Exp Med, 1933. **58**(1): p. 39-53.

29. Rivers, T.M. and F.F. Schwentker, *Encephalomyelitis accompanied by myelin destruction experimentally produced in monkeys.* J Exp Med, 1935. **61**(5): p. 689-702.

30. Tenembaum, S., et al., *Acute disseminated encephalomyelitis.* Neurology, 2007. **68**(16 Suppl 2): p. S23-36.

31. Kabat, E.A., A. Wolf, and A.E. Bezer, *The rapid production of acute disseminated encephalomyelitis in rhesus monkeys by injection of heterologous and homologous brain tissue with adjuvants.* J Exp Med, 1947. **85**(1): p. 117-30.

32. Wolf, A., E.A. Kabat, and A.E. Bezer, *The pathology of acute disseminated encephalomyelitis produced experimentally in the rhesus monkey and its resemblance to human demyelinating disease.* J Neuropathol Exp Neurol, 1947. **6**(4): p. 333-57.

33. Olitsky, P.K. and R.H. Yager, *Experimental disseminated encephalomyelitis in white mice.* J Exp Med, 1949. **90**(3): p. 213-24.

34. Laatsch, R.H., et al., *The encephalomyelitic activity of myelin isolated by ultracentrifugation.* J Exp Med, 1962. **115**: p. 777-88.

35. Miller, S.D. and W.J. Karpus, *Experimental autoimmune encephalomyelitis in the mouse.* Curr Protoc Immunol, 2007. **Chapter 15**: p. Unit 15.1.

36. Stills, H.F., Jr., *Adjuvants and antibody production: dispelling the myths associated with Freund's complete and other adjuvants.* ILAR J, 2005. **46**(3): p. 280-93.

37. Steinman, R.M. and H. Hemmi, *Dendritic cells: translating innate to adaptive immunity.* Curr Top Microbiol Immunol, 2006. **311**: p. 17-58.

38. Guermonprez, P., et al., *Antigen presentation and T cell stimulation by dendritic cells.* Annu Rev Immunol, 2002. **20**: p. 621-67.

39. Zhu, J., H. Yamane, and W.E. Paul, *Differentiation of effector CD4 T cell populations (*).* Annu Rev Immunol, 2010. **28**: p. 445-89.

40. Kugler, S., et al., *Pertussis toxin transiently affects barrier integrity, organelle organization and transmigration of monocytes in a human brain microvascular endothelial cell barrier model.* Cell Microbiol, 2007. **9**(3): p. 619-32.

41. Andreasen, C. and N.H. Carbonetti, *Pertussis toxin inhibits early chemokine production to delay neutrophil recruitment in response to Bordetella pertussis respiratory tract infection in mice.* Infect Immun, 2008. **76**(11): p. 5139-48.

42. Mangmool, S. and H. Kurose, *G(i/o) protein-dependent and -independent actions of Pertussis Toxin (PTX).* Toxins (Basel), 2011. **3**(7): p. 884-99.

43. Ronchi, F., et al., *Experimental priming of encephalitogenic Th1/Th17 cells requires pertussis toxin-driven IL-1beta production by myeloid cells.* Nat Commun, 2016. **7**: p. 11541.

44. Kivisakk, P., et al., *Human cerebrospinal fluid central memory CD4+ T cells: evidence for trafficking through choroid plexus and meninges via P-selectin.* Proc Natl Acad Sci U S A, 2003. **100**(14): p. 8389-94.

45. Kivisakk, P., et al., *Localizing central nervous system immune surveillance: meningeal antigen-presenting cells activate T cells during experimental autoimmune encephalomyelitis.* Ann Neurol, 2009. **65**(4): p. 457-69.

46. Schlager, C., et al., *Effector T-cell trafficking between the leptomeninges and the cerebrospinal fluid.* Nature, 2016. **530**(7590): p. 349-53.

47. Louveau, A., et al., *Structural and functional features of central nervous system lymphatic vessels.* Nature, 2015. **523**(7560): p. 337-41.

48. Langrish, C.L., et al., *IL-23 drives a pathogenic T cell population that induces autoimmune inflammation.* J Exp Med, 2005. **201**(2): p. 233-40.

49. Nath, N., et al., *T-bet is essential for the progression of experimental autoimmune encephalomyelitis.* Immunology, 2006. **118**(3): p. 384-391.

50. Stromnes, I.M. and J.M. Goverman, *Passive induction of experimental allergic encephalomyelitis.* Nat Protoc, 2006. **1**(4): p. 1952-60.

51. Toft-Hansen, H., et al., *Key metalloproteinases are expressed by specific cell types in experimental autoimmune encephalomyelitis.* J Immunol, 2004. **173**(8): p. 5209-18.

52. Agrawal, S., et al., *Dystroglycan is selectively cleaved at the parenchymal basement membrane at sites of leukocyte extravasation in experimental autoimmune encephalomyelitis.* J Exp Med, 2006. **203**(4): p. 1007-19.

53. Steinman, L. and S.S. Zamvil, *How to successfully apply animal studies in experimental allergic encephalomyelitis to research on multiple sclerosis.* Ann Neurol, 2006. **60**(1): p. 12-21.

54. Robinson, A.P., et al., *The experimental autoimmune encephalomyelitis (EAE) model of MS: utility for understanding disease pathophysiology and treatment.* Handb Clin Neurol, 2014. **122**: p. 173-89.

55. Baxter, A.G., *The origin and application of experimental autoimmune encephalomyelitis.* Nat Rev Immunol, 2007. **7**(11): p. 904-12.

56. Hauser, S.L., et al., *Immunohistochemical analysis of the cellular infiltrate in multiple sclerosis lesions.* Ann Neurol, 1986. **19**(6): p. 578-87.

57. Sriram, S. and I. Steiner, *Experimental allergic encephalomyelitis: a misleading model of multiple sclerosis.* Ann Neurol, 2005. **58**(6): p. 939-45.

58. Orkin, S.H. and L.I. Zon, *Hematopoiesis: an evolving paradigm for stem cell biology.* Cell, 2008. **132**(4): p. 631-44.

59. Gomez Perdiguero, E., et al., *Tissue-resident macrophages originate from yolk-sac-derived erythro-myeloid progenitors.* Nature, 2015. **518**(7540): p. 547-51.

60. Collin, M. and P. Milne, *Langerhans cell origin and regulation.* Curr Opin Hematol, 2016. **23**(1): p. 28-35.

61. Guilliams, M., et al., *Alveolar macrophages develop from fetal monocytes that differentiate into long-lived cells in the first week of life via GM-CSF*. J Exp Med, 2013. **210**(10): p. 1977-92.

62. Kopf, M., C. Schneider, and S.P. Nobs, *The development and function of lung-resident macrophages and dendritic cells.* Nat Immunol, 2015. **16**(1): p. 36-44.

63. Bain, C.C., et al., *Constant replenishment from circulating monocytes maintains the macrophage pool in the intestine of adult mice.* Nat Immunol, 2014. **15**(10): p. 929-37.

64. Ginhoux, F., et al., *Fate mapping analysis reveals that adult microglia derive from primitive macrophages.* Science, 2010. **330**(6005): p. 841-5.

65. Schulz, C., et al., *A lineage of myeloid cells independent of Myb and hematopoietic stem cells.* Science, 2012. **336**(6077): p. 86-90.

66. Alliot, F., I. Godin, and B. Pessac, *Microglia derive from progenitors, originating from the yolk sac, and which proliferate in the brain.* Brain Res Dev Brain Res, 1999. **117**(2): p. 145-52.

67. Yona, S., et al., *Fate mapping reveals origins and dynamics of monocytes and tissue macrophages under homeostasis.* Immunity, 2013. **38**(1): p. 79-91.

68. Doulatov, S., et al., *Hematopoiesis: a human perspective.* Cell Stem Cell, 2012. **10**(2): p. 120-36.

69. Kawamoto, H. and N. Minato, *Myeloid cells.* Int J Biochem Cell Biol, 2004. **36**(8): p. 1374-9.

70. Serafini, B., et al., *Dendritic cells in multiple sclerosis lesions: maturation stage, myelin uptake, and interaction with proliferating T cells.* J Neuropathol Exp Neurol, 2006. **65**(2): p. 124-41.

71. Trebst, C., et al., *CCR1+/CCR5+ mononuclear phagocytes accumulate in the central nervous system of patients with multiple sclerosis.* Am J Pathol, 2001. **159**(5): p. 1701-10.

72. Sriram, S., *Role of glial cells in innate immunity and their role in CNS demyelination.* J Neuroimmunol, 2011. **239**(1-2): p. 13-20.

73. Achiron, A., et al., *Blood transcriptional signatures of multiple sclerosis: unique gene expression of disease activity.* Ann Neurol, 2004. **55**(3): p. 410-7.

74. van Zwam, M., et al., *Brain antigens in functionally distinct antigen-presenting cell populations in cervical lymph nodes in MS and EAE.* J Mol Med (Berl), 2009. **87**(3): p. 273-86.

75. Bo, L., et al., *Induction of nitric oxide synthase in demyelinating regions of multiple sclerosis brains.* Ann Neurol, 1994. **36**(5): p. 778-86.

76. Tran, E.H., et al., *Immune invasion of the central nervous system parenchyma and experimental allergic encephalomyelitis, but not leukocyte extravasation from blood, are prevented in macrophage-depleted mice.* J Immunol, 1998. **161**(7): p. 3767-75.

77. Heppner, F.L., et al., *Experimental autoimmune encephalomyelitis repressed by microglial paralysis.* Nat Med, 2005. **11**(2): p. 146-52.

78. Greter, M., et al., *Dendritic cells permit immune invasion of the CNS in an animal model of multiple sclerosis.* Nat Med, 2005. **11**(3): p. 328-34.

79. Bartholomaus, I., et al., *Effector T cell interactions with meningeal vascular structures in nascent autoimmune CNS lesions.* Nature, 2009. **462**(7269): p. 94-8.

80. Yusuf-Makagiansar, H., et al., *Inhibition of LFA-1/ICAM-1 and VLA-4/VCAM-1 as a therapeutic approach to inflammation and autoimmune diseases.* Med Res Rev, 2002. **22**(2): p. 146-67.

81. Toft-Hansen, H., et al., *Metalloproteinases control brain inflammation induced by pertussis toxin in mice overexpressing the chemokine CCL2 in the central nervous system.* J Immunol, 2006. **177**(10): p. 7242-9.

82. Abraham, M., et al., *Gelatinases (MMP-2 and MMP-9) are preferentially expressed by Th1 vs. Th2 cells.* J Neuroimmunol, 2005. **163**(1-2): p. 157-64.

83. Yong, V.W., et al., *Elevation of matrix metalloproteinases (MMPs) in multiple sclerosis and impact of immunomodulators.* J Neurol Sci, 2007. **259**(1-2): p. 79-84.

84. Caldenhoven, E., et al., *STAT3beta, a splice variant of transcription factor STAT3, is a dominant negative regulator of transcription.* J Biol Chem, 1996. **271**(22): p. 13221-7.

85. Bharadwaj, U., et al., *Monoclonal Antibodies Specific for STAT3beta Reveal Its Contribution to Constitutive STAT3 Phosphorylation in Breast Cancer.* Cancers (Basel), 2014. **6**(4): p. 2012-34.

86. Levy, D.E. and J.E. Darnell, Jr., *Stats: transcriptional control and biological impact.* Nat Rev Mol Cell Biol, 2002. **3**(9): p. 651-62.

87. Meyer, T. and U. Vinkemeier, *Nucleocytoplasmic shuttling of STAT transcription factors.* Eur J Biochem, 2004. **271**(23-24): p. 4606-12.

88. Tworkoski, K., et al., *Phosphoproteomic screen identifies potential therapeutic targets in melanoma.* Mol Cancer Res, 2011. **9**(6): p. 801-12.

89. Wegrzyn, J., et al., *Function of mitochondrial Stat3 in cellular respiration.* Science, 2009. **323**(5915): p. 793-7.

90. Yang, J. and G.R. Stark, *Roles of unphosphorylated STATs in signaling.* Cell Res, 2008. **18**(4): p. 443-51.

91. Carow, B. and M.E. Rottenberg, *SOCS3, a Major Regulator of Infection and Inflammation.* Front Immunol, 2014. **5**: p. 58.

92. Niemand, C., et al., *Activation of STAT3 by IL-6 and IL-10 in primary human macrophages is differentially modulated by suppressor of cytokine signaling 3.* J Immunol, 2003. **170**(6): p. 3263-72.

93. Bourillot, P.Y., et al., *Novel STAT3 target genes exert distinct roles in the inhibition of mesoderm and endoderm differentiation in cooperation with Nanog.* Stem Cells, 2009. **27**(8): p. 1760-71.

94. Matsuda, T., et al., *STAT3 activation is sufficient to maintain an undifferentiated state of mouse embryonic stem cells.* EMBO J, 1999. **18**(15): p. 4261-9.

95. Takeda, K., et al., *Targeted disruption of the mouse Stat3 gene leads to early embryonic lethality.* Proc Natl Acad Sci U S A, 1997. **94**(8): p. 3801-4.

96. Kiuchi, N., et al., *STAT3 is required for the gp130-mediated full activation of the c-myc gene.* J Exp Med, 1999. **189**(1): p. 63-73.

97. Gomez-Nicola, D., et al., *Interleukin-15 regulates proliferation and self-renewal of adult neural stem cells.* Mol Biol Cell, 2011. **22**(12): p. 1960-70.

98. Bonni, A., et al., *Regulation of gliogenesis in the central nervous system by the JAK-STAT signaling pathway.* Science, 1997. **278**(5337): p. 477-83.

99. Nakanishi, M., et al., *Microglia-derived interleukin-6 and leukaemia inhibitory factor promote astrocytic differentiation of neural stem/progenitor cells.* Eur J Neurosci, 2007. **25**(3): p. 649-58.

100. Sepulveda, P., et al., *BCL-2 expression is mainly regulated by JAK/STAT3 pathway in human CD34+ hematopoietic cells.* Cell Death Differ, 2007. **14**(2): p. 378-80.

101. Catlett-Falcone, R., et al., *Constitutive activation of Stat3 signaling confers resistance to apoptosis in human U266 myeloma cells.* Immunity, 1999. **10**(1): p. 105-15.

102. Loffler, D., et al., *Interleukin-6 dependent survival of multiple myeloma cells involves the Stat3-mediated induction of microRNA-21 through a highly conserved enhancer.* Blood, 2007. **110**(4): p. 1330-3.

103. Fontaine, R.H., et al., *IL-9/IL-9 receptor signaling selectively protects cortical neurons against developmental apoptosis.* Cell Death Differ, 2008. **15**(10): p. 1542-52.

104. Abou-Ghazal, M., et al., *The incidence, correlation with tumor-infiltrating inflammation, and prognosis of phosphorylated STAT3 expression in human gliomas.* Clin Cancer Res, 2008. **14**(24): p. 8228-35.

105. Morton, G.J., et al., *Central nervous system control of food intake and body weight.* Nature, 2006. **443**(7109): p. 289-95.

106. Gao, Q., et al., *Disruption of neural signal transducer and activator of transcription 3 causes obesity, diabetes, infertility, and thermal dysregulation.* Proc Natl Acad Sci U S A, 2004. **101**(13): p. 4661-6.

107. Steelman, A.J., et al., *Activation of oligodendroglial Stat3 is required for efficient remyelination.* Neurobiol Dis, 2016. **91**: p. 336-46.

108. Chiba, T., M. Yamada, and S. Aiso, *Targeting the JAK2/STAT3 axis in Alzheimer's disease.* Expert Opin Ther Targets, 2009. **13**(10): p. 1155-67.

109. Nicolas, C.S., et al., *The Jak/STAT pathway is involved in synaptic plasticity.* Neuron, 2012. **73**(2): p. 374-90.

110. Wu, F., et al., *Extensive infiltration of neutrophils in the acute phase of experimental autoimmune encephalomyelitis in C57BL/6 mice.* Histochem Cell Biol, 2010. **133**(3): p. 313-22.

111. McLemore, M.L., et al., *STAT-3 activation is required for normal G-CSF-dependent proliferation and granulocytic differentiation.* Immunity, 2001. **14**(2): p. 193-204.

112. Lee, C.K., et al., *STAT3 is a negative regulator of granulopoiesis but is not required for G-CSF-dependent differentiation.* Immunity, 2002. **17**(1): p. 63-72.

113. Croker, B.A., et al., *SOCS3 is a critical physiological negative regulator of G-CSF signaling and emergency granulopoiesis.* Immunity, 2004. **20**(2): p. 153-65.

114. Liu, Y., et al., *Preferential Recruitment of Neutrophils into the Cerebellum and Brainstem Contributes to the Atypical Experimental Autoimmune Encephalomyelitis Phenotype.* J Immunol, 2015. **195**(3): p. 841-52.

115. Amsen, D., C.G. Spilianakis, and R.A. Flavell, *How are T(H)1 and T(H)2 effector cells made?* Curr Opin Immunol, 2009. **21**(2): p. 153-60.

116. Ivanov, II, L. Zhou, and D.R. Littman, *Transcriptional regulation of Th17 cell differentiation.* Semin Immunol, 2007. **19**(6): p. 409-17.

117. Egwuagu, C.E., *STAT3 in CD4+ T helper cell differentiation and inflammatory diseases.* Cytokine, 2009. **47**(3): p. 149-56.

118. Liu, X., et al., *Loss of STAT3 in CD4+ T cells prevents development of experimental autoimmune diseases.* J Immunol, 2008. **180**(9): p. 6070-6.

119. Lill, C.M., et al., *Independent replication of STAT3 association with multiple sclerosis risk in a large German case-control sample.* Neurogenetics, 2012. **13**(1): p. 83-6.

120. Frisullo, G., et al., *pSTAT1, pSTAT3, and T-bet expression in peripheral blood mononuclear cells from relapsing-remitting multiple sclerosis patients correlates with disease activity.* J Neurosci Res, 2006. **84**(5): p. 1027-36.

121. Lu, J.Q., et al., *The regulation of reactive changes around multiple sclerosis lesions by phosphorylated signal transducer and activator of transcription.* J Neuropathol Exp Neurol, 2013. **72**(12): p. 1135-44.

122. Hutchins, A.P., D. Diez, and D. Miranda-Saavedra, *The IL-10/STAT3-mediated anti-inflammatory response: recent developments and future challenges.* Brief Funct Genomics, 2013. **12**(6): p. 489-98.

123. Bettelli, E., et al., *IL-10 is critical in the regulation of autoimmune encephalomyelitis as demonstrated by studies of IL-10- and IL-4-deficient and transgenic mice.* J Immunol, 1998. **161**(7): p. 3299-306.

124. Takeda, K., et al., *Enhanced Th1 activity and development of chronic enterocolitis in mice devoid of Stat3 in macrophages and neutrophils.* Immunity, 1999. **10**(1): p. 39-49.

125. Gruys, E., et al., *Acute phase reaction and acute phase proteins.* J Zhejiang Univ Sci B, 2005. **6**(11): p. 1045-56.

126. Braun, D.A., M. Fribourg, and S.C. Sealfon, *Cytokine response is determined by duration of receptor and signal transducers and activators of transcription 3 (STAT3) activation.* J Biol Chem, 2013. **288**(5): p. 2986-93.

127. Qin, H., et al., *Signal transducer and activator of transcription-3/suppressor of cytokine signaling-3 (STAT3/SOCS3) axis in myeloid cells regulates neuroinflammation.* Proc Natl Acad Sci U S A, 2012. **109**(13): p. 5004-9.

128. Schroer, N., et al., *Molecular pathobiology of human cervical high-grade lesions: paracrine STAT3 activation in tumor-instructed myeloid cells drives local MMP-9 expression.* Cancer Res, 2011. **71**(1): p. 87-97.

129. Xie, T.X., et al., *Stat3 activation regulates the expression of matrix metalloproteinase-2 and tumor invasion and metastasis.* Oncogene, 2004. **23**(20): p. 3550-60.

130. Hauser, S.L. and J.R. Oksenberg, *The neurobiology of multiple sclerosis: genes, inflammation, and neurodegeneration.* Neuron, 2006. **52**(1): p. 61-76.

131. Steelman, A.J., *Infection as an environmental trigger of multiple sclerosis disease exacerbation.* Front Immunol, 2015. **6**: p. 520.

132. O'Gorman, C., R. Lucas, and B. Taylor, *Environmental risk factors for multiple sclerosis: a review with a focus on molecular mechanisms.* Int J Mol Sci, 2012. **13**(9): p. 11718-52.

133. Langrish, C.L., et al., *IL-23 drives a pathogenic T cell population that induces autoimmune inflammation.* Journal of Experimental Medicine, 2005. **201**(2): p. 233-240.

134. Kim, S., et al., *Aberrant upregulation of astroglial ceramide potentiates oligodendrocyte injury.* Brain Pathol, 2012. **22**(1): p. 41-57.

135. Takeda, K., et al., *Stat3 activation is responsible for IL-6-dependent T cell proliferation through preventing apoptosis: generation and characterization of T cell-specific Stat3-deficient mice.* J Immunol, 1998. **161**(9): p. 4652-60.

136. Clausen, B.E., et al., *Conditional gene targeting in macrophages and granulocytes using LysMcre mice.* Transgenic Res, 1999. **8**(4): p. 265-77.

137. Parkhurst, C.N., et al., *Microglia promote learning-dependent synapse formation through brain-derived neurotrophic factor.* Cell, 2013. **155**(7): p. 1596-609.

138. Stromnes, I.M. and J.M. Goverman, *Active induction of experimental allergic encephalomyelitis.* Nat Protoc, 2006. **1**(4): p. 1810-9.

139. Ying, W., et al., *Investigation of macrophage polarization using bone marrow derived macrophages.* J Vis Exp, 2013(76).

140. Li, J., et al., *Tumor necrosis factor alpha mediates lipopolysaccharide-induced microglial toxicity to developing oligodendrocytes when astrocytes are present.* J Neurosci, 2008. **28**(20): p. 5321-30.

141. Yamasaki, R., et al., *Differential roles of microglia and monocytes in the inflamed central nervous system.* J Exp Med, 2014. **211**(8): p. 1533-49.

142. Ajami, B., et al., *Infiltrating monocytes trigger EAE progression, but do not contribute to the resident microglia pool.* Nat Neurosci, 2011. **14**(9): p. 1142-9.

143. Furqan, M., et al., *STAT inhibitors for cancer therapy.* J Hematol Oncol, 2013. **6**: p. 90.

144. Furtek, S.L., et al., *Strategies and Approaches of Targeting STAT3 for Cancer Treatment.* ACS Chem Biol, 2016. **11**(2): p. 308-18.

145. Isomaki, P., et al., *The activity of JAK-STAT pathways in rheumatoid arthritis: constitutive activation of STAT3 correlates with interleukin 6 levels.* Rheumatology (Oxford), 2015. **54**(6): p. 1103-13.

146. Abad, C., et al., *Targeted STAT3 disruption in myeloid cells alters immunosuppressor cell abundance in a murine model of spontaneous medulloblastoma.* J Leukoc Biol, 2014. **95**(2): p. 357-67.

147. Reindl, W., et al., *Essential crosstalk between myeloid and lymphoid cells for development of chronic colitis in myeloid-specific signal transducer and activator of transcription 3-deficient mice.* Immunology, 2007. **120**(1): p. 19-27.

148. Matsukawa, A., et al., *Stat3 in resident macrophages as a repressor protein of inflammatory response.* J Immunol, 2005. **175**(5): p. 3354-9.

149. Melillo, J.A., et al., *Dendritic cell (DC)-specific targeting reveals Stat3 as a negative regulator of DC function.* J Immunol, 2010. **184**(5): p. 2638-45.

150. Kitamura, H., et al., *IL-6-STAT3 controls intracellular MHC class II alphabeta dimer level through cathepsin S activity in dendritic cells.* Immunity, 2005. **23**(5): p. 491-502.

151. Qi, Q.R. and Z.M. Yang, *Regulation and function of signal transducer and activator of transcription 3.* World J Biol Chem, 2014. **5**(2): p. 231-9.

152. Steinbach, K., et al., *Neutrophils amplify autoimmune central nervous system infiltrates by maturing local APCs.* J Immunol, 2013. **191**(9): p. 4531-9.

153. Martins, A., J. Han, and S.O. Kim, *The multifaceted effects of granulocyte colony-stimulating factor in immunomodulation and potential roles in intestinal immune homeostasis.* IUBMB Life, 2010. **62**(8): p. 611-7.

154. Nguyen-Jackson, H.T., et al., *G-CSF-activated STAT3 enhances production of the chemokine MIP-2 in bone marrow neutrophils.* J Leukoc Biol, 2012. **92**(6): p. 1215-25.

155. Panopoulos, A.D., et al., *STAT3 governs distinct pathways in emergency granulopoiesis and mature neutrophils.* Blood, 2006. **108**(12): p. 3682-90.

156. Kamezaki, K., et al., *Roles of Stat3 and ERK in G-CSF signaling.* Stem Cells, 2005. **23**(2): p. 252-63.

157. Kamada, N., et al., *Role of the gut microbiota in immunity and inflammatory disease.* Nat Rev Immunol, 2013. **13**(5): p. 321-35.

158. Ajami, B., et al., *Local self-renewal can sustain CNS microglia maintenance and function throughout adult life.* Nat Neurosci, 2007. **10**(12): p. 1538-43.

159. Bruttger, J., et al., *Genetic Cell Ablation Reveals Clusters of Local Self-Renewing Microglia in the Mammalian Central Nervous System.* Immunity, 2015. **43**(1): p. 92-106.

160. Aloisi, F., *Immune function of microglia.* Glia, 2001. **36**(2): p. 165-79.

161. Cronk, J.C. and J. Kipnis, *Microglia - the brain's busy bees.* F1000Prime Rep, 2013. **5**: p. 53.

162. Nimmerjahn, A., F. Kirchhoff, and F. Helmchen, *Resting microglial cells are highly dynamic surveillants of brain parenchyma in vivo.* Science, 2005. **308**(5726): p. 1314-8.

163. Oppenheim, R.W., *Cell death during development of the nervous system.* Annu Rev Neurosci, 1991. **14**: p. 453-501.

164. Yeo, W. and J. Gautier, *Early neural cell death: dying to become neurons.* Dev Biol, 2004. **274**(2): p. 233-44.

165. Sierra, A., et al., *Microglia shape adult hippocampal neurogenesis through apoptosis-coupled phagocytosis.* Cell Stem Cell, 2010. **7**(4): p. 483-95.

166. Ferrer, I., et al., *Naturally occurring cell death in the cerebral cortex of the rat and removal of dead cells by transitory phagocytes.* Neuroscience, 1990. **39**(2): p. 451-8.

167. Frade, J.M. and Y.A. Barde, *Microglia-derived nerve growth factor causes cell death in the developing retina.* Neuron, 1998. **20**(1): p. 35-41.

168. Sedel, F., et al., *Macrophage-derived tumor necrosis factor alpha, an early developmental signal for motoneuron death.* J Neurosci, 2004. **24**(9): p. 2236-46.

169. Chao, C.C., et al., *Activated microglia mediate neuronal cell injury via a nitric oxide mechanism.* J Immunol, 1992. **149**(8): p. 2736-41.

170. Wakselman, S., et al., *Developmental neuronal death in hippocampus requires the microglial CD11b integrin and DAP12 immunoreceptor.* J Neurosci, 2008. **28**(32): p. 8138-43.

171. Cunningham, C.L., V. Martinez-Cerdeno, and S.C. Noctor, *Microglia regulate the number of neural precursor cells in the developing cerebral cortex.* J Neurosci, 2013. **33**(10): p. 4216-33.

172. Gow, D.J., D.P. Sester, and D.A. Hume, *CSF-1, IGF-1, and the control of postnatal growth and development.* J Leukoc Biol, 2010. **88**(3): p. 475-81.

173. Butovsky, O., et al., *Microglia activated by IL-4 or IFN-gamma differentially induce neurogenesis and oligodendrogenesis from adult stem/progenitor cells.* Mol Cell Neurosci, 2006. **31**(1): p. 149-60.

174. Ueno, M., et al., *Layer V cortical neurons require microglial support for survival during postnatal development.* Nat Neurosci, 2013. **16**(5): p. 543-51.

175. Hua, J.Y. and S.J. Smith, *Neural activity and the dynamics of central nervous system development.* Nat Neurosci, 2004. **7**(4): p. 327-32.

176. Stevens, B., et al., *The classical complement cascade mediates CNS synapse elimination.* Cell, 2007. **131**(6): p. 1164-78.

177. Schafer, D.P., et al., *Microglia sculpt postnatal neural circuits in an activity and complement-dependent manner.* Neuron, 2012. **74**(4): p. 691-705.

178. Paolicelli, R.C., et al., *Synaptic pruning by microglia is necessary for normal brain development.* Science, 2011. **333**(6048): p. 1456-8.

179. Berbel, P. and G.M. Innocenti, *The development of the corpus callosum in cats: a light- and electron-microscopic study.* J Comp Neurol, 1988. **276**(1): p. 132-56.

180. Squarzoni, P., et al., *Microglia modulate wiring of the embryonic forebrain.* Cell Rep, 2014. **8**(5): p. 1271-9.

181. Duval, E.R., A. Javanbakht, and I. Liberzon, *Neural circuits in anxiety and stress disorders: a focused review.* Ther Clin Risk Manag, 2015. **11**: p. 115-26.

182. Kim, H., C.S. Lim, and B.K. Kaang, *Neuronal mechanisms and circuits underlying repetitive behaviors in mouse models of autism spectrum disorder.* Behav Brain Funct, 2016. **12**(1): p. 3.

183. Limatola, C. and R.M. Ransohoff, *Modulating neurotoxicity through CX3CL1/CX3CR1 signaling.* Front Cell Neurosci, 2014. **8**: p. 229.

184. Zhan, Y., et al., *Deficient neuron-microglia signaling results in impaired functional brain connectivity and social behavior.* Nat Neurosci, 2014. **17**(3): p. 400-6.

185. Erblich, B., et al., *Absence of colony stimulation factor-1 receptor results in loss of microglia, disrupted brain development and olfactory deficits.* PLoS One, 2011. **6**(10): p. e26317.

186. Nelson, L.H. and K.M. Lenz, *Microglia depletion in early life programs persistent changes in social, mood-related, and locomotor behavior in male and female rats.* Behav Brain Res, 2017. **316**: p. 279-293.

187. VanRyzin, J.W., et al., *Temporary Depletion of Microglia during the Early Postnatal Period Induces Lasting Sex-Dependent and Sex-Independent Effects on Behavior in Rats.* eNeuro, 2016. **3**(6).

188. Bilbo, S.D., et al., *Neonatal infection induces memory impairments following an immune challenge in adulthood.* Behav Neurosci, 2005. **119**(1): p. 293-301.

189. Malkova, N.V., et al., *Maternal immune activation yields offspring displaying mouse versions of the three core symptoms of autism.* Brain Behav Immun, 2012. **26**(4): p. 607-16.

190. Nayak, D., T.L. Roth, and D.B. McGavern, *Microglia development and function.* Annu Rev Immunol, 2014. **32**: p. 367-402.

191. Ponomarev, E.D., T. Veremeyko, and H.L. Weiner, *MicroRNAs are universal regulators of differentiation, activation, and polarization of microglia and macrophages in normal and diseased CNS.* Glia, 2013. **61**(1): p. 91-103.

192. Kierdorf, K., et al., *Microglia emerge from erythromyeloid precursors via Pu.1- and Irf8-dependent pathways.* Nat Neurosci, 2013. **16**(3): p. 273-80.

193. Friedman, A.D., *C/EBPalpha induces PU.1 and interacts with AP-1 and NF-kappaB to regulate myeloid development.* Blood Cells Mol Dis, 2007. **39**(3): p. 340-3.

194. Huynh, J., et al., *CSF-1 receptor signalling from endosomes mediates the sustained activation of Erk1/2 and Akt in macrophages.* Cell Signal, 2012. **24**(9): p. 1753-61.

195. Lee, A.W. and D.J. States, *Colony-stimulating factor-1 requires PI3-kinase-mediated metabolism for proliferation and survival in myeloid cells.* Cell Death Differ, 2006. **13**(11): p. 1900-14.

196. Jack, G.D., L. Zhang, and A.D. Friedman, *M-CSF elevates c-Fos and phospho-C/EBPalpha(S21) via ERK whereas G-CSF stimulates SHP2 phosphorylation in marrow progenitors to contribute to myeloid lineage specification.* Blood, 2009. **114**(10): p. 2172-80.

197. Novak, U., et al., *Colony-stimulating factor 1-induced STAT1 and STAT3 activation is accompanied by phosphorylation of Tyk2 in macrophages and Tyk2 and JAK1 in fibroblasts.* Blood, 1995. **86**(8): p. 2948-56.

198. Wang, Y., et al., *IL-34 is a tissue-restricted ligand of CSF1R required for the development of Langerhans cells and microglia.* Nat Immunol, 2012. **13**(8): p. 753-60.

199. Cheng, X., Q.L. Wan, and Z.B. Li, *AG490 suppresses interleukin-34-mediated osteoclastogenesis in mice bone marrow macrophages.* Cell Biol Int, 2017. **41**(6): p. 659-668.

200. Yang, S., et al., *Interleukin 34 Upregulation Contributes to the Increment of MicroRNA 21 Expression through STAT3 Activation Associated with Disease Activity in Rheumatoid Arthritis.* J Rheumatol, 2016. **43**(7): p. 1312-9.

201. Francisco-Cruz, A., et al., *Granulocyte-macrophage colony-stimulating factor: not just another haematopoietic growth factor.* Med Oncol, 2014. **31**(1): p. 774.

202. Shibata, Y., et al., *GM-CSF regulates alveolar macrophage differentiation and innate immunity in the lung through PU.1.* Immunity, 2001. **15**(4): p. 557-67.

203. Panopoulos, A.D., et al., *Control of myeloid-specific integrin alpha Mbeta 2 (CD11b/CD18) expression by cytokines is regulated by Stat3-dependent activation of PU.1.* J Biol Chem, 2002. **277**(21): p. 19001-7.

204. Hegde, S., et al., *Stat3 promotes the development of erythroleukemia by inducing Pu.1 expression and inhibiting erythroid differentiation.* Oncogene, 2009. **28**(38): p. 3349-59.

205. Lu, Y., et al., *Differential pro-inflammatory responses of astrocytes and microglia involve STAT3 activation in response to 1800 MHz radiofrequency fields.* PLoS One, 2014. **9**(9): p. e108318.

206. Przanowski, P., et al., *The signal transducers Stat1 and Stat3 and their novel target Jmjd3 drive the expression of inflammatory genes in microglia.* J Mol Med (Berl), 2014. **92**(3): p. 239-54.

207. Dominguez, D., et al., *Phenotypic and biochemical analyses of BACE1- and BACE2-deficient mice.* J Biol Chem, 2005. **280**(35): p. 30797-806.

208. Lai, W.S., et al., *Akt1 deficiency affects neuronal morphology and predisposes to abnormalities in prefrontal cortex functioning.* Proc Natl Acad Sci U S A, 2006. **103**(45): p. 16906-11.

209. Crawley, J.N., *Mouse behavioral assays relevant to the symptoms of autism.* Brain Pathol, 2007. **17**(4): p. 448-59.

210. Weitzner, D.S., et al., *Morris water maze test: optimization for mouse strain and testing environment.* J Vis Exp, 2015(100): p. e52706.

211. Vorhees, C.V. and M.T. Williams, *Morris water maze: procedures for assessing spatial and related forms of learning and memory.* Nat Protoc, 2006. **1**(2): p. 848-58.

212. Frost, J.L. and D.P. Schafer, *Microglia: architects of the developing nervous system.* Trends Cell Biol, 2016. **26**(8): p. 587-97.

213. Angoa-Perez, M., et al., *Marble burying and nestlet shredding as tests of repetitive, compulsive-like behaviors in mice.* J Vis Exp, 2013(82): p. 50978.

214. Silverman, J.L., et al., *Behavioural phenotyping assays for mouse models of autism.* Nat Rev Neurosci, 2010. **11**(7): p. 490-502.

215. Thomas, A., et al., *Marble burying reflects a repetitive and perseverative behavior more than novelty-induced anxiety.* Psychopharmacology (Berl), 2009. **204**(2): p. 361-73.

216. Choleris, E., et al., *A detailed ethological analysis of the mouse open field test: effects of diazepam, chlordiazepoxide and an extremely low frequency pulsed magnetic field.* Neurosci Biobehav Rev, 2001. **25**(3): p. 235-60.

217. Carola, V., et al., *Evaluation of the elevated plus-maze and open-field tests for the assessment of anxiety-related behaviour in inbred mice.* Behav Brain Res, 2002. **134**(1-2): p. 49-57.

218. Tatem, K.S., et al., *Behavioral and locomotor measurements using an open field activity monitoring system for skeletal muscle diseases.* J Vis Exp, 2014(91): p. 51785.